

DISS. ETH NO. 28496

**FUNGAL MELANIN AND ITS COMPOSITES FOR
WATER REMEDIATION AND WOOD TREATMENT**

A thesis submitted to attain the degree of
DOCTOR OF SCIENCES of ETH ZÜRICH
(Dr. sc. ETH Zürich)

presented by
NGUYET ANH TRAN LY

Dipl.-Ing.in, BOKU Wien, Austria

born on 09.06.1993
citizen of Vietnam

accepted on the recommendation of

Prof. Dr. Ingo Burgert (examiner)
Prof. Dr. Francis Schwarze (co-examiner)
Prof. Dr. Siegfried Fink (co-examiner)
Prof. Dr. Markus Linder (co-examiner)

2022

Abstract

Melanin is a pigment that is found in most organisms. In nature, many different sources of melanin are available, with the most common ones being the ink of cephalopods, sheep wool, human hair and different types of bacteria and fungi. Structural studies suggest that melanin has diverse and heterogeneous polymeric structures, and has slightly different compositions, sizes, colors and functions depending on its sources.

During the past decade, melanin has attracted increasing attention for use in organic semiconductors and bioelectronics, drug delivery, photo-protection and environmental remediation processes. Although considerable advances in these fields have been achieved, real-world applications of melanin are still scarce, due to the limited and expensive source of natural melanin. In addition, its insolubility in water and many organic solvents as well as its diverse structure and properties makes it more difficult to study and to use in practical applications.

Recent biotechnological advances from our research group and others have allowed a relatively large-scale production of fungal melanin, which could replace current expensive commercial melanin. Fungal melanin is soluble in aqueous solutions, facilitating its use, either directly or as a component in composites with other natural polymers. In this thesis, fungal melanin and composites with other biodegradable polymers were investigated for water remediation and wood protection, with the aim to bring fungal melanin closer to practical and sustainable applications.

It is well known that heavy metal and organic dye pollution in water resources has become a severe environmental and public health problem worldwide due to rapid urbanization and industrialization. Thereby, enhanced treatments are urgently required with respect to eco-friendliness, filtration efficiencies and low operational costs. Within the scope of the doctoral thesis, first, fungal melanin was incorporated into polymeric nanofibrous membranes via an

electrospinning method to obtain stable and highly porous filtration systems, which were used to absorb heavy metal ions from water. Adsorption assays were performed on both raw melanin and melanized membranes. At phytotoxic concentrations of Pb^{2+} , Cd^{2+} , Ni^{2+} and Cr^{3+} , fungal melanin was able to remove more than 90% of heavy metals in single-component solutions, showing a strong affinity for binding Pb^{2+} a low affinity for essential metals such as Ca^{2+} and Zn^{2+} . The metal adsorption profiles also showed that melanized membranes were able to maintain the adsorption capacity of raw melanin. Thus, these membranes can be efficiently used as filtration membranes for the removal of heavy metals.

Secondly, fungal melanin was used to develop melanized-cationic cellulose nanofiber foams that can successfully remove crystal violet, a common organic dye used in textile industry, reducing its concentrations in water down to the sub-ppm level. The foam can be recycled several times while retaining its adsorption/desorption properties, demonstrating a high practicability for adsorbing the cationic dye crystal violet. This work highlights the opportunity to combine both advanced features of sustainable polymers such as cellulose and the unique properties of fungal melanin for manufacturing bio-hybrid composites for water purification.

Besides being an effective scavenger for toxic chemicals, fungal melanin can be used directly as an antimicrobial agent for wood protection. When melanin was used together with plant oils for wood treatment, a double impregnation process resulted in an accelerated and superior antibacterial response when compared to oil(s) without melanin. A significant antifungal effect was also obtained, i.e. the lethal effect against *Chaetomium globosum* was 90% on walnut wood after 2 weeks incubation. In addition, the treated wood samples absorbed less water than the untreated ones and resulted in a higher dimensional stability of treated wood at different humidity conditions, highlighting the practicability of this approach for wood protection.

Overall, the knowledge obtained in this doctoral thesis helps to better understand the functions and applicability of fungal melanin and opens avenues for future research to design new materials and systems that can be applied in real life.

Kurzfassung

Melanin ist ein Pigment, das in den meisten Organismen vorkommt. In der Natur sind viele verschiedene Melaninquellen verfügbar, wobei die häufigsten die Tinte von Kopffüßern, Schafwolle, menschliches Haar und verschiedene Arten von Bakterien und Pilzen sind. Strukturelle Studien legen nahe, dass Melanin vielfältige und heterogene Polymerstrukturen besitzt und je nach Herkunft leicht unterschiedliche Zusammensetzungen, Größen, Farben und Funktionen aufweisen kann.

In den letzten zehn Jahren hat Melanin eine zunehmende Aufmerksamkeit für die Verwendung in organischen Halbleitern und Bioelektronik, Arzneimittelabgabe, Lichtschutz und Umweltsanierungsprozessen auf sich gezogen. Obwohl auf diesen Gebieten beträchtliche Fortschritte erzielt wurden, sind reale Anwendungen von Melanin aufgrund der begrenzten und teuren Quelle von natürlichem Melanin immer noch selten. Ausserdem ist Melanin in Wasser und vielen organischen Lösungsmitteln unlöslich und seine vielfältige Struktur und Eigenschaften erschweren die Untersuchung und Verwendung in praktischen Anwendungen.

Die jüngsten biotechnologischen Fortschritte unserer Forschungsgruppe und anderer Wissenschaftler haben eine höhere Produktion von Pilzmelanin ermöglicht, das in Zukunft das derzeit teure kommerzielle Melanin ersetzen könnte. Pilzmelanin ist in wässrigen Lösungen löslich, was seine Verwendung erleichtert, entweder direkt oder als Bestandteil in Verbundstoffen mit anderen natürlichen Polymeren. In dieser Dissertation wurden Pilzmelanin und Komposite mit anderen biologisch abbaubaren Polymeren zur Wasserreinigung und zum Holzschutz untersucht, mit dem Ziel, das Potential von Pilzmelanin für nachhaltige Anwendungen aufzuzeigen.

Es ist allgemein bekannt, dass die Verschmutzung von Wasserressourcen durch Schwermetalle und organische Farbstoffe aufgrund der schnellen Urbanisierung und Industrialisierung weltweit zu einem ernsthaften Problem für die Umwelt und die öffentliche Gesundheit geworden ist. Daher sind verbesserte Behandlungen im Hinblick auf Umweltfreundlichkeit, Filtrationseffizienz und niedrige Herstellungskosten dringend erforderlich. Im Rahmen meiner Doktorarbeit wurde Pilzmelanin über ein Elektrospleinverfahren in polymere Nanofasermembranen eingearbeitet, um stabile und hochporöse Filtersysteme zu entwickeln, die zur Absorption von Schwermetallionen aus Wasser verwendet wurden. Adsorptionsstudien wurden sowohl an rohem Melanin als auch an melanierten Membranen durchgeführt. Bei physiotoxischen Konzentrationen von Pb^{2+} , Cd^{2+} , Ni^{2+} und Cr^{3+} war Pilzmelanin in der Lage, mehr als 90% der Schwermetalle in Einkomponentenlösungen zu entfernen, wobei es eine starke Affinität zur Bindung von Pb^{2+} und eine geringe Affinität zu essentiellen Metallen wie Ca^{2+} und Zn^{2+} nachweisbar war. Die Metalladsorptionsprofile zeigten auch, dass melanierte Membranen in der Lage waren, die Adsorptionskapazität von Rohmelanin aufrechtzuerhalten. Somit können diese Membranen effizient als Filtrationsmembranen zur Entfernung von Schwermetallen verwendet werden. Ausserdem wurde Pilzmelanin verwendet, um melanierte kationische Zellulose-Nanofaserschäume zu entwickeln, die Kristallviolett, ein in der Textilindustrie häufig verwendeten organischen Farbstoff, erfolgreich absorbieren und die Konzentrationen im verschmutzten Wasser auf das Niveau von unter ppm reduzieren können. Der melanierte Schaumstoff kann unter Beibehaltung seiner Adsorptions-/Desorptionseigenschaften mehrmals recycelt werden, was eine hohe Praktikabilität für die Adsorption des kationischen Farbstoffs Kristallviolett demonstriert. Diese Arbeit hebt die Möglichkeit hervor, sowohl fortschrittliche Eigenschaften nachhaltiger Polymere wie Zellulose als auch die einzigartigen Eigenschaften von Pilzmelanin für die Herstellung von Bio-Hybrid-Verbundwerkstoffen für die Wasserreinigung zu kombinieren.

Pilzmelanin ist nicht nur ein effektiver Fänger für toxische Chemikalien, sondern kann auch direkt als antimikrobielles Mittel für den Holzschutz verwendet werden. Wenn Melanin zusammen mit Pflanzenölen zur Holzbehandlung verwendet wird, führt ein doppelter Imprägnierungsprozess zu einer beschleunigten und erhöhten antibakteriellen Reaktion im Vergleich zu Öl(en) ohne Melanin. Es wurde auch eine zufriedenstellende, nicht signifikante antimykotische Wirkung erhalten, d. h. die letale Wirkung gegen *Chaetomium globosum* betrug 90% auf Walnussholz nach 2-wöchiger Inkubation. Darüber hinaus absorbierten die behandelten Holzproben weniger Wasser als die unbehandelten. Dies führte zu einer höheren Dimensionsstabilität des behandelten Holzes bei unterschiedlichen Feuchtebedingungen, was die Praktikabilität dieses Ansatzes für den Holzschutz unterstreicht.

Insgesamt trägt das in dieser Doktorarbeit gewonnene Wissen dazu bei, die Funktionen und Anwendbarkeit von Pilzmelanin besser zu verstehen und Türen für zukünftige Forschungen zu öffnen, um neue Materialien und Systeme mit Melanin zu entwickeln, die im wirklichen Leben angewendet werden können.

Table of Contents

Abstract.....	3
Kurzfassung	6
1. General introduction	11
1.1. <i>Motivation and Objectives</i>	11
1.2. <i>Structure of the Thesis</i>	12
1.3. <i>Melanin</i>	14
1.3.1. Introduction.....	15
1.3.2. Melanin pigments	16
1.3.3. Melanin isolation from conventional natural sources	17
1.3.4. Melanin production by chemical synthesis.....	19
1.3.5. Melanin production by microorganisms.....	20
1.3.6. Applications of microbial melanins	25
1.3.7. Conclusions and outlook	27
Bibliography.....	27
1.4. <i>Materials Processing Technologies</i>	35
1.4.1. Electrospinning.....	35
1.4.2. Freeze-drying	35
1.4.3. Vacuum pressure impregnation	36
1.5. <i>Materials Characterization Techniques</i>	37
1.5.1. Fourier transform infrared (FTIR) spectroscopy.....	37
1.5.2. Ultraviolet-Visible (UV-Vis) spectroscopy	38
1.5.3. Inductively coupled plasma mass spectrometry (ICP-MS)	38
1.5.4. X-ray photoelectron spectroscopy (XPS).....	38
1.5.5. Scanning electron microscopy (SEM)	39
1.5.6. Mechanical testing.....	39
1.5.7. Adsorption	40
2. Main investigations	44
2.1. <i>Fungal Melanin-based Electrospun Membranes for Heavy Metal Detoxification of Water</i>	46
2.1.1. Introduction.....	47
2.1.2. Materials and methods.....	50
2.1.3. Results and discussion	56
2.1.4. Conclusions.....	69
References	70
Supporting Information	74
2.2. <i>Melanized-Cationic Cellulose Nanofibers Foams for Bioinspired Removal of Cationic Dyes</i>	78
2.2.1. Introduction.....	79
2.2.2. Materials and methods.....	80
2.2.3. Results and discussion	87
2.2.4. Conclusions.....	101

References	102
Supporting Information	106
<i>2.3. Antimicrobial Effect of Fungal Melanin in Combination with Plant Oils for the Treatment of Wood</i>	111
2.3.1. Introduction.....	112
2.3.2. Materials and methods	114
2.3.3. Results and discussions.....	121
2.3.4. Conclusions	131
References	132
Supporting Information	135
3. General discussion and conclusions.....	139
3.1. <i>Relationship between Synthesis, Extraction and Structure of Melanin</i>	139
3.2. <i>Different Material Processing Strategies to Utilize Melanin</i>	142
3.2.1. Electrospinning.....	143
3.2.2. Freeze-drying	145
3.3. <i>Metal Binding to Melanin</i>	146
3.4. <i>Aggregation versus Dispersion Affecting Adsorption</i>	148
3.5. <i>Mechanical Improvement of Melanin-based Composites</i>	150
3.6. <i>Synergy between Fungal Melanin and Plant Oils</i>	151
4. Outlook.....	153
References of chapter 1, 3 and 4.....	155
Acknowledgements.....	160
Curriculum Vitae.....	162
Declaration.....	164

1. General introduction

1.1. Motivation and Objectives

Melanin is the common term for a group of multifunctional biopolymers that often exhibit interesting physical, chemical and biological properties. During the past decade, melanin has attracted increasing attention, as it has been shown to act as photo-protectants, toxic-compound scavengers, and antimicrobial and anti-inflammatory agent. Other promising applications include organic semiconductors, bioelectronics, and drug delivery. Although considerable advances in these different research fields have been achieved, the expensive production cost of melanin (Sigma Aldrich, CHF 1760/g) either via extraction from sepia ink or by chemical synthesis), its insolubility in water and many organic solvents, and its heterogeneous chemical structures inhibit melanin's use for practical applications.

Recent studies from our group and others have enabled the production of melanin at a large scale using *Armillaria cepistipes*. The biosynthesis of fungal melanin is rather sustainable, simple and of low cost (CHF 25/g). In addition, fungal melanin produced with this method is homogeneously dispersed in an aqueous media, which makes it easier for studies than using highly aggregated and insoluble commercial melanin. The high melanin production yields (25 – 30 g melanin/L medium) allowed us to investigate the functions and applicability of fungal melanin. The incentive for me to initially study fungal melanin for water remediation is based on the fact that water pollution has developed into a severe environmental and public health problem due to rapid urbanization and industrialization, especially in some developing countries. Finding solutions to tackle water pollution is urgently required and of global importance. Currently, a range of water treatment methods are available, however, a water remediation process that is simple, inexpensive, eco-friendly, and effective for removal of pollutants down to ppm/ppb concentrations, has long been sought after.

I was also motivated by the request from musicians and music instrument makers to study fungal melanin for wood protection. Microbial deterioration of wood gradually destroys precious and historic musical instruments. For example, the Serpentino (English: serpent/little snake), a wind instrument used over 400 years ago and considered the godfather of modern instruments such as the saxophone and the tuba, was totally ruined as the last original specimens were destroyed due to the colonization of bacteria and fungi. Reconstructing the serpent in particular and other ancient instruments in general requires the preservation of wood against bio-deterioration.

The first objective of the project was to examine whether the obtained fungal melanin displays similar physical, chemical, and biological properties as that of other types of melanin. The second objective was to investigate the ability of using melanin for practical applications. For this purpose, I aimed to answer several key questions:

- i) Is fungal melanin an effective scavenger for toxic compounds?
- ii) Does fungal melanin exhibit antimicrobial properties?
- iii) How can fungal melanin be incorporated into biodegradable polymer substrates to develop materials such as membranes and foams?
- iv) How can these materials be used for practical applications? The work performed and the results obtained in this thesis provide answers to these questions.

1.2. Structure of the Thesis

The thesis first provides the state of the art of melanin research, and then presents research work and findings achieved. It is concluded with a summary and an outlook for future work. The published research of this cumulative thesis is organized in two chapters:

Subchapter 1.3 provides an exclusive overview of melanin, its isolation from natural sources, as well as different routes of synthesis, ranging from chemical to electrochemical and microbial

methods. Based on the advantages of melanin production from fungi compared to other conventional methods and sources, the focus of this research (Chapter 2) was set on using fungal melanin to develop different multifunctional melanin-based materials.

Chapter 2 describes the research conducted in detail. Specifically, in sub-chapter 2.1, I investigated the binding of toxic metals to fungal melanin and its composites, which were prepared by the incorporation of melanin powder into polycaprolactone and polyurethane membranes by electrospinning. It was apparent that fungal melanin is an excellent scavenger for these positively charged metal ions, and in all cases, the toxic compounds were adsorbed with high capacities and rapid adsorption rates.

In sub-chapter 2.2, fully bio-derived composites were developed from melanin solution and cellulose nanofibers by freeze-drying. The resulting porous foams offered high specific surface areas to adsorb toxic organic dyes. The concentrations of the remnant after adsorption were at the ppm/sub-ppm level. These membranes and foams not only allowed for easy handling of the materials, but also displayed improved performance due to the synergistic effect between the highly dispersed melanin supramolecules and the substrates. More detail on these studies will be provided in sub-chapters 2.1 and 2.2.

In sub-chapter 2.3, I also examined the antimicrobial effect of melanin for wood protection. We found that when melanin was used together with plant oils, the double-impregnation with plant oils and melanin resulted in an accelerated and superior antibacterial effect when compared to that of the oil(s) alone. A significant antifungal effect was also achieved, while the treated wood samples still preserved their dimensions at different humidity conditions. The latter highlights the practicability of this approach for wood protection.

1.3. Melanin

This chapter was published as an open-access review paper:

Anh N. Tran-Ly, Carolina Reyes, Francis W. M. R. Schwarze, Javier Ribera, *Microbial production of melanin and its various applications*, World Journal of Microbiology and Biotechnology, **2020**, *36*, 170.

Author contributions

Anh N. Tran-Ly: conceptualization, writing - original draft, writing - review & editing, visualization; **Carolina Reyes**: visualization, editing; **Francis W. M. R. Schwarze**: review & editing; **Javier Ribera**: conceptualization, review and editing, project administration.

Corresponding authors: Correspondence to Anh N. Tran-Ly or Javier Ribera.

Microbial production of melanin and its various applications

Anh N. Tran-Ly,^{a,b*} Carolina Reyes^a, Francis W.M.R. Schwarze,^a Javier Ribera^{a*}

^aLaboratory for Cellulose & Wood Materials, Empa, 9014 St. Gallen, Switzerland

^bDepartment of Civil, Environmental and Geomatic Engineering, ETH Zürich, 8093 Zürich, Switzerland

Abstract

Melanins are natural biopolymers that are known to contribute to different biological processes and to protect organisms from adverse environmental conditions. During the past decade, melanins have attracted increasing attention for their use in organic semiconductors and bioelectronics, drug delivery, photoprotection and environmental bioremediation. Although considerable advances in these fields have been achieved, real-world applications of melanins are still scarce, probably due to the limited and expensive source of natural melanin. Nevertheless, recent biotechnological advances have allowed for relatively large-scale production of microbial melanins, which could replace current commercial melanin. In this review, we first describe different melanin sources and highlight the advantages and

disadvantages of each production method. Our focus is on the microbial synthesis of melanins, including the methodology and mechanism of melanin formation. Applications of microbial melanins are also discussed, and an outlook on how to push the field forward is discussed.

1.3.1. Introduction

Melanin is an ancient pigment that occurred very early in all living organisms (Zhang et al. 2010; Glass et al. 2012). Melanin is typically known for its unique ability to absorb a wide range of radiations (Brenner and Hearing 2008; Liu et al. 2013). Moreover, melanization is considered a survival strategy for many organisms inhabiting unfavorable environmental conditions. Owing to the multifunctionality of the pigment, it has been known to serve as: (a) an antioxidant and radical scavenger (Ju et al. 2011; Le Na et al. 2019), (b) a photo-protector that efficiently absorbs and dissipates solar radiation in the form of heat (d'Ischia et al. 2015), (c) an absorber that chelates metals and binds organic compounds (Karlsson and Lindquist 2016; Tran-Ly et al. 2020) and (d) an organic semiconductor (Bothma et al. 2008). Besides these functions, melanin is considered eco-friendly and biocompatible since it is naturally synthesized by most organisms. Melanin has recently burst onto the scene of materials science and green technology as a functional additive or coating that can substantially improve the performance of conventional materials for different applications. However, upscaling production and extraction protocols of melanin needs further optimization so that it can be used for developing novel materials.

In this review, we first introduce the current understanding of melanin, along with its chemical structures and physical properties. We then present the strategies of melanin production, including the chemical synthesis and methods based on natural resources with emphasis on promising biotechnology processes using microorganisms. We highlight several recent

applications of microbial melanins, and provide our perspectives on how to bring melanin closer to practical applications in materials science.

1.3.2. Melanin pigments

Recent studies suggest that melanin is in fact a general term for a group of heterogeneous pigments produced by organisms of all domains of life from bacteria to mammals (the plural form “melanins” is occasionally used in sections below indicating the heterogeneous nature of melanin). In humans, melanin is the prominent pigment responsible for the colour of skin, hair and eyes (Solano 2014; d’Ischia et al. 2015). As melanin usually appears black or dark brown, the pigment derives its name "melanin" from "melanos" – an ancient Greek word for black (Borovanský and Riley 2011). However, there are other pigments in this group that produce reddish or yellowish colours such as the pheomelanin found in red hair, freckles, and feathers. Melanin has a relatively diverse and heterogeneous structure. This is due to the ubiquitous sources of melanin, which leads to its heterogeneity in composition, size, color and function. Moreover, the physicochemical properties of melanin (a highly negative charge, high molecular weight and hydrophobic nature) hinder analytical approaches to identify and characterize its structure (Pralea et al. 2019). Additionally, the pigment is insoluble in most solvents and is resistant to chemical degradation (Nosanchuk et al. 2015; Pralea et al. 2019). Chemical treatments, such as using a strong base, can be used to dissolve melanin but often alter its native structure and may even break the initial polymer into fragments. Enzymatic digestion is relatively inefficient in eliminating the protein and lipid content of natural samples (Pralea et al. 2019).

A widespread definition of melanin is “a heterogeneous polymer derived from the oxidation of phenolic or indolic compounds and subsequent polymerization of intermediate phenols and their resulting quinones” (Solano 2014). Melanin pigments can be categorized based on their chemical structures, namely, eumelanin, pheomelanin, neuromelanin and allomelanin (d’Ischia

et al. 2013). Eumelanin is the black-to-brown subgroup of melanin formed by oxidative polymerization of tyrosine derivatives such as L-3,4-dihydroxyphenylalanine (L-Dopa), and it is the most common melanin found in animals, including humans (Solano 2014). Eumelanin is, therefore, by far the most relevant source from a biological and technological perspective and has been widely studied and used as a model for synthetic melanin. Pheomelanin is another type of animal melanin, found in red hair, freckles or feathers, which differs from eumelanin by the presence of sulfur in the composition since its precursor is 5-cysteinyl-Dopa. Neuromelanin is explicitly produced within human neurons by the oxidation of dopamine and other catecholamine precursors. In plants, fungi and bacteria, the identified melanin is called allomelanin. This group encompasses a variety of non-nitrogenous subgroups of melanin derived from different catecholic and dihydroxynaphthalene precursors, which are usually mentioned as catechol melanin (in plants), DHN-melanin and pyomelanin (in bacteria and fungi). Lastly, it is notable that many microorganisms can produce different types of melanin, including eumelanin via a similar pathway with mammalian melanin synthesis (Eisenman and Casadevall 2012; Cordero and Casadevall 2017) (Table 1).

Table 1. Summary of common melanins, sources and their corresponding precursors

Type of melanin	Producing sources	Melanin precursor
Eumelanin (DOPA-melanin)	Animals, bacteria, fungi	Tyrosine or L-Dopa
Pheomelanin	Animals	5-S-cys-Dopa
Neuromelanin	Human (brain)	Dopamine and 5-S-cys-dopamine
Catechol-melanin	Plants	Catechol
DHN-melanin	Fungi, bacteria	1,8-dihydroxynaphthalene (DHN)
Pyomelanin	Fungi, bacteria	Homogentisic acid

1.3.3. Melanin isolation from conventional natural sources

Conventionally, melanin is extracted from sepia ink or animals' dark hair/feathers. One of the challenges for melanin production and extraction from these sources is that most melanins are

formed inside melanosomes and are tightly bound to some cellular components such as proteins or minerals (Prota 1995). Therefore, the isolation procedure of melanin usually involves harsh chemical treatments to remove the entire protein fraction, cell debris and unconsumed nutrients. Normally, these treatments include extensive hydrolysis with boiling mineral acids or bases followed by successive washing steps with organic solvents such as chloroform, acetone or absolute ethanol (Liu and Simon 2003; Pralea et al. 2019). However, during the latter process, the melanin polymeric skeleton suffers chemical alterations (Pralea et al. 2019). Alternative strategies reported in the literature have described the use of milder isolation methodologies such as: mechanical separation using ultracentrifugation; proteolytic digestion using enzymes to eliminate the residue protein matrix; or a combination of both strategies (Novellino et al. 2000; Xiao et al. 2018) (Figure 1). Some studies have shown that enzymatic extraction methods can retain the melanin structure and its morphology in the form of intact melanosomes better than the acid/base extraction protocols (Liu et al. 2003).

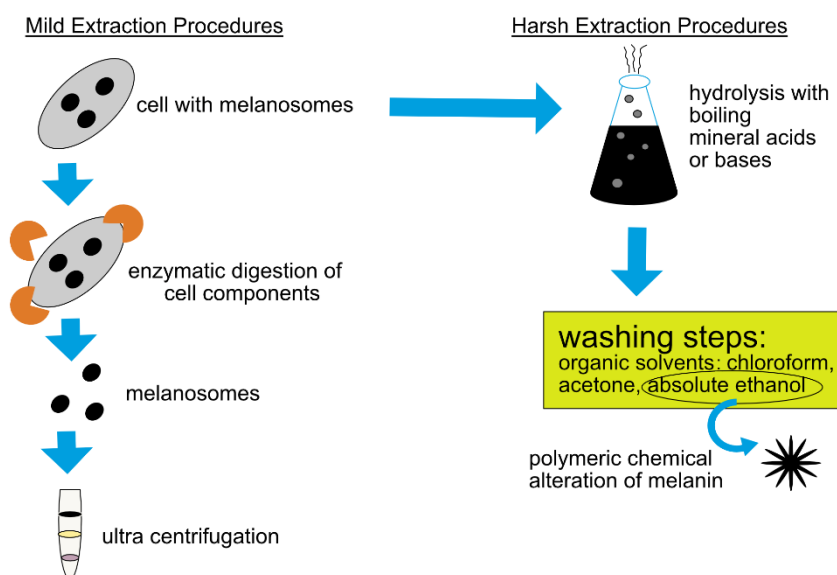


Figure 1. Mild and harsh melanin extraction steps currently used to obtain melanin from living cells.

Natural melanins are complete polymers with limited potential for modification. Besides, the final drying method can have a great influence on the physical properties of melanin such as the aggregation, the surface area-to-mass ratio, and porosity (d'Ischia et al. 2013). This source-

dependency makes natural melanin supply difficult and expensive for up-scaling and can result in contamination depending on its source. For example, melanin extracted from feathers of birds or the ink sac of sepia may have an increased amount of associated toxic metals related to their environmental exposure. Moreover, these melanin sources are of ethical concern as the animals, from which melanin is extracted, may need to be killed. All these factors emphasize the cautious use of natural melanin for applied research.

1.3.4. Melanin production by chemical synthesis

In the last decade, the synthesis of materials with properties mimicking that of natural melanins has been extensively investigated (Lee et al. 2007; Liu et al. 2013; D’Ischia et al. 2014; Solano 2017). In chemical synthesis, polydopamine, which shares some properties with natural melanin due to their similar functional groups such as catechol, amine and imine groups (Solano 2017), is synthesized via oxidative polymerization of dopamine. The high tunability of polydopamine has rapidly promoted research on this material (Liu et al. 2014). Notably, when studies on synthetic melanin-based materials are cited, they usually refer to polydopamine and its derivatives.

Three common approaches for the synthesis of polydopamine are: 1) solution oxidation, 2) enzymatic oxidation, and 3) electropolymerization (Liu et al. 2014). Solution oxidation under alkaline conditions is widely used and involves the oxidation with oxygen and self-polymerization of the dopamine monomers. The second approach is often related to the enzymatic oxidation of L-tyrosine using the enzyme tyrosinase. Another method in this approach involves the oxidation of diphenolic groups of dopamine, followed by its polymerization into polydopamine using the enzyme laccase. Lastly, the electropolymerization method has mainly been used for the formation of polydopamine on an electrode. In a deoxygenated solution, a polymeric film with high thickness can be effectively obtained by applying an appropriate electrical voltage. One disadvantage of this method, however, is the

requirement that the surface of the electrode is conductive, hence polydopamine can only be deposited on conductive materials.

Despite a number of attempts to mimic natural melanins, synthetic melanins often have altered structural and functional properties compared to natural melanins (Ligonzo et al. 2009; Bridelli and Crippa 2010). Some reports have demonstrated that natural melanins in biotechnological applications outperform synthetic melanins. For instance, sepia melanin exhibits a higher specific capacity (16.1 in comparison with 7.9 mAhg⁻¹) in aqueous sodium-ion batteries compared to polydopamine (Kim et al. 2013). The higher efficiency of natural melanins may be attributed to their innate features, including the carboxyl content of the starting precursor (i.e. tyrosine or L-DOPA vs. dopamine, which is devoid of a carboxylic group), the melanogenesis mechanism (Pezzella et al. 1997), the unique nanostructure of melanin granules attached to small amounts of proteins, and the higher hydration degree of the molecules (Bernsmann et al. 2010).

1.3.5. Melanin production by microorganisms

The diverse biological roles of melanin in bacteria and fungi have been extensively reported in the literature (Nosanchuk and Casadevall 2003; Plonka and Grabacka 2006; Eisenman and Casadevall 2012; Solano 2014; Cordero and Casadevall 2017). However, the control of melanin synthesis in different microorganisms has only recently been investigated. Considering the advantages of using microorganisms to produce melanin, such as no seasonal growth constraint, cost-effectiveness, and eco-friendliness, microbial melanin is a valuable source of natural melanin.

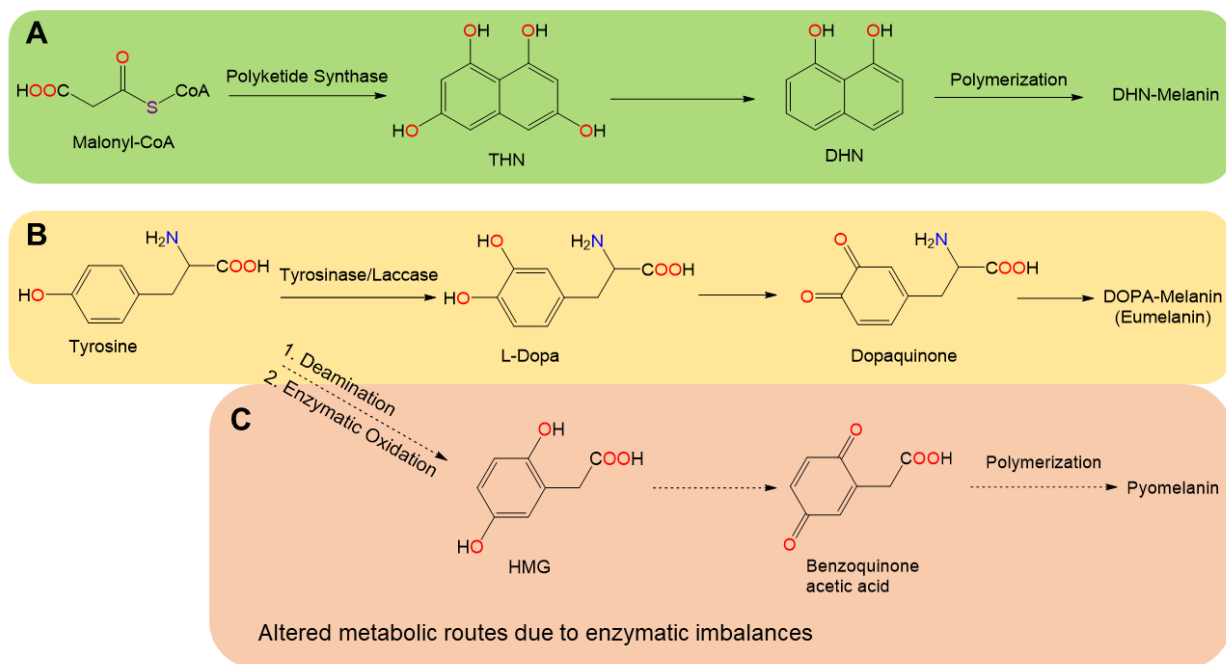


Figure 2. Schematic representation of melanin synthesis in bacteria and fungi, indicating key chemical transformations common to microbial melanin forming processes. A. DHN-pathway; B. DOPA-pathway; C. In the event of enzymatic imbalances, altered metabolic pathways can occur, leading to different types of melanins, for example pyomelanin.

Generally, most microbial melanins are formed through the transformation of either tyrosine (DOPA-pathway) or malonyl-coenzyme A (DHN-pathway), facilitated by different sets of enzymes (Figure 2). The first pathway is very similar to mammalian melanin synthesis. In this pathway, the melanin precursor, tyrosine, is converted to L-Dopa, then to dopaquinone by tyrosinase and laccase. Dopaquinones are highly active and spontaneously oxidized and autopolymerized to form melanin. Synthesis of melanin via the DOPA-pathway is referred to as DOPA-melanin or eumelanin. However, during the catabolic process, other hydroxylated aromatic compounds such as homogentisic acid, can accumulate due to enzymatic imbalances or interruptions, which may result in different types of melanins. In the second pathway, the corresponding precursor, malonyl-coenzyme A, is produced endogenously. Catalyzed by polyketide synthases, the sequential decarboxylative condensation of five molecules of malonyl-coenzyme A creates 1,3,6,8-tetrahydroxynaphthalene (THN). THN then undergoes a

series of reduction and dehydration reactions to form 1,8-dihydroxynaphthalene (DHN). The polymerization of DHN results in DHN-melanin as the final product (Plonka and Grabacka 2006; Eisenman and Casadevall 2012; Pavan et al. 2020). Notably, both pathways can be found in bacteria and fungi. Nevertheless, most bacteria and basidiomycetous fungi synthesize melanin via the DOPA-pathway, whereas, ascomycetous and some imperfect fungi including non-microscopic fungi, for instance *Tuber* spp., use the DHN-pathway to produce melanin.

With respect to high-yield melanin production, microorganisms using the DHN-pathway are not preferred since in this pathway, the pigment is synthesized endogenously and is tightly attached to the inner side of the cell wall (Toledo et al. 2017). This makes melanin extraction extremely difficult and can generate artifacts derived from harsh extracting chemicals. Alternatively, melanogenesis via the DOPA-pathway is a mechanism microorganisms use to neutralize toxic phenolic compounds from the environment, such as those released by microorganisms during host defense (Schmaler-Ripcke et al. 2009; Almeida-Paes et al. 2012). Consequently, many microbes depend on exogenous tyrosine or tyrosine derivative substrates for melanin synthesis. This is of great interest for scientists that study microbial melanization since melanin is produced extracellularly and harsh extraction can therefore be avoided. Several bacteria and fungi in this category are summarized in Table 2.

Additionally, these characteristics allow considerable control of the yield and the type of resulting melanin. Although tyrosine is identified as the main melanin substrate, other catecholamines such as dopamine and norepinephrine can also be used as substrates. However, it is important to note that melanins resulting from different substrates may differ in structure due to various catabolic processes with different enzymes involved. This creates room for tuning the physicochemical properties and optimizing the production of microbial melanins.

Table 2. Studies focused on optimization of microbial melanin production

Microorganisms	Melanin type	Max. melanin production / g L ⁻¹ , (Incubation time / days)	Tyrosine added	Metal ions added	Substrates	Reference
Bacteria						
<i>Actinoalloteichus</i> MA-32	sp. DOPA	0.1 (7)	Yes	Fe, Mg	Glycerol	(Manivasagan et al. 2013)
<i>Bacillus safensis</i>	nd	6.9 (24h)	None	None	Fruit waste extract	(Tarangini and Mishra 2014)
<i>Brevundimonas</i> sp. SGJ	DOPA	6.8 (54h)	Yes	Cu	Tryptone	(Surwase et al. 2013)
<i>Nocardiopsis</i> MSA10	<i>alba</i> nd	3.4 (7)	Yes	nd	Sucrose	(Kiran et al. 2014)
<i>Pseudomonas</i> WH001 55	sp. nd	7.6 (6)	Yes	None	Starch, yeast extract	(Kiran et al. 2017)
<i>Pseudomonas</i> HMGM-7	<i>stutzeri</i> DOPA	7.2 (3)	Yes	None	Nutrient broth in sea water	(Ganesh Kumar et al. 2013)
<i>Streptomyces</i> NEAE-H	<i>glaucescens</i> DOPA	0.4 (6)	Yes	Fe	Protease peptone	(El-Naggari and El-Ewasy 2017)
<i>Streptomyces</i> SC-1	<i>kathirae</i> DOPA	13.7 (5)	Yes	Cu	Amylodextrine, yeast extract	(Guo et al. 2014)
<i>Streptomyces</i> DMZ-3	<i>lusitanus</i> nd	5.3 (6)	Yes	Cu	Beef extract	(Madhusudhan et al. 2014)
<i>Streptomyces</i> sp. ZL-24	DOPA	4.2 (5)	None	Fe, Ni	Soy peptone	(Wang et al. 2019)
Fungi						
<i>Armillaria borealis</i>	DOPA	11.58 (97)	Yes	Cu, Fe, Mg	Glucose, yeast extract	(Ribera et al. 2019)
<i>Armillaria cepistipes</i>	DOPA	27.98 (161)	Yes	Cu, Fe, Mg	Glucose, yeast extract	(Ribera et al. 2019)
<i>Armillaria ostoyae</i>	DOPA	24.80 (153)	Yes	Cu, Fe, Mg	Glucose, yeast extract	(Ribera et al. 2019)
<i>Aspergillus fumigatus</i>	nd	0.01 (10)	No	None	Dextrose, peptone	(Raman et al. 2015)
<i>Auricularia auricula</i>	DOPA	2.97 (8)	Yes	Mg	Lactose, yeast extract	(Sun et al. 2016)

<i>Daldinia concentrica</i>	DOPA	1.78 (73)	Yes	Cu, Fe, Mg	Glucose, yeast extract	(Ribera et al. 2019)
<i>Gliocephalotrichum simplex</i>	DOPA	6.60 (6)	Yes	Cu, Fe	Peptone, yeast extract	(Jalmi et al. 2012)

nd: not defined

The formation of melanin depends highly on the regulation of melanin synthesis enzymes, which is driven by multiple nutritional factors and physicochemical conditions. Peptone, glucose and yeast extract are widely chosen as carbon and nitrogen sources. Recent studies have also exploited agricultural residues, such as fruit waste extract, corn steep liquor and wheat bran extract, to lower the production cost while ensuring the high yield of production (Hamano and Kilikian 2006; Silveira et al. 2008; Zou and Tian 2017). Copper is an important element for melanin production because of its role as a cofactor for laccases and tyrosinases (Sendovski et al. 2011; Reiss et al. 2013; Yang et al. 2017). Variation in the amount of added copper leads to irregular pigmentation in several fungal and bacterial species (Held and Kutzner 1990; Griffith et al. 2007). On the one hand, besides copper, other metals can also enhance melanin formation. A recent study by Wang et al. (2019) showed a strong increase in tyrosinase activity and melanin production driven by the addition of iron and nickel. On the other hand, the presence of metals may induce stress responses in microbes, resulting in melanin formation (Gowri and Srivastava 1996). In other cases, melanin synthesis is promoted by different kinds of stress, for instance: high temperature, nutrient-poor growth media, hyperosmotic pressure, etc. (Coyne and Al-Harhi 1992; Fogarty and Tobin 1996; Cordero and Casadevall 2017). Because of the multiple and diverse factors that affect melanin biosynthesis, there is no universal culture media or cultivation condition for growing melanogenic microorganisms. Instead, the composition and ratio of each component should be identified depending on the microbe. Similarly, environmental factors, i.e. temperature, pH, the presence of oxygen and aeration, light, stress and irradiation during cultivation, can greatly affect the cell growth and pigment biosynthesis, and should be carefully considered. Some statistic tools such as the Taguchi method, the Plackett-Burman design, or the Response surface methodology are usually used to design

multifactorial experiments and to evaluate the impact of each factor in the production process (Surwase et al. 2013; Saini and Melo 2015; Sun et al. 2016; El-Naggar and El-Ewasy 2017).

Previously, most melanin-related studies involving other microorganisms, such as *Aspergillus carbonarius* or *Streptomyces glaucescens* NEAE-H (El-Naggar and El-Ewasy 2017), could not achieve melanin suitable for industrial application yields ($< 1 \text{ g L}^{-1}$ medium) even after optimizing the growth conditions. In contrast, studies focused on optimizing melanin production utilize fungi and bacteria with the ability to produce melanin via tyrosine transformation. The optimized protocols usually involve the exogenous supply of tyrosine, copper and/or other metal ions and show the possibility to produce melanin pigments in significant yields. For instance, melanin can now be produced by *Armillaria cepistipes* at gram-scale (28 g L^{-1} medium) in laboratory condition, which paves the way for industrial scaling up and future applications of melanin (Ribera et al. 2019).

Last but not least, microbial melanin production can be further improved by applying genetic engineering techniques to increase the natural melanogenic capacity of some organisms or generating novel melanin-producing strains. The most common genetic modification to enhance/generate a production strain, targets the expression of genes encoding the enzymes involved in melanin formation, mostly tyrosinases. The latest advances in the generation of recombinant melanogenic strains and production processes were already summarized by (Martínez et al. 2019) and are not the focus of this review.

1.3.6. Applications of microbial melanins

In fungi and bacteria, melanins are usually reported for its important role in the virulence of pathogenic organisms (Jacobson 2000; Cordero and Casadevall 2017). With the advancement of new knowledge and technologies, melanin pigments can now be turned into valuable materials in various fields of green technology, materials science, biomedicine, cosmetics and environmental remediation (Figure 3).

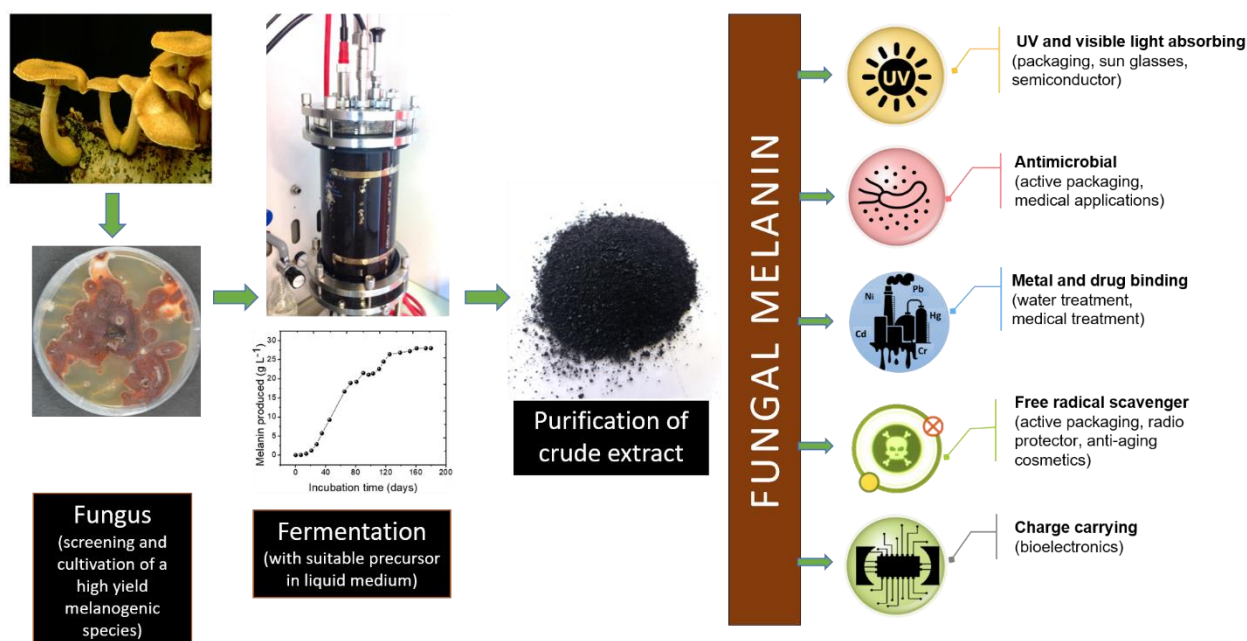


Figure 3. Biotechnological production of fungal melanin and its potential applications

From a physicochemical viewpoint, melanin is a natural "sunscreen" that absorbs the broadband of UV-visible light spectrum. In addition to blocking UV light, this pigment is a powerful antioxidant. Melanin also exhibits a hydration-dependent semiconductor-like behavior. As such, it is evaluated as a component for organic electronic devices (Bothma et al. 2008; Kim et al. 2013). Other advantages of microbial melanin are its bioavailability, biocompatibility and biodegradability, making it a promising candidate for biomedical applications; for example, implantable devices (Vahidzadeh et al. 2018). In another type of application, melanin has been employed for the environmentally benign synthesis of silver nanostructures. These melanin-mediated silver nanostructures show broad-spectrum antimicrobial activity against food pathogens and have potential uses in the food and health industries (Kiran et al. 2014; Patil et al. 2018). Dermal and cosmetic applications of melanin include its use for sunscreen and hair dyeing (Koike and Ebato, 2013). Melanin can act as metal chelators, which can be employed in environmental applications. By incorporating fungal melanin with other polymers such as polycaprolactone and polyurethane, the melanin-based composites can remove up to 94% Pb(II) in water systems (Tran-Ly et al. 2020). Although there are a lot of studies reporting the potential applications of melanin, they are mostly in the developmental stage and have not yet been

commercialized. In the era of transition towards sustainable materials, microbial melanin research has not yet reached its full potential.

1.3.7. Conclusions and outlook

Melanins are a unique class of natural pigments that can be considered functional materials for multiple potential applications in industry. The future of melanin-based materials and technology development depends on the ability to produce melanin at a large scale with a chemically defined structure and low cost. As discussed in this review, conventional approaches are the isolation of melanins from natural sources like sepia ink and chemical synthesis. They are, however, unsustainable and difficult to scale up. A feasible alternative approach is using melanogenic microorganisms and melanin precursors. Although no universal protocol is available, good tips for producing high-yield microbial melanins are: i) choosing the microorganisms that can produce melanin extracellularly from the exogenous substrate, and ii) improving the metabolic process by adding tyrosine and copper to the culture media. However, it is worth pointing out that melanins comprise a chemically-diverse group of polymers. So far, most of the published works on microbial melanin production focused on eumelanin. However, the chemical diversity of melanin, which can be controlled by the supplied melanin precursors, has not yet been fully explored. Furthermore, the accumulated knowledge on the biochemistry and genetic engineering of melanin in various organisms can contribute to the direct manipulation and enhancement of melanin production. With this perspective, melanin can be used beyond basic research and encourage more researchers from industry to deploy bio-inspired melanin-based materials for biomedical, environmental and technological applications.

Bibliography

Almeida-Paes R, Nosanchuk JD, Zancope-Oliveira RM (2012) Fungal melanins: biosynthesis and biological functions. In: *Melanin: biosynthesis, functions and health effects*. Nova Science Publishers, Inc, pp 77–107

Bernsmann F, Frisch B, Ringwald C, Ball V (2010) Protein adsorption on dopamine-melanin

- films: role of electrostatic interactions inferred from ζ -potential measurements versus chemisorption. *J Colloid Interface Sci* 344:54–60. <https://doi.org/10.1016/j.jcis.2009.12.052>
- Borovanský J, Riley PA (2011) History of melanosome research. In: *Melanins and melanosomes: biosynthesis, biogenesis, physiological, and pathological functions*. Wiley-VCH, pp 1–19
- Bothma JP, De Boor J, Divakar U, et al (2008) Device-quality electrically conducting melanin thin films. *Adv Mater* 20:3539–3542. <https://doi.org/10.1002/adma.200703141>
- Brenner M, Hearing VJ (2008) The protective role of melanin against UV damage in human skin. *Photochem Photobiol* 84:539–549. <https://doi.org/10.1111/j.1751-1097.2007.00226.x>
- Bridelli MG, Crippa PR (2010) Infrared and water sorption studies of the hydration structure and mechanism in natural and synthetic melanin. *J Phys Chem B* 114:9381–9390. <https://doi.org/10.1021/jp101833k>
- Cordero RJB, Casadevall A (2017) Functions of fungal melanin beyond virulence. *Fungal Biol Rev* 31:99–112. <https://doi.org/10.1016/j.fbr.2016.12.003>
- Coyne VE, Al-Harhi L (1992) Induction of melanin biosynthesis in *Vibrio cholerae*. *Appl Environ Microbiol* 58:2861–2865. <https://doi.org/10.1128/aem.58.9.2861-2865.1992>
- d’Ischia M, Napolitano A, Ball V, et al (2014) Polydopamine and eumelanin: from structure-property relationships to a unified tailoring strategy. *Acc Chem Res* 47:3541–3550. <https://doi.org/10.1021/ar500273y>
- d’Ischia M, Pezzella A, Napolitano A, et al (2015) Melanins and melanogenesis: from pigment cells to human health and technological applications. *Pigment Cell Melanoma Res* 28:520–544. <https://doi.org/10.1111/pcmr.12393>
- d’Ischia M, Wakamatsu K, Napolitano A, et al (2013) Melanins and melanogenesis: methods, standards, protocols. *Pigment Cell Melanoma Res* 26:616–633. <https://doi.org/10.1111/pcmr.12121>
- Eisenman HC, Casadevall A (2012) Synthesis and assembly of fungal melanin. *Appl Microbiol Biotechnol* 93:931–940. <https://doi.org/10.1007/s00253-011-3777-2>
- El-Naggar NEA, El-Ewasy SM (2017) Bioproduction, characterization, anticancer and

- antioxidant activities of extracellular melanin pigment produced by newly isolated microbial cell factories *Streptomyces glaucescens* NEAE-H. *Sci Rep* 7:42129. <https://doi.org/10.1038/srep42129>
- Fogarty R V., Tobin JM (1996) Fungal melanins and their interactions with metals. *Enzyme Microb Technol* 19:311–317. [https://doi.org/10.1016/0141-0229\(96\)00002-6](https://doi.org/10.1016/0141-0229(96)00002-6)
- Ganesh Kumar C, Sahu N, Narender Reddy G, et al (2013) Production of melanin pigment from *Pseudomonas stutzeri* isolated from red seaweed *Hypnea musciformis*. *Lett Appl Microbiol* 57:295–302. <https://doi.org/10.1111/lam.12111>
- Glass K, Ito S, Wilby PR, et al (2012) Direct chemical evidence for eumelanin pigment from the Jurassic period. *Proc Natl Acad Sci U S A* 109:10218–10223. <https://doi.org/10.1073/pnas.1118448109>
- Gowri PM, Srivastava S (1996) Encapsulation as a response of *Azospirillum brasilense* sp7 to zinc stress. *World J Microbiol Biotechnol* 12:319–322. <https://doi.org/10.1007/BF00340207>
- Griffith GW, Easton GL, Detheridge A, et al (2007) Copper deficiency in potato dextrose agar causes reduced pigmentation in cultures of various fungi. *FEMS Microbiol Lett* 276:165–171. <https://doi.org/10.1111/j.1574-6968.2007.00923.x>
- Guo J, Rao Z, Yang T, et al (2014) High-level production of melanin by a novel isolate of *Streptomyces kathirae*. *FEMS Microbiol Lett* 357:85–91. <https://doi.org/10.1111/1574-6968.12497>
- Hamano PS, Kilikian B V. (2006) Production of red pigments by *Monascus ruber* in culture media containing corn steep liquor. *Brazilian J Chem Eng* 23:443–449. <https://doi.org/10.1590/S0104-66322006000400002>
- Held T, Kutzner HJ (1990) Transcription of the tyrosinase gene in *Streptomyces michiganensis* DSM 40015 is induced by copper and repressed by ammonium. *J Gen Microbiol* 136:12. <https://doi.org/10.1099/00221287-136-12-2413>
- Jacobson ES (2000) Pathogenic roles for fungal melanins. *Clin Microbiol Rev* 13:708–717. <https://doi.org/10.1128/CMR.13.4.708-717.2000>
- Jalmi P, Bodke P, Wahidullah S, Raghukumar S (2012) The fungus *Gliocephalotrichum simplex* as a source of abundant, extracellular melanin for biotechnological applications.

- World J Microbiol Biotechnol 28:505–512. <https://doi.org/10.1007/s11274-011-0841-0>
- Ju KY, Lee Y, Lee S, et al (2011) Bioinspired polymerization of dopamine to generate melanin-like nanoparticles having an excellent free-radical-scavenging property. *Biomacromolecules* 12:625–632. <https://doi.org/10.1021/bm101281b>
- Karlsson O, Lindquist NG (2016) Melanin and neuromelanin binding of drugs and chemicals: toxicological implications. *Arch Toxicol* 90:1883–1891. <https://doi.org/10.1007/s00204-016-1757-0>
- Kim YJ, Wu W, Chun SE, et al (2013) Biologically derived melanin electrodes in aqueous sodium-ion energy storage devices. *Proc Natl Acad Sci U S A* 110:20912–20917. <https://doi.org/10.1073/pnas.1314345110>
- Kiran GS, Dhasayan A, Lipton AN, et al (2014) Melanin-templated rapid synthesis of silver nanostructures. *J Nanobiotechnology* 12:1. <https://doi.org/10.1186/1477-3155-12-18>
- Kiran GS, Jackson SA, Priyadharsini S, et al (2017) Synthesis of Nm-PHB (nanomelanin-polyhydroxy butyrate) nanocomposite film and its protective effect against biofilm-forming multi drug resistant *Staphylococcus aureus*. *Sci Rep* 7:9167. <https://doi.org/10.1038/s41598-017-08816-y>
- Le Na NT, Duc Loc S, Minh Tri N Le, et al (2019) Nanomelanin potentially protects the spleen from radiotherapy-associated damage and enhances immunoactivity in tumor-bearing mice. *Materials (Basel)* 12:1725. <https://doi.org/10.3390/ma12101725>
- Lee H, Dellatore SM, Miller WM, Messersmith PB (2007) Mussel-inspired surface chemistry for multifunctional coatings. *Science* 318:426–430. <https://doi.org/10.1126/science.1147241>
- Ligonzo T, Ambrico M, Augelli V, et al (2009) Electrical and optical properties of natural and synthetic melanin biopolymer. *J Non Cryst Solids* 355:1221–1226. <https://doi.org/10.1016/j.jnoncrysol.2009.05.014>
- Liu Y, Ai K, Liu J, et al (2013) Dopamine-melanin colloidal nanospheres: An efficient near-infrared photothermal therapeutic agent for in vivo cancer therapy. *Adv Mater* 25:1353–1359. <https://doi.org/10.1002/adma.201204683>
- Liu Y, Ai K, Lu L (2014) Polydopamine and its derivative materials: synthesis and promising applications in energy, environmental, and biomedical fields. *Chem Rev* 114:5057–5115.

<https://doi.org/10.1021/cr400407a>

- Liu Y, Kempf VR, Nofsinger JB, et al (2003) Comparison of the structural and physical properties of human hair eumelanin following enzymatic or acid/base extraction. *Orig Res Artic* 16:355–365. <https://doi.org/10.1034/j.1600-0749.2003.00059.x>
- Liu Y, Simon JD (2003) Isolation and biophysical studies of natural eumelanins: applications of imaging technologies and ultrafast spectroscopy. *Pigment Cell Res* 16:606–618. <https://doi.org/10.1046/j.1600-0749.2003.00098.x>
- Madhusudhan DN, Mazhari BBZ, Dastager SG, Agsar D (2014) Production and cytotoxicity of extracellular insoluble and droplets of soluble melanin by *Streptomyces lusitanus* DMZ-3. *Biomed Res Int* 2014:306895. <https://doi.org/10.1155/2014/306895>
- Manivasagan P, Venkatesan J, Senthilkumar K, et al (2013) Isolation and characterization of biologically active melanin from *Actinoalloteichus* sp. MA-32. *Int J Biol Macromol* 58:263–274. <https://doi.org/10.1016/j.ijbiomac.2013.04.041>
- Martínez LM, Martínez A, Gosset G (2019) Production of melanins with recombinant microorganisms. *Front Bioeng Biotechnol* 7:285. <https://doi.org/10.3389/fbioe.2019.00285>
- Nosanchuk JD, Casadevall A (2003) The contribution of melanin to microbial pathogenesis. *Cell Microbiol* 5:203–223. <https://doi.org/10.1046/j.1462-5814.2003.00268.x>
- Nosanchuk JD, Stark RE, Casadevall A (2015) Fungal melanin: what do we know about structure? *Front Microbiol* 6:1463. <https://doi.org/10.3389/fmicb.2015.01463>
- Novellino L, Napolitano A, Prota G (2000) Isolation and characterization of mammalian eumelanins from hair and irides. *Biochim Biophys Acta - Gen Subj* 1475:295–306. [https://doi.org/10.1016/S0304-4165\(00\)00080-5](https://doi.org/10.1016/S0304-4165(00)00080-5)
- Patil S, Sistla S, Bapat V, Jadhav J (2018) Melanin-mediated synthesis of silver nanoparticles and their affinity towards tyrosinase. *Appl Biochem Microbiol* 54:163–172. <https://doi.org/10.1134/S0003683818020096>
- Pavan ME, López NI, Pettinari MJ (2020) Melanin biosynthesis in bacteria, regulation and production perspectives. *Appl Microbiol Biotechnol* 104:1821–1822. <https://doi.org/10.1007/s00253-019-10245-y>
- Pezzella A, d'Ischia M, Napolitano A, et al (1997) An integrated approach to the structure of

- sepia melanin. Evidence for a high proportion of degraded 5,6-Dihydroxyindole-2-carboxylic acid units in the pigment backbone. *Tetrahedron* 53:8281–8286. [https://doi.org/10.1016/S0040-4020\(97\)00494-8](https://doi.org/10.1016/S0040-4020(97)00494-8)
- Plonka PM, Grabacka M (2006) Melanin synthesis in microorganisms - biotechnological and medical aspects. *Acta Biochim Pol* 53:429–443. https://doi.org/10.18388/abp.2006_3314
- Pralea I-E, Moldovan R-C, Petrache A-M, et al (2019) From extraction to advanced analytical methods: the challenges of melanin analysis. *Int J Mol Sci* 20:3943. <https://doi.org/10.3390/ijms20163943>
- Prota G (1995) The chemistry of melanins and melanogenesis. In: Herz W., Kirby G.W., Moore R.E., Steglich W. TC (ed) *Fortschritte der Chemie organischer Naturstoffe. Progress in the chemistry of organic natural products / Progrès dans la chimie des substances organiques naturelles*. Springer, Vienna, pp 93–148
- Raman NM, Shah PH, Mohan M, Ramasamy S (2015) Improved production of melanin from *Aspergillus fumigatus* AFGRD105 by optimization of media factors. *AMB Express* 5:72. <https://doi.org/10.1186/s13568-015-0161-0>
- Reiss R, Ihssen J, Richter M, et al (2013) Laccase versus laccase-like multi-copper oxidase: a comparative study of similar enzymes with diverse substrate spectra. *PLoS One* 8:6. <https://doi.org/10.1371/journal.pone.0065633>
- Ribera J, Panzarasa G, Stobbe A, et al (2019) Scalable biosynthesis of melanin by the basidiomycete *Armillaria cepistipes*. *J Agric Food Chem* 67:132–139. <https://doi.org/10.1021/acs.jafc.8b05071>
- Saini AS, Melo JS (2015) One-pot green synthesis of eumelanin: process optimization and its characterization. *RSC Adv* 5:47671–47680. <https://doi.org/10.1039/c5ra01962a>
- Schmalzer-Ripcke J, Sugareva V, Gebhardt P, et al (2009) Production of pyomelanin, a second type of melanin, via the tyrosine degradation pathway in *Aspergillus fumigatus*. *Appl Environ Microbiol* 75:493–503. <https://doi.org/10.1128/AEM.02077-08>
- Sendovski M, Kanteev M, Ben-Yosef VS, et al (2011) First structures of an active bacterial tyrosinase reveal copper plasticity. *J Mol Biol* 405:227–237. <https://doi.org/10.1016/j.jmb.2010.10.048>
- Silveira ST, Daroit DJ, Brandelli A (2008) Pigment production by *Monascus purpureus* in

- grape waste using factorial design. *LWT - Food Sci Technol* 41:170–174.
<https://doi.org/10.1016/j.lwt.2007.01.013>
- Solano F (2014) Melanins: skin pigments and much more—types, structural models, biological functions, and formation routes. *New J Sci* 2014:498276.
<https://doi.org/10.1155/2014/498276>
- Solano F (2017) Melanin and melanin-related polymers as materials with biomedical and biotechnological applications—cuttlefish ink and mussel foot proteins as inspired biomolecules. *Int J Mol Sci* 18:1561. <https://doi.org/10.3390/ijms18071561>
- Sun S, Zhang X, Chen W, et al (2016) Production of natural edible melanin by *Auricularia auricula* and its physicochemical properties. *Food Chem* 196:486–492.
<https://doi.org/10.1016/j.foodchem.2015.09.069>
- Surwase SN, Jadhav SB, Phugare SS, Jadhav JP (2013) Optimization of melanin production by *Brevundimonas* sp. SGJ using response surface methodology. *3 Biotech* 3:187–194.
<https://doi.org/10.1007/s13205-012-0082-4>
- Tarangini K, Mishra S (2014) Production of melanin by soil microbial isolate on fruit waste extract: two step optimization of key parameters. *Biotechnol Reports* 4:139–146.
<https://doi.org/10.1016/j.btre.2014.10.001>
- Toledo AV, Franco MEE, Yanil Lopez SM, et al (2017) Melanins in fungi: types, localization and putative biological roles. *Physiol Mol Plant Pathol* 99:2–6.
<https://doi.org/10.1016/j.pmpp.2017.04.004>
- Tran-Ly AN, Ribera J, Schwarze FWMR, et al (2020) Fungal melanin-based electrospun membranes for heavy metal detoxification of water. *Sustain Mater Technol* 23:e00146.
<https://doi.org/10.1016/j.susmat.2019.e00146>
- Vahidzadeh E, Kalra AP, Shankar K (2018) Melanin-based electronics: from proton conductors to photovoltaics and beyond. *Biosens Bioelectron* 122:127–139.
<https://doi.org/10.1016/j.bios.2018.09.026>
- Wang L, Li Y, Li Y (2019) Metal ions driven production, characterization and bioactivity of extracellular melanin from *Streptomyces* sp. ZL-24. *Int J Biol Macromol* 123:521–530.
<https://doi.org/10.1016/j.ijbiomac.2018.11.061>
- Xiao M, Chen W, Li W, et al (2018) Elucidation of the hierarchical structure of natural

eumelanins. *J R Soc Interface* 15:20180045. <https://doi.org/10.1098/rsif.2018.0045>

Yang J, Li W, Bun Ng T, et al (2017) Laccases: production, expression regulation, and applications in pharmaceutical biodegradation. *Front Microbiol* 8:832. <https://doi.org/10.3389/fmicb.2017.00832>

Zhang F, Kearns SL, Orr PJ, et al (2010) Fossilized melanosomes and the colour of Cretaceous dinosaurs and birds. *Nature* 463:1075–1078. <https://doi.org/10.1038/nature08740>

Zou Y, Tian M (2017) Fermentative production of melanin by *Auricularia auricula*. *J Food Process Preserv* 41:e12909. <https://doi.org/10.1111/jfpp.12909>

1.4. Materials Processing Technologies

1.4.1. Electrospinning

Electrospinning is a spinning technology using electrostatic forces to fabricate micro- and nanoscale fibers from polymer solutions. In a basic lab-scale set up, the electrospinning system typically involves a high-voltage power supply, a polymer reservoir (typically a syringe) connected with a spinneret (a blunt tip needle), a pump and a conductive collector. During the spinning process, the polymer solution is pumped from the spinneret at a constant flow rate and creates pendant droplets. Upon electrification, the electric field between the needle tip and the collector initiates the spinning process by accumulating charge at the liquid surface. When the electrostatic repulsion is higher than the surface tension, the droplet is deformed into a Taylor cone, from which a charged jet is ejected and deposited onto the collector [1]. In general, the applied voltage, liquid flow rate, needle diameter and the polymer concentration (solution viscosity) determine the properties of the electrospun product. In an optimized set up, uniform solid fibers will be produced as the solvent evaporates quickly during the thinning of the jet and the growth of the whipping instability that happens during the flight time from the needle to the collector [2].

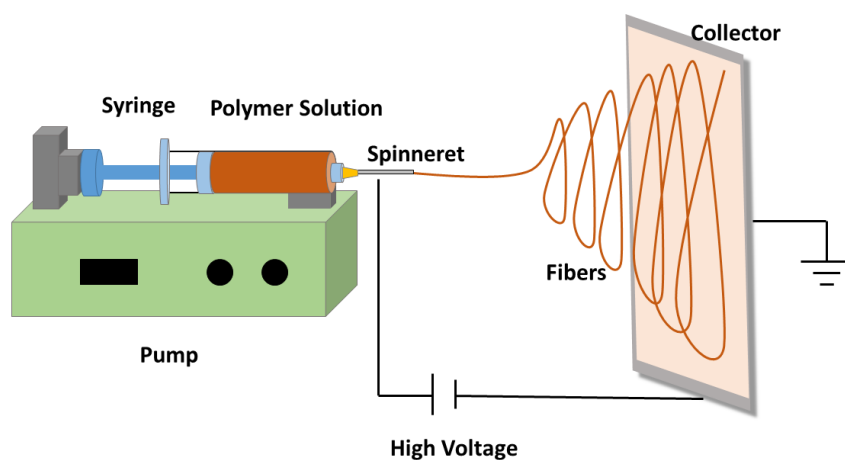


Figure 1.1. Schematic of a basic electrospinning set up.

1.4.2. Freeze-drying

Freeze-drying or lyophilization is a sample preparation technique in which the complete frozen water or solvent from a material turns directly into vapor without going through a liquid phase (i.e. sublimation), and thus is removed from the sample [3]. During the procedure, the sample must be kept at a low temperature to avoid any effect on the final dried product, before being placed under a vacuum where the sublimation occurs. The whole process can be simplified into three main steps:

1. Freeze: The sample is completely frozen either in a freezer or liquid nitrogen
2. Vacuum: The sample is placed in a vacuum chamber where the pressure is kept below the triple point of the targeted solvent (Figure 1.2)
3. Dry: Temperature is increased to cause the ice to evaporate

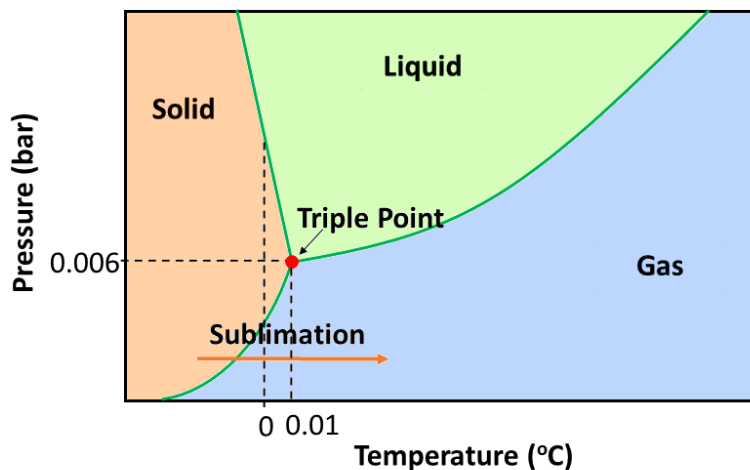


Figure 1.2. Phase diagram showing the triple point of water.

Freeze-drying has been widely used to preserve many sensitive products from food, pharmaceuticals to biological specimens for a long time. In materials processing, freeze-drying has become a common approach for fabrication of aerogels. It allows removing the liquid component from a colloidal system while preserving its framework structure to form a shaped material.

1.4.3. Vacuum pressure impregnation

Vacuum pressure impregnation is a common practice for wood preservation. The process is to allow preservative agents to penetrate deeply into the wood in order to stabilize its dimensions,

increase its resistance to water and/or other deteriorating agents including wood-decay fungi and insects. Wood structure comprises cell cavities and cell walls. To maximize the penetration of preservative, vacuum is used to remove air from the cavities. The wood is then infused in the preservative solution under high pressure. Although the duration and process parameters vary depending on the permeability of the wood type, the basic procedures are similar, which consist of five steps:

1. Initial vacuum: Once the wood is loaded in the chamber, air is removed from the wood cell under vacuum. This step helps expand the wood structure to allow the later impregnation treatment more effective.
2. Filling: The chamber is flooded with the preservative solution under vacuum.
3. Application of pressure: The pressure is increased to press the preservative solution into the airless wood cells and held until the desired penetration is achieved.
4. Discharging the solution: The remaining solution not absorbed by the wood is drained out to the storage tank for reuse. At this step, a final vacuum is usually applied to extract excess preservative solution.
5. End of procedure: The vessel is vented to ambient pressure and the treated wood is removed and left to dry in a designated area.

1.5. Materials Characterization Techniques

1.5.1. Fourier transform infrared (FTIR) spectroscopy

The vibrations of chemical bonds such as the stretching, bending, and oscillatory motions of atoms have energy similar to electromagnetic radiation in the infrared (IR) range (400–4000 cm^{-1}). Therefore, infrared spectroscopy is an analytical tool to prove the presence of specific functional groups. For example, the stretching band of an O-H group normally appears as a broad band with its frequency ranging from 3300–3600 cm^{-1} . The stretching band(s) for C-H is at around 3000 cm^{-1} , while those for double bonds such as C=C, C=N, and C=O are at 1600-

1800 cm^{-1} . The bands in the 400–1500 cm^{-1} region are called the fingerprint, and are characteristic for a given compound, i.e. the identity of a compound of interest is defined if it has the same fingerprint as that of the reference.

1.5.2. Ultraviolet-Visible (UV-Vis) spectroscopy

UV-Vis spectroscopy is based on the absorption of the ultraviolet (UV) or the visible (Vis) light of a molecule. This technique is useful for the identification and quantification of compounds that contain chromophoric groups. According to the Beer-Lambert law, the light absorption of a substance is proportional to its molecular concentration and the length of the light path:

$$A = \log \frac{I_0}{I} = \epsilon l C \quad (1)$$

where A is the absorbance, I_0 and I are the intensity of the light from the source and the light passed through the sample, ϵ is the molar absorptivity (or molar extinction coefficient) ($\text{M}^{-1} \text{cm}^{-1}$), l is the path length (cm) equal to the width of the cuvette, and C is the concentration (M).

The molar absorptivity measures the probability of the electronic transition of a chromophoric group and is a constant in a given solution (and can change in different solvents). At wavelengths where there is no light absorption, the absorbance is of 0.

1.5.3. Inductively coupled plasma mass spectrometry (ICP-MS)

ICP-MS is a technique primarily used for the detection and precise quantification of trace metal elements (ppb to ppm concentrations) in liquid samples. This technique uses an inductively coupled plasma that atomizes the sample into constituent elements and ionizes those elements into ions. The ions are then extracted into a mass spectrometer, equipped with a detector that creates signals proportional to the concentration of each ion.

For solid samples, it is important to completely dissolve the solid in strong acidic solutions, e.g. HNO_3 . The concentration of an ion is determined through calibration with reference solutions.

1.5.4. X-ray photoelectron spectroscopy (XPS)

XPS is a technique allowing for quantitative study of the atomic composition from the outer 5 - 10 nanometers of a solid surface. The fundamental of XPS is based on the photoelectric effect, in which a photoelectron is emitted when an X-ray (e.g. Al(K α) at 1486.7eV) interacts with an atom.

The kinetic energy (E_k) of the photoelectron is given by the Einstein's equation:

$$E_k = h\nu - E_b - \varphi_{sp} \quad (2)$$

where $h\nu$ is the photon energy, E_b is the atomic core level binding energy of the photoelectron, and φ_{sp} is the work function of the spectrometer.

An XPS spectrum displays bands corresponding to various core-level binding energies, with the Carbon 1s at 284.5 eV being used as the calibration reference. The obtained binding energies allow the identification of elements within the sample of interest. It is worth noting that binding energies are sensitive to the chemical environment of the atom; for example pyridinic, pyrrolic, and graphitic N atoms possess slightly different binding energies.

1.5.5. Scanning electron microscopy (SEM)

A scanning electron microscope creates images by scanning the sample with a focused electron beam. The electrons are accelerated with a voltage ranging from 1 to 30 keV. The focused electron beam hits the sample and the secondary electrons are detected by the detector, which digitizes the signal and converts it into a gray level. SEM is routinely used to study the nano- and micrometer-scale morphology of objects. In addition, chemical compositions can also be achieved using Energy-Dispersive X-Ray Spectroscopy (EDS).

Non-conductive samples often collect charge and cause artifacts on SEM images. Non-conducting materials such as organic polymers are usually coated with an electrically conducting layer, such as gold/palladium, via sputter coating or by high-vacuum evaporation.

1.5.6. Mechanical testing

Mechanical testing is used to investigate different mechanical aspects of a material. Insights into properties of materials are gained via tests such as tensile, compression, bending shear, impact, tearing, and fatigue testing. Tensile testing is the most commonly performed for film materials, while compression is normally done for foams. Tensile and compression stress-strain characteristics are obtained by monitoring the force required to pull or compress a material and the displacement as a result of the applied force. Brittle materials exhibit fracture at a low strain (ε) while rubber-like behavior is characteristic by a low stress at a high strain percentage. The stiffness of a material is defined by its elastic modulus (also called Young modulus or E modulus), which is the slope in the linear (elastic) region of a stress-strain diagram (equations 3, 4).

$$E = \frac{\sigma_2 - \sigma_1}{\varepsilon_2 - \varepsilon_1} \quad (3)$$

$$E = \frac{d\sigma}{d\varepsilon} \quad (4)$$

1.5.7. Adsorption

Adsorption is the phenomenon in which substances from a gas/liquid phase are transferred onto the surface of a solid. Adsorption isotherms and kinetics are often studied to gain insights into the adsorption process.

Adsorption isotherms

Adsorption isotherms are established via a series of adsorption measurements and the data are fit based on mathematical models. Three isotherm models, Langmuir [4], Freundlich [5] and Redlich-Peterson [6], which establish the relationship between the adsorption capacity (q_e) and equilibrium concentration (C_e) at a constant temperature are often employed to study how the adsorbate interacts with the adsorbent.

The Langmuir model assumes that the adsorbent surface is homogeneous and the adsorption is a monolayer process. The expression of the Langmuir isotherm is represented by the following equation:

$$\frac{1}{q_e} = \frac{1}{Q_m} + \frac{1}{K_L Q_m} \times \frac{1}{C_e} \quad (5)$$

where Q_m (mg g⁻¹) is the maximum adsorption capacity, C_e is the concentration at equilibrium and K_L (L g⁻¹) is the Langmuir constant, which represents the energy of adsorption. The plot of $1/q_e$ as a function of $1/C_e$ allows the determination of Q_m and K_L .

Furthermore, the separation factor R_L can be obtained from the following equation:

$$R_L = \frac{1}{1 + K_L C_0} \quad (6)$$

The constant R_L indicates the favorability of the adsorption process. If $R_L=0$, the adsorption is irreversible; if $0 < R_L < 1$ the adsorption is favorable. The adsorption profile is linear when $R_L = 1$ ($K_L = 0$). When $R_L > 1$ ($K_L < 0$), the adsorption is unfavorable.

The Freundlich isotherm describes non-ideal, multilayer adsorption at a heterogeneous adsorbent surface. The adsorptive sites are presumed to exhibit different binding energies. The model is represented by the following equation:

$$\log(q_e) = \log K_F + \left(\frac{1}{n}\right) \log C_e \quad (7)$$

where K_F and $1/n$ are the Freundlich constants that indicate the adsorption capacity and the adsorption intensity, respectively. When $1/n < 1$, the adsorption is strong, e.g. chemisorption, whereas $1/n > 1$ is indicative of cooperative adsorption. The values of K_F and n were obtained from the plot of $\log(q_e)$ versus $\log C_e$.

The Redlich-Peterson (R-P) model is a combination of both Langmuir and Freundlich approaches. The model can be applied in either homogeneous or heterogeneous systems, providing a more accurate representation of adsorption equilibrium over a wide range of concentration. The equation for R-P model is described as follows:

$$q_e = \frac{K_R C_e}{1 + a_R C_e^\beta} \quad (8)$$

where K_R ($L g^{-1}$) and a_R ($L mg^{-1}$) are the R-P constants and the exponent β varies between 0 and 1. A nonlinear plot of q_e versus C_e gives out the values of K_R , a_R and β .

Adsorption kinetic models

The adsorption kinetics control the adsorption rate. Three kinetic models, namely pseudo-first-order, pseudo-second-order and Weber's intraparticle diffusion are often applied to understand the characteristics of the adsorption process such as the adsorption pathways and probable mechanism involved.

According to Lagergren [7], the pseudo-first-order model is expressed as:

$$\frac{dq_t}{dt} = k_1(q_e - q_t) \quad (9)$$

Equation (9) can, however, be converted to the linear form:

$$\log(q_e - q_t) = \log(q_e) - \frac{k_1}{2.303} t \quad (10)$$

where q_e and q_t ($mg g^{-1}$) are the adsorption capacities at equilibrium and at time t , respectively; k_1 is the rate constant (min^{-1}) in the pseudo-first-order kinetic model. The value of k_1 can be found from the linear plot of $\log(q_e - q_t)$ versus time.

The differential equation for the pseudo-second-order kinetic model is given by Ho and McKay [8] as follows:

$$\frac{dq_t}{dt} = k_2(q_e - q_t)^2 \quad (11)$$

After mathematical development, the linearized form of the above equation is expressed as:

$$\frac{t}{q_t} = \frac{1}{k_2 q_e^2} + \frac{t}{q_e} \quad (12)$$

where q_e and q_t ($mg g^{-1}$) are the adsorption capacity at equilibrium and at time t while k_2 ($g mg^{-1} min^{-1}$) is the pseudo-second-order rate constant. By plotting t/q_t as a function of time t , the values of q_e and k_2 can be calculated.

To study the diffusion mechanism in the adsorption process, the intraparticle mass transfer diffusion model proposed by Weber and Morris [9] can be employed:

$$q_t = k_i t^{0.5} + C \quad (13)$$

where k_i ($\text{mg g}^{-1} \text{min}^{-1/2}$) is the intraparticle diffusion rate while C gives information about the thickness of the boundary layer.

2. Main investigations

The research work is mainly based on three first-author publications, which are reprinted in the following subchapters.

Publication 1

Anh N. Tran-Ly, Javier Ribera, Francis W.M.R. Schwarze, Marzia Brunelli, Giuseppino Fortunato, *Fungal Melanin-based Electrospun Membranes for Heavy Metal Detoxification of Water*, *Sustainable Materials and Technologies*, **2020**, *23*, e00146.

<https://doi.org/10.1016/j.susmat.2019.e00146>

Author contributions

Anh N. Tran-Ly: conceptualization, methodology, experiment conduction, data collection and treatment, discussion, visualization, writing - original draft, writing - review & editing; **Javier Ribera**: methodology, review & editing; **Francis W.M.R. Schwarze**: review & editing; **Marzia Brunelli**: mechanical testing; **Giuseppino Fortunato**: conceptualization, methodology, discussion, review & editing.

Publication 2

Anh N. Tran-Ly, Kevin J. De France, Patrick Rupper, Francis W.M.R. Schwarze, Carolina Reyes, Gustav Nyström, Gilberto Siqueira, Javier Ribera, *Melanized-Cationic Cellulose Nanofiber Foams for Bioinspired Removal of Cationic Dyes*, *Biomacromolecules*, **2021**, *22*, 4681–4690.

<https://doi.org/10.1021/acs.biomac.1c00942>

Author contributions

Anh N. Tran-Ly: conceptualization, methodology, experiment conduction, data collection and treatment, discussion, visualization, writing - original draft, writing - review & editing; **Kevin J. De France**: mechanical testing, methodology, writing, review & editing; **Patrick Rupper**:

FTIR and XPS measurements; **Francis W.M.R. Schwarze**: review & editing; **Carolina Reyes**: discussion; **Gustav Nyström**: discussion; **Gilberto Siqueira**: resources, **Javier Ribera**: review & editing, project administration.

Publication 3

Anh N. Tran-Ly, Markus Heeb, Tine Kalac, Francis W.M.R. Schwarze, *Antimicrobial Effect of Fungal Melanin in Combination with Plant Oils for the Treatment of Wood*, *Frontiers in Materials*, **2022**, 9:915607.

<https://doi.org/10.3389/fmats.2022.915607>

Author contributions

Anh N. Tran-Ly: conceptualization, methodology, experiment conduction, data collection and treatment, discussion, visualization, writing - original draft, writing - review & editing; **Markus Heeb**: conceptualization, methodology, experiment conduction, discussion; **Tine Kalac**: fungal culture preparation; **Francis W.M.R. Schwarze**: conceptualization, methodology, discussion, writing- review & editing, project administration

2.1. Fungal Melanin-based Electrospun Membranes for Heavy Metal Detoxification of Water

Anh N. Tran-Ly^{a,b}, Javier Ribera^b, Francis W.M.R. Schwarze^b, Marzia Brunelli^c, Giuseppino Fortunato^c

^aDepartment of Civil, Environmental and Geomatic Engineering, ETH Zurich, Stefano-Francini-Platz 5, Postfach 193, CH-8093 Zurich, Switzerland

^bLaboratory for Cellulose and Wood Materials, Empa, Lerchenfeldstrasse 5, CH-9014 St. Gallen, Switzerland

^cLaboratory for Biomimetic Membranes and Textiles, Empa, Lerchenfeldstrasse 5, CH-9014 St. Gallen, Switzerland

Abstract

In recent years, heavy metal pollution in water resources has become a severe environmental and public health problem worldwide. Thereby, enhanced treatments are urgently needed with respect to eco-friendliness, filtration efficiencies and low operational costs. This study demonstrates how fungal melanin extracted from *Armillaria cepistipes* (Empa 655) can be applied as a promising biosorbent for removal of toxic heavy metals from water. For this aim, an electrospinning technique was developed to incorporate fungal melanin particles, a novel source of adsorptive species, into polymeric nanofibrous membranes to obtain stable and highly porous filtration systems. Starting spinning dispersions were investigated with respect to their rheological behaviour and electrical conductivity and related to morphological and surface properties of the resulting composite fibres and membranes. Metal adsorption assays were then performed on both raw melanin and melanised membranes. At the phytotoxic concentrations of Pb^{2+} , Cd^{2+} , Ni^{2+} and Cr^{3+} , fungal melanin was able to remove more than 90% of heavy metals in single-component solutions. In multi-component solutions incorporating Ca^{2+} and Zn^{2+} , fungal melanin showed a different affinity to different metals in the following order: $\text{Pb}^{2+} > \text{Cr}^{3+} >$

$\text{Ni}^{2+} > \text{Cd}^{2+} > \text{Zn}^{2+} > \text{Ca}^{2+}$ with an extreme preference for Pb^{2+} (80% removal) over the essential metals (0% and 12% removal for Ca^{2+} and Zn^{2+} , respectively). The metal adsorption profiles also showed that melanised membranes were able to maintain the adsorption capacity of the raw melanin. Thus, these novel membranes can be efficiently used as filtration membranes for removal of heavy metals from water.

2.1.1. Introduction

The access to clean and safe water is essential for a healthy living [1]; however, this fact cannot be taken for granted worldwide. Due to increased human activity from, for example, intensive agriculture and industrialisation, a wide range of physical, biological and chemical pollutants have entered water bodies and have affected human lives. Among the latter pollutant classes, heavy metals are of great concern owing to their toxicity, persistence in nature, bioaccumulation and bio-magnification in the food chain [2].

In recent decades, human exposure to toxic heavy metals has increased globally, but the prevalence of heavy metal pollution is most prominent in developing countries due to rapid urbanisation, industrialisation and non-restrictive legislation [3, 4, 5]. Contaminated water systems have become a major public health and environmental concern. Heavy metals can be transformed into ions in water systems and thus enter our bodies through contaminated drinking water and food. Due to the natural persistence of heavy metals, they tend to remain in body organs and soft tissues for extended periods. Once in the body, they compete and displace essential minerals such as zinc, copper, magnesium, and calcium, and interfere with organ system function [6, 7, 8]. Continuous exposure to heavy metals has been proven to cause several health risks for living organisms, including human beings.

Traditionally, a wide range of water treatment technologies such as chemical precipitation, ion exchange, adsorption, multistep coagulation-flocculation or electrodeposition have been used for heavy metal removal. The latter conventional methods are, however, time-consuming and

suffer from problems related to recyclability. Moreover, some of the methods have a tendency to release secondary pollutants to the environment [9]. Beside those problems, removal of heavy metal at very low concentration (<10 mg/L) has long been a challenge for most adsorbents owing to mass transfer limitations. In other words, due to low collision frequency between adsorbate and adsorbent in dilute solution, a decrease in adsorption capacity is usually observed with a decrease of initial ion concentration [10]. Recent environmental regulations have become increasingly restrictive, which is encouraging the continuous development of water-cleaning technologies. Therefore, sustainable, profitable, and safer methods are required. In recent years, membrane-based water purification using tailor-made electrospun nanofibres has received widespread attention owing to the advantage of relative production ease, low cost, high efficiency, high porosity, large contact area and versatility [11]. Concerning water treatment applications, polyurethane (PUR) and polycaprolactone (PCL) are among the most widely used polymers. Thermoplastic PUR possesses a wide range of desirable properties, e.g. high mechanical strength, thermal stability and good hydrolytic stability [12]. PCL is usually known for its applications in tissue engineering for its good biodegradability and biocompatibility [13, 14]. It has also become a good choice as a nanofibrous template for wastewater treatment owing to its sound electrospinnability and long degradation time.

Furthermore, a great motivation for using electrospun filtration membranes stems from the possibility of combining chelating agents to develop nanocomposite membranes with optimal scavenging efficiency for heavy metals [15]. Many sophisticated systems, materials and mechanisms have been inspired by nature from where the transfer to technical applications is considered highly desirable. For instance, it has been well documented that the proportion of dark, pigmented individuals within an organism group were found to be more resistant to atmospheric metal pollution in industrial areas for many species, including insects, fungi and avians [16, 17, 18]. To explain the latter phenomenon, melanin, the naturally existing pigment in many organisms, has been reported for its chelating power. Melanin is negatively charged,

giving it the ability to bind different metal ions by forming ionic and charge transfer complexes [19]. In addition, melanin is resistant to acid degradation and insoluble in most substances, including common organic solvents and water [20]. These properties, coupled with its intrinsic biocompatibility and sustainability, make melanin a good substrate to develop green technology for metal detoxification in environmental and medical applications. Currently, commercial melanins are either extracted from hair, or squid, or are chemically synthesised. However, the high production cost has raised challenges in applying those melanins in most industrial-based applications. Moreover, melanin extracted from squid carries the risk of heavy metal loading from the polluted environment.

In a recent study, fungal melanin was introduced as a natural and renewable resource to produce high yields of melanin in liquid media. The cultivation procedure was optimised, up-scaled and characterised in a previous study [21]. Using fungal melanin for biosorption is, therefore, cost effective and avoids toxic by-products generation. The objective of the current study was to functionalise electrospun PCL and PUR membranes with fungal melanin by electrostatic spinning to remove toxic heavy metals from aqueous solutions. This approach can combine both the advanced characteristics of a non-woven membrane with nanometer range fibrous diameters, micron-sized interconnected pore diameters and the metal biosorption capacity of fungal melanin. Furthermore, as one of the challenges of water treatment technologies is metal removal at dilute concentration, fungal melanin and melanised membranes were proposed to adsorb metal solutions at reference level of risk (from 25 to 600 $\mu\text{g/L}$ depending on the metal). At this dilute concentration, these heavy metals can still cause toxic effect to human body if being consumed daily in drinking water [22, 23]. The morphology and surface properties of the acquired melanised polymeric membranes were examined by scanning electron microscopy (SEM) and X-ray photoelectron spectroscopy (XPS) to examine embedding of melanin particles into and onto the fibres. Metal adsorption investigations were performed by placing melanin powders and melanised membranes into selected heavy metal solutions, while elemental

contents were analysed before and after adsorption to determine the removal efficiency of the different forms of melanin.

2.1.2. Materials and methods

Melanin production and extraction

Growth medium was prepared according to Jalmi et al [24]. and contained 1% (w/v) peptone, 1% (w/v) D-Glucose, 0.1% (w/v) yeast extract with 0.05% (w/v) KH_2PO_4 , 0.02% (w/v) $\text{MgSO}_4 \cdot 7\text{H}_2\text{O}$, 0.01% $\text{FeSO}_4 \cdot 7\text{H}_2\text{O}$, 0.0005% (w/v) CuSO_4 and 2.5% (w/v) tyrosine. The growth medium was sterilised by autoclaving for 20 min at 121°C . It was then inoculated with five plugs taken with a cork borer from fresh cultures of *A. cepistipes* (Empa 655). The fungus was cultivated in 500 mL Erlenmeyer flasks with 300 mL of the growth medium under continuous shaking at 150 rpm and 22°C for 4 months. Thereafter, the supernatant was centrifuged at 4800 rpm for 15 min to remove the biomass and other debris. The extracted solution was adjusted to $\text{pH} = 13$ with NaOH (10 M) to dissolve all the melanin. Chloroform (0.2 vol) was mixed with the above solution to deproteinise the melanin pigment. The mixture was then centrifuged at 4800 rpm for 15 min, while the supernatant was adjusted to $\text{pH} = 2$ with HCl (5 M). The precipitated melanin was centrifuged again at 4800 rpm for 30 min. Melanin was obtained after it was washed once with 100% methanol (0.1 vol) and 70% ethanol (0.1 vol), respectively, and air-dried for 24 h. Finally, the generated melanin pellets were ground into fine powder using a pestle and mortar.

Polymer solution preparation

PCL ($M_w = 80000 \text{ g mol}^{-1}$), glacial acetic acid (AA, 99%), formic acid (FA, $\geq 95\%$), and tetraethylammonium bromide (TEAB, 98%) were purchased from Sigma-Aldrich (Switzerland). PUR (Elastollan C95A55, $M_w 85790 \text{ g mol}^{-1}$) was obtained from BASF (Germany) and dimethylformamide (DMF, $\geq 99.8\%$) was from VWR (France).

Spinning solutions of 15% w/v PCL were prepared by dissolving PCL in a mixture of AA/FA (3:1), while for PUR 14.5% w/v spinning solutions were prepared by dissolving PUR in pure DMF solvent. Additionally, 0.01% v/v TEAB were added into the PUR solutions to increase its electrical conductivity as described in Table 1. The concentration ratios were used according to our previous spinning studies [25, 26].

For preparation of melanin-blended membranes (PCL/Mel and PUR/Mel), fungal melanin powder was added into the solvent and dispersed with a Branson Ultrasonics™ Sonifier 250/450 at 83.3 W 30% amplitude for 20 min. The ultrasonic treatment alternated 2 sec of stop and go under ice cooling step. The polymers (PCL and PUR) were added afterwards and kept shaking for 24h to 125h to obtain homogeneous solutions.

Table 1. Electrospinning dispersion preparation

Polymer	Solvent ratio (v/v)	Total concentration of polymer in solution (wt%)	Concentration of melanin in the fibres (wt%)
PCL	AA:FA (3:1)	15	-
PCL/Mel	AA:FA (3:1)	15	10
PUR	DMF:TEAB (1000:1)	14.5	-
PUR/Mel	DMF	14.5	10

Fibre membranes were generated on the pilot scale needless Nanospider electrospinning instrument (NS 1WS500U, Elmarco, Czech Republic). In this setup, the solution reservoir continuously moves along a wire source electrode and deposits a thin film of solution on it. Applying a high electrical field forms multiple Taylor cones along the wire; electrospinning jets are pulled toward a counter wire electrode and fibres are deposited onto a paper substrate placed before

the counter electrode. Spinning parameters including: applied voltage, electrode distance, reservoir speed, temperature and relative humidity are described in Table 2.

Table 2. Spinning parameters for pure polymeric and composite melanised membranes fabrication

Solution	Applied voltage (kV)	Relative humidity – Temperature (% - °C)	Electrode distance (mm)	dis-	Reservoir speed (mm s ⁻¹)	Orifice diameter (mm)
PCL	+60/-10	10 - 22	261		195	0.6
PCL/Mel	+60/-10	10 - 22	261		214	0.6
PUR	+60/-10	10 - 22	200		245	0.7
PUR/Mel	+60/-10	10 - 22	250		218	0.7

Characterisation of spinning solutions and dispersions

The conductivity of the spinning solutions and dispersions was measured at room temperature using a 660 conductometer from Metrohm (Herisau, Switzerland) equipped with a Pt 100 dip-type conductometric cell ($c = 0.83 \text{ cm}^{-1}$).

A rheometer (Anton Paar Physica MCR 300, Switzerland) equipped with a plate-cone system was applied in controlled shear rate mode to assess the shear viscosity as a function of the shear rate. Flow curves with shear rates varying from 0.01 to 100 s⁻¹ were determined. Solutions were equilibrated at 22 °C prior to measurements.

Fibre and membrane analysis

i) Scanning electron microscopy (SEM)

The fibre morphologies were analysed by scanning electron microscope (SEM) imaging on a Hitachi S-4800 (Hitachi High-Technologies, Canada) at an accelerating voltage of 2 kV and current flow of 10 μA . For characterisation of the latter, a small piece of every sample was sputter coated with 9 nm of gold/palladium to reduce the effect of charging before imaging

(Polaron Equipment, SEM coating Unit E5100, Kontron AG, Switzerland). The ImageJ software 1.47v (National Institutes of Health, USA) was used to measure the average fibre diameter of 100 different randomly selected fibres from each SEM image.

ii) X-ray photoelectron spectroscopy (XPS)

Surface elemental compositions were characterised by X-ray photoelectron spectroscopy (XPS) measurements and performed on a PHI 5000 VersaProbe II instrument (USA) with a monochromatic AlK α X-ray source. Energy resolution of the spectrometer was set to 0.8 eV/step at a pass-energy of 187.85 eV for the survey scans. Carbon 1s at 284.5 eV was used as a calibration reference to correct for charge effects. Elemental compositions were determined using instrument dependent atom sensitivity factors. The photoelectron-transitions C1s, O1s and N1s were selected to determine the elemental concentrations. Data analysis was performed by use of CasaXPS software (Casa Software Ltd, United Kingdom).

iii) Mechanical testing

To test the mechanical properties of the fabricated membranes, samples (N=5) were cut to rectangular shape (10x130 mm) and thickness was measured in 3 different points of each sample using a profilometer (Dektak150, Veeco, Bruker, Germany).

Mechanical tensile tests were performed using a tensile test machine (Zwick, Intron, Germany) at 20 mm/min up to rupture or until a maximum of 100% strain was achieved at environmental conditions of 23°C and 40% relative humidity. The distance between grips was kept at 80 mm. The Young Modulus (E) was calculated considering an interval between 1-3% strain. For mechanical tests, statistical differences among samples were evaluated through one-way ANOVA and post-hoc Tukey test.

iv) Porosity measurements

Overall membrane porosities were measured by weighing the membranes and using the following relation:

$$\text{Porosity } (\varepsilon) = 1 - \frac{\text{Solid volume of fibre } (V_F)}{\text{Total volume } (V)} \quad (1)$$

Here, solid volume V_F was measured by density of the nanofibers (*Mass/Density*) and the total volume V was measured by membrane dimensions (*Length* \times *Width* \times *Thickness*). Thickness measurements were described in section 2.4.3.

Adsorption capacity of fungal raw melanin

Metal solutions were diluted from stock metal solutions of 1 g L^{-1} in 5% HNO_3 (Specpure[®] *Plasma Standards*, Alfa Aesar, Germany) to prepare the target concentrations: $600 \mu\text{g L}^{-1} \text{Pb}^{2+}$, $50 \mu\text{g L}^{-1} \text{Cd}^{2+}$, $250 \mu\text{g L}^{-1} \text{Ni}^{2+}$ and $120 \mu\text{L}^{-1} \text{Cr}^{3+}$. The concentrations were selected based on their toxicity level described in previous literature [22, 23] and were kept consistent throughout all adsorption assays, except the test for selectivity of melanin. 10 mg of extracted fungal melanin were then added to 10 mL metal solutions. The experiments were performed at room temperature and at a constant pH = 6. In order to optimise the adsorption process, the solutions were shaken at 150 rpm for 120 min. Finally, melanin powder was precipitated by centrifugation and the remaining liquid phase were analysed by Inductively Coupled Plasma - Mass Spectrometry (ICP-MS) (ELEMENT 2[™] ICP-MS, Thermo Finnigan, Germany), using the following isotopes: ^{207}Pb , ^{111}Cd , ^{60}Ni and ^{52}Cr . Calibration was performed by linear regression of a set of reference solutions.

Metal removal efficiency ($Y \%$) and adsorption capacity (q_e) were calculated as follows:

$$Y \% = \frac{C_0 - C_e}{C_0} \times 100\% \quad (2)$$

$$q_e = \frac{(C_0 - C_e) \times V}{m} \quad (3)$$

where, C_0 and C_e are the initial and equilibrium metal ions concentrations (mg L^{-1}), respectively; V is the aqueous solution volume (L) and m is the amount of used adsorbent in the adsorption process (g), q_e (mg g^{-1}) is the adsorption amount at equilibrium.

To determine the metal selectivity of fungal melanin, further measurements were performed in multi-component ion water systems. Some of the most relevant and essential metals normally present in drinking water or the human body were also added to the mixture for this study: Ca^{2+} and Zn^{2+} [27]. 10 mL of multicomponent solution was prepared by mixing 500 mg L^{-1} of each metal. Selective adsorption studies were also performed according to the experimental conditions previously described.

Adsorption capacity of fungal melanin-based electrospun membranes

To determine the optimal contact/adsorption time for the membranes to reach the maximum adsorption capacity, 50 mg of each produced membrane was submerged into the water systems, each contained 10 mL of $600 \mu\text{g L}^{-1} \text{Pb}^{2+}$, $50 \mu\text{g L}^{-1} \text{Cd}^{2+}$, $250 \mu\text{g L}^{-1} \text{Ni}^{2+}$ and $120 \mu\text{g L}^{-1} \text{Cr}^{3+}$ separately. After selected contact times (5, 10, 20, 40, 60, 80 min), the membranes were removed and the remaining metal concentration in solution was analysed by ICP-MS. After the optimum time was determined, a new set of experiments was prepared to compare the adsorption efficiency of different adsorbents including: PCL/Mel membranes, PUR/Mel membranes, raw melanin as positive control and pure polymer (PCL and PUR) membranes as negative controls. The initial metal concentrations were the same as described above for the contact time tests. It should be noted that due to sedimentation, not all melanin particles from the starting dispersion were encapsulated within and onto the fibres. Therefore, to obtain comparable adsorption results for raw melanin and the melanised membranes, the actual amount of melanins incorporated during the spinning process was determined by re-dissolving the melanised membranes in their corresponding solvents followed by centrifugal collection of the melanin for quantification by weighing. These data were then used to calculate the adsorption capacities per 1 gram of blended melanin following formula (2).

Statistical analysis

For metal adsorption assays, all measurements were performed in triplicates and were represented as mean value \pm SD. The difference in adsorption capacity between different adsorbents were analysed by independent samples T-test using the statistical software IBM[®] SPSS[®] (Version 25, SPSS Inc., Chicago, IL, USA). The difference was considered significant when the $P < 0.05$.

2.1.3. Results and discussion*Membrane fabrication and characterisation*

Freestanding nonwoven membranes, incorporating nanoscale-diameter fibres, were successfully produced by optimising electrospinning parameters (e.g. polymer concentration, polymer solvents, electrical field, electrode distance, humidity, temperature, etc.) to obtain PCL, PCL/Mel, PUR and PUR/Mel (Fig. 1). As viscosity and conductivity of the solutions are major factors affecting fibre morphology, these properties were measured (Table 3). The viscosities changed slightly by the addition of melanin: for PCL samples an increase was determined while the opposite trend was observed for PUR samples (Fig. S1). This can be explained by the fact that the polymer PCL is more hydrophobic than PUR and supposedly has less interaction with melanin. Hence, the viscosity of the polymeric solution for PCL was barely affected by melanin. In the case of PUR, melanin might interact and partially disentangle the polymer chains. With increasing shear rates, the chains were able to align themselves in the direction of the flow, which resulted in a viscosity drop. Furthermore, the addition of melanin highly influenced the conductivity of the polymeric solutions because melanin is a charge-carrying pigment [28].

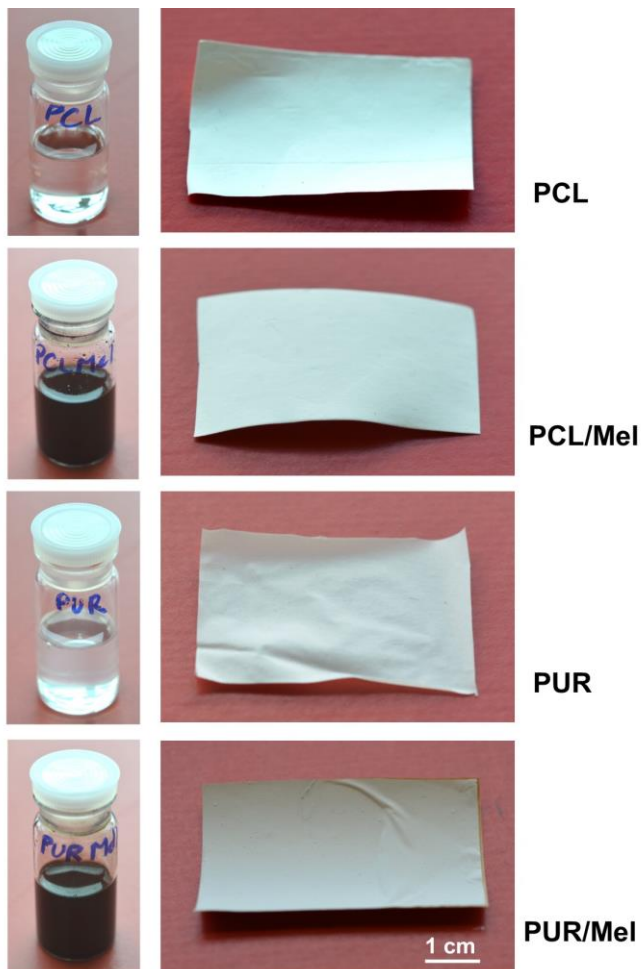


Figure 1. Spinning polymer solutions/dispersions with corresponding electrospun membranes.

Table 3. Characteristics of spinning samples

	Conductivity [$\mu S cm^{-1}$]	Viscosity at shear rate of $1 s^{-1}$ [Pa·s]	Viscosity at shear rate of $10 s^{-1}$ [Pa·s]	Viscosity at shear rate of $100 s^{-1}$ [Pa·s]
PCL	12.6	1.27	1.27	1.25
PCL/10wt% Mel	175.0	1.33	1.32	1.32
PUR	2.7	2.37	2.27	2.12
PUR/10wt% Mel	173.5	1.94	1.90	1.78

SEM pictures revealed that only melanin-containing samples were able to form smooth and homogenous fibres, whereas the pure polymeric electrospun fibres appeared to contain beads.

For PCL, the beads space widely apart along the fibre length (Fig. 2a), while elongated beads were highly packed within the membrane of the PUR polymer (Fig. 2c).

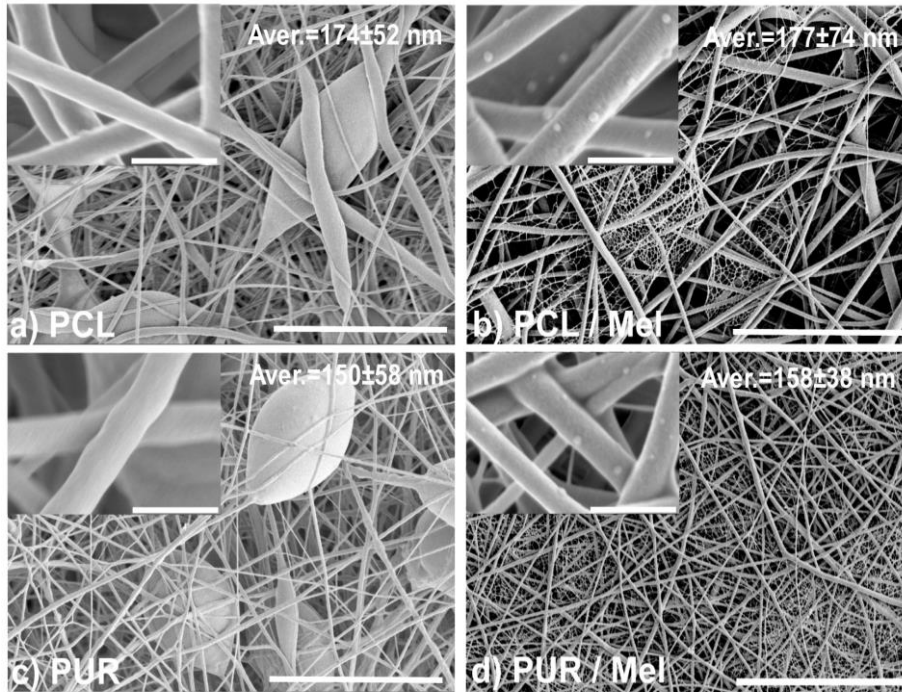


Figure 2: SEM images of nanofibre membranes of (a) PCL, (b) PCL/Mel, (c) PUR and (d) PUR/Mel with their average fibre diameters. Scale bar = $10\mu\text{m}$, scale bar within the insert = 500 nm.

According to the principle of electrospinning, the stretching of viscoelastic filaments during the spinning process depends on the electric force that elongates the solution [29]. Based on the solution characteristics, low electrical conductivity may not generate sufficient strength to stretch the highly viscous pure PUR solution to form fibres. In the case of pure PCL control samples, the spinning solution is less viscous and the solution conductivity is also higher, which explains the lower rate of beads forming for PCL compared to PUR. Different morphologies were found for electrospun fibers containing melanin (Fig. 2b and 2d). The negatively charged groups of melanin significantly increased the conductivity of the spinning dispersions, hence, bead formation on the composite nanofibers was eliminated, thus improving the e-spinning process leading to homogenous fibre morphologies.

At higher magnifications, secondary spider-web-like structures notably appeared between electrospun fibres incorporating melanin (Figs. 3a and 3b). It is worth stating that the mechanism of the spider-web-like structures is rather complex in its nature and a full consistent explanation has not been reached yet. However, according to several studies, such nanoweb structures can be attributed to the phase separation of charged droplets. It is supposed that the addition of melanin increased conductivity of the solution that followed a higher charge distribution on the flying jets [30, 31]. When the charge to mass ratio of the Taylor cone apex exceeds a critical value, it forms not only jets but also generated micron-sized charged droplets due to the stronger electric repulsion [31]. During the flight to the collector, the droplets expand quickly, the fast phase separation between polymer and solvent as a result of fast solvent evaporation leads to the splitting of the thin film into nanowebs. The nanoweb structures were stable and were present within the membranes after the adsorption assays (Fig. S3).

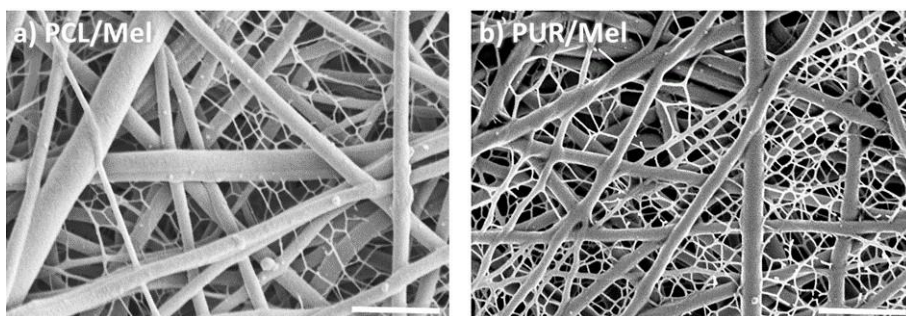


Figure 3. Spider-web-like secondary structures between fibres of (a) PCL/Mel and (b) PUR/Mel electrospun membranes. Scale bar = 2 μm .

The porosity of the electrospun membranes was influenced by the presence of melanin (Table S2). Specifically, the membranes containing melanin (PCL/Mel and PUR/Mel) were slightly more porous than the ones without (PCL and PUR). We suggest that the lower porosities of the pure polymeric membranes were the result of highly dense beads present in the spun fibres and confirmed by SEM (Fig. 2). The beads, in fact, brought mass into the membranes and occupied more space between submicron-scaled fibres. In contrast, the addition of melanin enhanced the

spinnability of the polymer solutions, resulting in the formation of homogeneous and uniform fibres with low weight.

As illustrated in the SEM images (Fig. 2), the diameters of the fibres were all at the nanoscale, ranging from 100 to 200 nm. Homogeneously distributed nanoparticles with a size of approximately 55 ± 8 nm were observed along the fibres' surfaces of PCL/Mel and PUR/Mel (Fig. 2b and 2d). These particles are suggested to be melanin encapsulated by the polymer during the spinning process, which explains its absence in the control membranes of PUR and PCL (Fig. 2a and 2c). To determine the amount of melanin on the fibre surfaces, the atomic content of each membrane was examined by XPS analysis, exhibiting a surface information depth of 8 - 10 nm (Table 4). Based on the elemental characterisation of raw melanin, we expected to witness an increased nitrogen concentration in the melanin blended samples. However, nitrogen was not detected in PCL/Mel and the measured nitrogen concentration of PUR/Mel was only slightly higher when compared to the nitrogen concentration of pure PUR (Fig. S2). These results suggest that melanin particles are mostly encapsulated within the fibres or a polymer layer is covering the melanin particles.

Table 4. Atomic surface composition of electrospun membranes and raw melanin determined by XPS

Sample	Atomic composition (at.%)				
	C	N	O	Na	Cl
PCL	78.8	-	21.2	-	-
PCL/Mel	74.5	-	25.6	-	-
PUR	76.2	2.3	21.6	-	-
PUR/Mel	73.1	3.0	23.9	-	-
Melanin	65.4	6.4	23.4	2.4	2.3

Mechanical properties of the fabricated membranes

Mechanical tests revealed the differences in the mechanical response of PCL and PUR membranes. Indeed, considering membranes electrospun from the pure polymers, PUR membranes are stiffer materials with higher elastic Modulus as compared to PCL membranes (Fig. 5a). Despite this, PUR is able to withstand elongations up to 100% strain with a minimal plastic deformation of $16.6\pm 0.7\%$, while PCL shows maximum elongations at break at $44.4\pm 9.5\%$ (Fig. 5b). Melanin encapsulated within the fibres influences the mechanical response of membranes, causing a decrease in the elastic Modulus for PUR while increasing the average Modulus for PCL. A difference due to the addition of melanin can also be noticed by the shape of the loading curves (Fig. 4). Indeed, while the overall stress/strain curve pattern retains the same shape for PCL (Fig. 4a,c), the characteristic viscoelastic behaviour of PUR [32] disappears in PUR/Mel, showing a higher linear elastic response and limited maximum elongation before failure (Fig. 5b). Such phenomenon is believed to correspond to the different interactions between melanin and the polymers as it was already reflected in terms of change in viscosity of the initial spinning solutions.

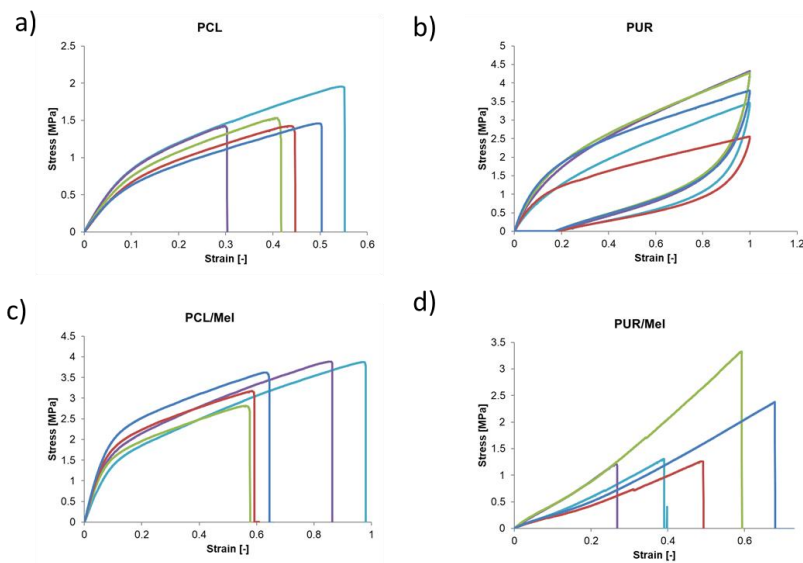


Figure 4. Stress/strain curves for a) PCL, b) PUR, c) PCL/Mel, d) PUR/Mel.

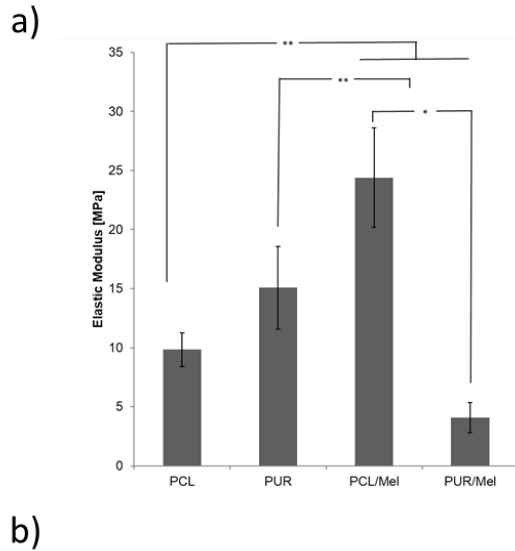


Figure 5. a) Young Modulus of membranes. * $p < 0.05$, ** $p < 0.01$; b) table depicting the average values of Young Modulus and Elongation at break.

The addition of melanin led to a slight increase in the PCL solution viscosity while causing a more significant decrease in the PUR solution viscosity, suggesting high interaction between the less hydrophobic PUR and melanin. Moreover, as noticed by SEM pictures melanin acts also as filler forming nanoparticles within the fibres. The presence of fillers is known to greatly affect the final mechanical properties of materials depending on the interaction between the materials as well as the size and concentration of the fillers [33, 34, 35].

Adsorption studies with raw melanin

Several studies reported that melanin-rich strains of fungus had biosorbed high concentrations of cations from their surrounding environments [18, 19]. However, since most of the current commercial melanins are either extracted from sepia or chemically synthesised, limited information on metal adsorption characteristics of fungal melanin is available. In our batch experiments, significant amounts of metals were eliminated from the solution by the fungal melanin

in single-component solutions. The adsorption efficiencies were more than 90.0% for all studied heavy metals: 95.9% for Pb^{2+} , 98.1% for Cd^{2+} , 94.8% for Ni^{2+} and 91.0% for Cr^{3+} (Fig. 6).

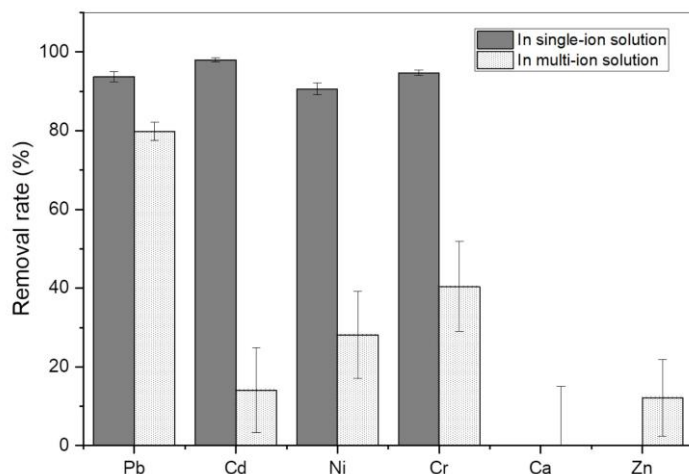


Figure 6. Metal removal efficiency of melanin in single and multi-component metal solutions.

Contaminated water systems are usually affected by several heavy metals [36]. Therefore, the behavior of melanin in multi-component solution provides information on its selectivity towards different metals. The metal adsorption efficiencies of raw melanin in the multi-component solutions revealed significantly reduced values compared to the single-component experiments (Fig. 6). The latter result is predictable since melanin was introduced at the same amount while the concentrations of metals were much higher than in the previous single component assay. Interestingly, the reduction rate varied between metals, from 94% to 80% for Pb^{2+} , 98% to 14% for Cd^{2+} , 91% to 28% for Ni^{2+} and 95% to 40% for Cr^{3+} . To set the stage for the discussion about metal binding selectivity of melanin, it is important to stress from the outset that the complete and detailed molecular structure of melanin in general, and for fungal melanin in particular, is still under investigation. Therefore, when addressing the biophysics of metal binding to fungal melanin, the proposed arguments are based on the current knowledge of functional groups existing in the fungal melanin structure and comparisons with reported metal binding

behaviour of melanin from different sources, e.g. sepia melanin, neuromelanin and fungal melanin from other strains, etc. Moreover, since our fungal melanin is eumelanin, we restrict the cited literature and discussion to this pigment category.

A recent physicochemical study of fungal melanin extracted from *A. cepistipes* (Empa 655) indicated that this pigment, which is derived from L-Dopa precursor, should contain carboxyl, amine, hydroxyl (phenolic), quinone and semiquinone groups [21]. Each of these functional groups, or combinations of them, can potentially serve as a metal binding site. As mentioned above, some metals may share the same binding sites, while others have unique binding locations. According to the results of adsorption study regarding the presence of different metals together in a system, fungal melanin showed an extreme affinity to Pb^{2+} (nearly 80% removal) while its affinity for other metals was significantly lower. Similar results were reported in the study of Chen et al. [37], in which macrosalts such as NaCl, MgCl_2 , and CaCl_2 had no obvious effect on the binding of Pb^{2+} but greatly diminished the adsorption of Cd^{2+} . Both studies indicated that different functional groups within melanin are responsible for their adsorption. For instance, Pb^{2+} can be bound to various sites including catechol (OH), amine (NH) and carboxyl (COOH) groups. In contrast, Cd^{2+} , Zn^{2+} and Ca^{2+} bind specifically to carboxyl (COOH) groups [37]. As a result, in multi-component ion systems, they have to compete with each other for the same binding sites, which leads to a greatly reduced adsorption while Pb^{2+} can, more or less, remain bound to melanin. It was also reported that alkaline and earth alkaline metals such as Na^+ , K^+ or Ca^{2+} show a weak affinity to melanin compared to heavier metals [38]. This was illustrated clearly in the results, where no significant amount of Ca^{2+} was adsorbed by fungal melanin.

Although natural melanins are sometimes found to accumulate high amounts of Ca^{2+} and/or Zn^{2+} , its affinity to these two metal ions is only modest, where under certain conditions, melanin can release them [38, 39, 40]. Thus, one of the biological roles ascribed to metal binding of melanin is to serve as a reservoir for Ca^{2+} and Zn^{2+} [41, 42]. In contrast, heavy metals bind

tightly to melanin [43]. For instance, the affinity of Pb^{2+} to melanin outcompeted many metals. Compared to the strong affinity of Pb^{2+} , the affinities of Cd^{2+} , Ni^{2+} , Cr^{3+} to fungal melanin are considered to be moderate. Nevertheless, melanin can still bind strongly to those heavy metals and prefer them over other alkaline metals. In this study, the adsorption affinity of fungal melanin to the heavy metals followed the order $\text{Pb}^{2+} > \text{Cr}^{3+} > \text{Ni}^{2+} > \text{Cd}^{2+} > \text{Zn}^{2+} > \text{Ca}^{2+}$. Except for Pb^{2+} , Zn^{2+} and Ca^{2+} , the adsorption order of the remaining three metals may differ from some reported literature, which may be related to the various types and origins of the melanin within those studies, as the relative abundance of binding sites varies among different sources of melanin [38]. It is evident that more analytical studies should be performed on the interaction of heavy metals with fungal melanin. Nevertheless, these findings indicate that fungal melanin is strongly considered to be a selective adsorbent of heavy metals in contaminated water without removing other co-existing essential metals such as Zn^{2+} and Ca^{2+} .

Adsorption studies with melanised membranes

The effects of contact time on the biosorption were determined within a range from 5 to 80 min (Fig. 7). In the first 20 min, the adsorption efficiency for all heavy metals increased rapidly due to the abundant availability of active binding sites on melanin. With gradual occupancy of these sites, the adsorption efficiency slowed down in the latter stages. As observed, the amount of cations adsorbed increased with increasing contact time. For PUR/Mel membranes, more than 90% of total adsorption occurred in the first 40 min and equilibria were reached after 60 min. In the parallel assays, the adsorption kinetics for PCL/Mel membranes was slightly slower but also revealed greater than 90% metal removal after 60 min as well. This may be explained by the different wettability behaviour of PCL and PUR where it is suggested that PCL shows highly hydrophobic wettability properties when compared to PUR [44]. This means the contact of the membrane with the liquid is less pronounced for PCL, resulting in slower diffusion rates of the cations towards the melanin encapsulated within the fibres. Furthermore, as melanin was

found on PUR surfaces as determined by nitrogen XPS quantification, a faster adsorption efficiency has to be considered due to more accessible binding sites. Fibre diameters of the two polymeric membranes may also influence the adsorption efficiency results. For instance, thinner fibres in PUR/Mel membranes (aver. 158 nm) are assumed to have greater surface area to interact with metals than the PCL/Mel membranes (aver. 177 nm). Regardless, it is interesting to note that the adsorption efficiencies of these metal ions onto both types of melanised membranes were considerably faster than that of other biosorbents and nanofibres (Table S1) [10, 45].

Knowing the optimum time for the melanised membranes to reach the saturation of binding sites, the following batch adsorption assays were performed with different adsorbents at the same time period to evaluate the adsorption capacity of melanins after electrospinning.

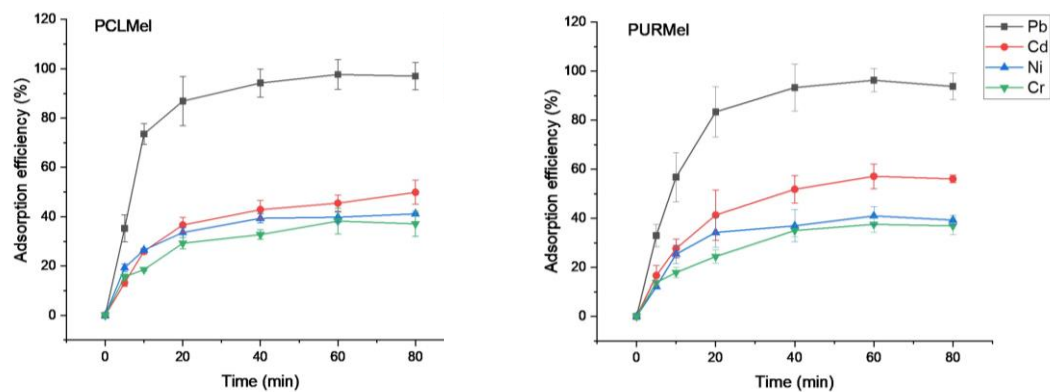


Figure 7. Effect of contact time on the metal adsorption efficiency of PCL/Mel and PUR/Mel electrospun membranes.

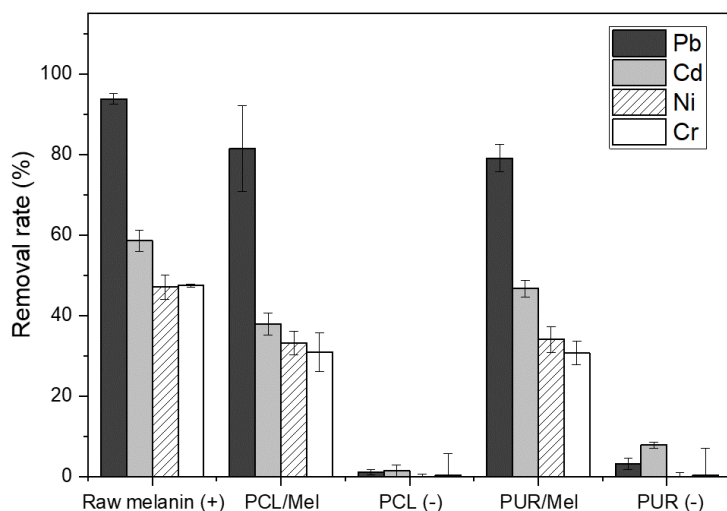


Figure 8. Metal removal efficiency of melanised membranes in comparison with raw melanin (positive control) and pure polymeric membranes (negative controls), for 5 mg melanin per 10 mL metal solution after 60 min.

The ability of melanised membranes to remove heavy metals from solutions depends on the heavy metal retainability of either the polymer fibres, or the melanin incorporated within them, or both. According to the results, the pure polymer membranes (negative control) showed very little to almost no effect on metal removal (< 2%). Therefore, it can be inferred that the polymer fibres played very little role in binding heavy metals. Instead, the high porosity of the electrospun membranes facilitates fast diffusion of metal ions into the fibres. There, the polymeric structure of the fibres, which is composed of amorphous and crystalline phases with often low ordering properties [46], let the metals diffuse into the fibres and be chelated by the encapsulated melanin, resulting in high metal adsorption capacities of the melanised membranes.

Secondly, the removal efficiency of Pb^{2+} and Ni^{2+} by the melanised membranes was in the same range when compared to raw melanin particles (positive control). However, for Cr^{3+} and Cd^{2+} , slightly but significantly lower removal efficiency were determined, which might be an indication for non-accessible binding sites on the encapsulated melanin particles. Furthermore, we calculated the heavy metal adsorption capacity of the melanised membranes based on the actual amount of the existing melanin in the membranes (Table 5). Unlike the metal removal efficiency data, the adsorption capacity values revealed almost no significant difference between

the melanised membranes and the raw melanin (with 95% confidence interval), which indicated that the incorporated melanin within the polymer fibres can maintain its capacity to bind heavy metals.

Table 5. Metal removal efficiency and metal adsorption capacity of melanised membranes in comparison with raw melanin and pure polymeric membranes

Adsorbent	Metal	Removal efficiency (%)	Adsorption capacity (mg g ⁻¹ melanin)
Raw melanin (positive control)	Pb ²⁺	93.8 ± 1.3	1.12 ± 0.02
	Cd ²⁺	58.6 ± 2.6	0.06 ± 0.00
	Ni ²⁺	47.1 ± 3.1	0.24 ± 0.02
	Cr ³⁺	47.5 ± 0.4	0.11 ± 0.00
PCL (negative control)	Pb ²⁺	1.06 ± 0.7	
	Cd ²⁺	1.5 ± 1.4	
	Ni ²⁺	0.0 ± 0.7	
	Cr ³⁺	0.3 ± 5.5	
PCL/Mel	Pb ²⁺	97.7 ± 12.8	1.17 ± 0.15
	Cd ²⁺	45.5 ± 3.3	0.05 ± 0.00
	Ni ²⁺	39.8 ± 3.6	0.20 ± 0.02
	Cr ³⁺	37.1 ± 5.8	0.09 ± 0.01
PUR (negative control)	Pb ²⁺	3.2 ± 1.4	
	Cd ²⁺	7.9 ± 0.7	
	Ni ²⁺	0.0 ± 0.9	
	Cr ³⁺	0.3 ± 6.7	
PUR/Mel	Pb ²⁺	94.8 ± 4.0	1.14 ± 0.05

Cd ²⁺	55.9 ± 2.5	0.06 ± 0.00
Ni ²⁺	40.9 ± 3.8	0.21 ± 0.02
Cr ³⁺	36.8 ± 3.5	0.09 ± 0.01

Finally, there was no significant difference between the adsorption behaviour of the two polymer membranes - PCL/Mel and PUR/Mel - except in case of Cd²⁺ interaction. Since PUR membranes can retain, albeit not much, Cd²⁺ ions, the removal efficiency of PUR/Mel for Cd²⁺ was better than that of PCL/Mel. This phenomenon might be explained by the slight interaction between Cd²⁺ and the amide groups of PUR; however, this hypothesis would require more chemical analyses before it can be confirmed.

2.1.4. Conclusions

In this study, we demonstrated the metal removal potential of in-house biosynthesised melanin from the basidiomycete *A. cepistipes* (Empa 655) and the use of electrospinning techniques to immobilise this melanin into and onto PCL and PUR polymer membranes for water treatment. The resulting extracted melanin and the melanised membranes can effectively sequester trace amount of toxic metals to achieve drinking-water quality (according to WHO standard). It was also confirmed that fungal melanins expressed different affinities to different metal types. The adsorption efficiencies of the tested metals in multi-component systems fall in the order Pb²⁺ > Cr³⁺ > Ni²⁺ > Cd²⁺ > Zn²⁺ > Ca²⁺. The notably low affinity of fungal melanin towards essential metals such as Ca²⁺ and Zn²⁺ opens up the possibility to develop a customised treatment technology to chelate particular heavy metals. These results are promising for the field of water treatment however, further studies are required to investigate the interactions between melanin and polymer fibres as well as their adsorption kinetics to different metals and aqueous matrices for improving and optimising the adsorption potential of the melanised membranes.

Conflicts of interest

There are no conflicts to declare.

Acknowledgement

We thankfully acknowledge the technical assistance provided by Adrian Wichser of the Laboratory for Particles-Biology Interactions, Empa, for his support with ICP-MS elemental analysis.

References

- [1] United Nation Office of the High Commissioner for Human Rights (OHCHR), Fact Sheet No. 35, The Right to Water, Geneva, 2010.
- [2] C. G. Tchounwou, P. B. and Yedjou, A. K. Patlolla, D. J. Sutton, Heavy metal toxicity and the environment, *Exp. Suppl.* 101 (2012) 133–164. [doi: 10.1007/978-3-7643-8340-4_6](https://doi.org/10.1007/978-3-7643-8340-4_6).
- [3] F. Fernandez-Luqueno, F. Lopez-Valdez, P. Gamero-Melo, S. Luna-Suarez, A. I. M. Elsa Nadia Aguilera-Gonzalez, Heavy metal pollution in drinking water - a global risk for human health: A review, *Afr. J. Environ. Sci. Technol.* 7 (7) (2013) 567–584.
- [4] H. Hu, Q. Jin, P. Kavan, A study of heavy metal pollution in china: Current status, pollution-control policies and countermeasures, *Sustainability* 6 (9) (2014) 5820–5838.
- [5] M. Kumar, A. Gogoi, D. Kumari, R. Borah, P. Das, P. Mazumder, , V. K. Tyagi, Review of perspective, problems, challenges, and future scenario of metal contamination in the urban environment, *J. Hazard Toxic. Radioact. Waste* 21 (4) (2017) 04017007. [doi:10.1061/\(ASCE\)HZ.2153-5515.0000351](https://doi.org/10.1061/(ASCE)HZ.2153-5515.0000351).
- [6] H. J. Hapke, Heavy metal transfer in the food chain to humans, Springer Netherlands, Dordrecht, 1996.
- [7] M. Jaishankar, T. Tseten, N. Anbalagan, B. B. Mathew, K. N. Beeregowda, 510 Toxicity, mechanism and health effects of some heavy metals, *Interdiscip. Toxicol.* 7 (2) (2014) 60–72. [doi:10.2478/intox-2014-0009](https://doi.org/10.2478/intox-2014-0009).
- [8] X. Wu, S. J. Cobbina, G. Mao, H. Xu, Z. Zhang, L. Yang, A review of toxicity and mechanisms of individual and mixtures of heavy metals in the environment, *Environ. Sci. Pollut. R.* 23 (9) (2016) 8244–8259. [doi: 515 10.1007/s11356-016-6333-x](https://doi.org/10.1007/s11356-016-6333-x).
- [9] F. Fu, Q. Wang, Removal of heavy metal ions from wastewaters: A review, *J. Environ. Manage.* 92 (3) (2011) 407–418. [doi:10.1016/j.jenvman.2010.11.011](https://doi.org/10.1016/j.jenvman.2010.11.011).

- [10] V. Manirethan, K. Raval, R. Rajan, H. Thaira, R. M. Balakrishnan, Kinetic and thermodynamic studies on the adsorption of heavy metals from aqueous solution by melanin nanopigment obtained from marine source: *Pseudomonas stutzeri*, *J. Environ. Manage.* 214 (2018) 18619–18629. [doi:10.1016/j.jenvman.2018.02.084](https://doi.org/10.1016/j.jenvman.2018.02.084).
- [11] P. S. Suja, C. R. Reshmi, P. Sagitha, A. Sujith, Electrospun nanofibrous membranes for water purification, *Polym. Rev.* 57 (3) (2017) 467–504. [doi: 10.1080/15583724.2017.1309664](https://doi.org/10.1080/15583724.2017.1309664).
- [12] J. Akindoyo, M. D. H. Beg, S. Ghazali, M. R. Islam, N. Jeyaratnam, A. R. Yuvaraj, Polyurethane types, synthesis and applications – a review, *Rsc Adv.* 6 (115) (2016) 114453–114482. [doi:10.1039/C6RA14525F](https://doi.org/10.1039/C6RA14525F).
- [13] J. Williams, A. Adewunmi, R. Schek, C. Flanagan, P. Krebsbach, S. Feinberg, S. Hollister, S. Das, Bone tissue engineering using polycaprolactone scaffolds fabricated via selective laser sintering, *Biomaterials* 26 (23) (2005) 4817–4827. [doi:10.1016/j.biomaterials.2004.11.057](https://doi.org/10.1016/j.biomaterials.2004.11.057).
- [14] N. Wismer, S. Grad, G. Fortunato, S. J. Ferguson, M. Alini, D. Eglin, Biodegradable electrospun scaffolds for annulus fibrosus tissue engineering: Effect of scaffold structure and composition on annulus fibrosus cells in vitro, *Tissue Eng. Part A* 20 (3-4) (2014) 672–682. [doi:10.1089/ten.TEA.2012.0679](https://doi.org/10.1089/ten.TEA.2012.0679).
- [15] S. Homaeigohar, M. Elbahri, Nanocomposite electrospun nanofiber membranes for environmental remediation, *Materials* 7 (2) (2014) 1017–1045. [doi:10.3390/ma7021017](https://doi.org/10.3390/ma7021017).
- [16] P. A. Riley, A proposed selective mechanism based on metal chelation in industrial melanic moths, *Biol. J. Linnean Soc.* 109 (2) (2013) 298–301. [doi:10.1111/bij.12062](https://doi.org/10.1111/bij.12062).
- [17] M. Chatelain, J. Gasparini, L. Jacquin, A. Frantz, The adaptive function of melanin-based plumage coloration to trace metals, *Biol. Lett.* 10 (3) (2014) 20140164. [doi:10.1098/rsbl.2014.0164](https://doi.org/10.1098/rsbl.2014.0164).
- [18] N. N. Gessler, A. S. Egorova, T. A. Belozerskaya, Melanin pigments of fungi under extreme environmental conditions (review), *Appl. Biochem. Micro.* 50 (2) (2014) 105–113. [doi:10.1134/S0003683814020094](https://doi.org/10.1134/S0003683814020094).
- [19] J. Nosanchuk, A. Casadevall, The contribution of melanin to microbial pathogenesis, *Cell. Microbiol.* 5 (4) (2003) 203–223.
- [20] H. C. Eisenman, A. Casadevall, Synthesis and assembly of fungal melanin, *Appl. Microbiol. Biotechnol.* 93 (3) (2012) 931–940. [doi:10.1007/s00253-011-3777-2](https://doi.org/10.1007/s00253-011-3777-2).
- [21] J. Ribera, G. Panzarasa, A. Stobbe, A. Osypova, P. Rupper, D. Klose, F. W. M. R. Schwarze, Scalable biosynthesis of melanin by the basidiomycete *Armillaria cepistipes*, *J. Agric. Food Chem.* 67 (1) (2019) 132–139. [doi:10.1021/acs.jafc.8b05071](https://doi.org/10.1021/acs.jafc.8b05071).

- [22] S. Thomas, I. Watson, Laboratory analyses for poisoned patients, *Ann. Clin. Biochem.* 39 (2002) 327–339.
- [23] W. H. Organization, *Guidelines for Drinking-water Quality*, 3rd Edition, Geneva, 2004.
- [24] P. Jalmi, P. Bodke, S. Wahidullah, S. Raghukumar, The fungus *Gliocephalotrichum simplex* as a source of abundant, extracellular melanin for biotechnological applications, *World J. Microbiol. Biotechnol.* 28 (2) (2012) 505–512. [doi:10.1007/s11274-011-0841-0](https://doi.org/10.1007/s11274-011-0841-0).
- [25] A. G. Guex, F. M. Kocher, G. Fortunato, E. Korner, D. Hegemann, T. P. Carrel, H. T. Tevaearai, M. N. Giraud, Fine-tuning of substrate architecture and surface chemistry promotes muscle tissue development, *Acta Biomater.* 8 (4) (2012) 1481–1489. [doi:10.1016/j.actbio.2011.12.033](https://doi.org/10.1016/j.actbio.2011.12.033).
- [26] A. G. Guex, L. Weidenbacher, K. Maniura-Weber, R. M. Rossi, G. Fortunato, Hierarchical self-assembly of poly(urethane)/poly(vinylidene fluoride-co-hexafluoropropylene) blends into highly hydrophobic electrospun fibers with reduced protein adsorption profiles, *Macromol. Mater. Eng.* 302 (10) (2017) 1700081. [doi:10.1002/mame.201700081](https://doi.org/10.1002/mame.201700081).
- [27] A. Azoulay, P. Garzon, M. Eisenberg, Comparison of the mineral content of tap water and bottled waters, *J. Gen. Intern. Med.* 16 (3) (2001) 168–175.
- [28] J. D. Nosanchuk, R. E. Stark, A. Casadevall, Fungal melanin: What do we know about structure?, *Front. Microbiol.* 6 (3) (2015) 1463. [doi:10.3389/fmicb.2015.01463](https://doi.org/10.3389/fmicb.2015.01463).
- [29] G. L. Garg, K.; Bowlin, Electrospinning jets and nanofibrous structures, *Biomicrofluidics* 5 (1) (2011) 13403. [doi:10.1063/1.3567097](https://doi.org/10.1063/1.3567097).
- [30] B. Ding, C. Li, Y. Miyauchi, O. Kuwaki, S. Shiratori, Formation of novel 2d polymer nanowebs via electrospinning, *Nanotechnology* 17 (15) (2006) 3685–3691. [doi:10.1088/0957-4484/17/15/011](https://doi.org/10.1088/0957-4484/17/15/011).
- [31] S. Zhang, K. Chen, J. Yu, B. Ding, Model derivation and validation for 2d polymeric nanonets: Origin, evolution, and regulation, *Polymer* 74 (2015) 182–192. [doi:10.1016/j.polymer.2015.08.002](https://doi.org/10.1016/j.polymer.2015.08.002).
- [32] H. Qi, M. Boyce, Stress–strain behavior of thermoplastic polyurethanes, *Mech. Mater.* 37 (2005) 817–839. [doi:10.1016/j.mechmat.2004.08.001](https://doi.org/10.1016/j.mechmat.2004.08.001).
- [33] R. Scaffaro, F. Lopresti, A. Maio, L. Botta, S. Rigogliuso, G. Ghersi, Electrospun pcl/gog-peg structures: Processing-morphology-properties relationships, *Compos. Part A Appl. Sci. Manuf.* 92 (2017) 97–107. [doi: 10.1016/j.compositesa.2016.11.005](https://doi.org/10.1016/j.compositesa.2016.11.005).

- [34] F. Saint-Michel, L. Chazeau, J.-Y. Cavaill e, Mechanical properties of high density polyurethane foams: Effect of the filler size, *Compos. Sci. Technol.* 66 (15) (2006) 2709–2718. [doi:10.1016/j.compscitech.2006.03.008](https://doi.org/10.1016/j.compscitech.2006.03.008).
- [35] Y. Wang, T. Li, X. Wang, P. Ma, H. Bai, W. Dong, Y. Xie, M. Chen, Superior performance of polyurethane based on natural melanin nanoparticles, *Biomacromolecules* 17 (11) (2016) 3782–3789. [doi:10.1021/acs.biomac.6b01298](https://doi.org/10.1021/acs.biomac.6b01298).
- [36] V. Masindi, K. L. Muedi, [Environmental contamination by heavy metals](#), in: H. E.-D. M. Saleh, R. F. Aglan (Eds.), *Heavy Metals*, IntechOpen, Rijeka, 2018, Ch. 7. [doi:10.5772/intechopen.76082](https://doi.org/10.5772/intechopen.76082). URL <https://doi.org/10.5772/intechopen.76082>
- [37] S. Chen, C. Xue, J. Wang, H. Feng, Y. Wang, Q. Ma, D. Wang, Adsorption of pb(ii) and cd(ii) by squid *Ommastrephes bartrami* melanin, *Bioinorg. Chem. Appl.* 2009 (7) (2009) 901563. [doi:10.1155/2009/901563](https://doi.org/10.1155/2009/901563).
- [38] L. Hong, J. D. Simon, Current understanding of the binding sites, capacity, affinity, and biological significance of metals in melanin, *J. Phys. Chem. B* 111 (28) (2007) 7938–7947. [doi:10.1021/jp071439h](https://doi.org/10.1021/jp071439h).
- [39] J. Borovansky, Zinc in pigmented cells and structures, interactions and possible roles, *Sborn. Lek.* 95 (4) (1994) 309–320.
- [40] R. Salceda, G. Sanchez-Chavez, Calcium uptake, release and ryanodine binding in melanosomes from retinal pigment epithelium, *Cell Calcium* 27 (4) (2000) 223–229.
- [41] J. M. Bowness, R. A. Morton, Distribution of copper and zinc in the eyes of fresh-water fishes and frogs. occurrence of metals in melanin fractions from eye tissues, *Biochem. J.* 51 (4) (1952) 530–535.
- [42] J. A. Panessa, B. J.; Zadunaisky, Pigment granules: a calcium reservoir in the vertebrate eye, *Exp. Eye Res.* 32 (5) (1981) 593–604. [doi:10.1016/S0014-4835\(81\)80008-5](https://doi.org/10.1016/S0014-4835(81)80008-5).
- [43] B. Larsson, H. Tjalve, Studies on melanin-affinity of metal-ions, *Acta Physiol. Scand.* 104 (4) (1978) 479–484. [doi:10.1111/j.1748-1716.1978.tb06303.x](https://doi.org/10.1111/j.1748-1716.1978.tb06303.x).
- [44] L. Weidenbacher, E. Muller, A. G. Guex, M. Zundel, P. Schweizer, V. Marina, C. Adlhart, L. Vejsadova, R. Pauer, E. Spiecker, K. Maniura-Weber, S. J. Ferguson, R. M. Rossi, M. Rottmar, G. Fortunato, *In Vitro* endothelialization of surface-integrated nanofiber networks for stretchable blood interfaces, *ACS Appl. Mater. Interfaces* 11 (6) (2019) 5740–5751. [doi:10.1021/acsami.8b18121](https://doi.org/10.1021/acsami.8b18121).

[45] J. E. Efome, D. Rana, T. Matsuura, C. Q. Lan, Insight studies on metal-organic framework nanofibrous membrane adsorption and activation for heavy metal ions removal from aqueous solution, *ACS Appl. Mater. Interfaces* 10 (22) (2018) 315–324. [doi:10.1021/acsami.8b01454](https://doi.org/10.1021/acsami.8b01454).

[46] A. Morel, S. C. Oberle, S. Ulrich, G. Yazgan, F. Spano, S. J. Ferguson, G. Fortunato, R. M. Rossi, Revealing non-crystalline polymer superstructures within electrospun fibers through solvent-induced phase rearrangements, *Nanoscale* 11 (2019) 16788–16800. [doi:10.1039/C9NR04432A](https://doi.org/10.1039/C9NR04432A).

Supporting Information

Fungal Melanin-Based Electrospun Membranes for Heavy Metal Detoxification of Water

Anh N. Tran-Ly^{a,b}, Javier Ribera^b, Francis W.M.R. Schwarze^b, Marzia Brunelli^c, Giuseppino Fortunato^c

^aDepartment of Civil, Environmental and Geomatic Engineering, ETH Zurich, Stefano-Francini-Platz 5, Postfach 193, CH-8093 Zurich, Switzerland

^bLaboratory for Cellulose and Wood Materials, Empa, Lerchenfeldstrasse 5, CH-9014 St. Gallen, Switzerland

^cLaboratory for Biomimetic Membranes and Textiles, Empa, Lerchenfeldstrasse 5, CH-9014 St. Gallen, Switzerland

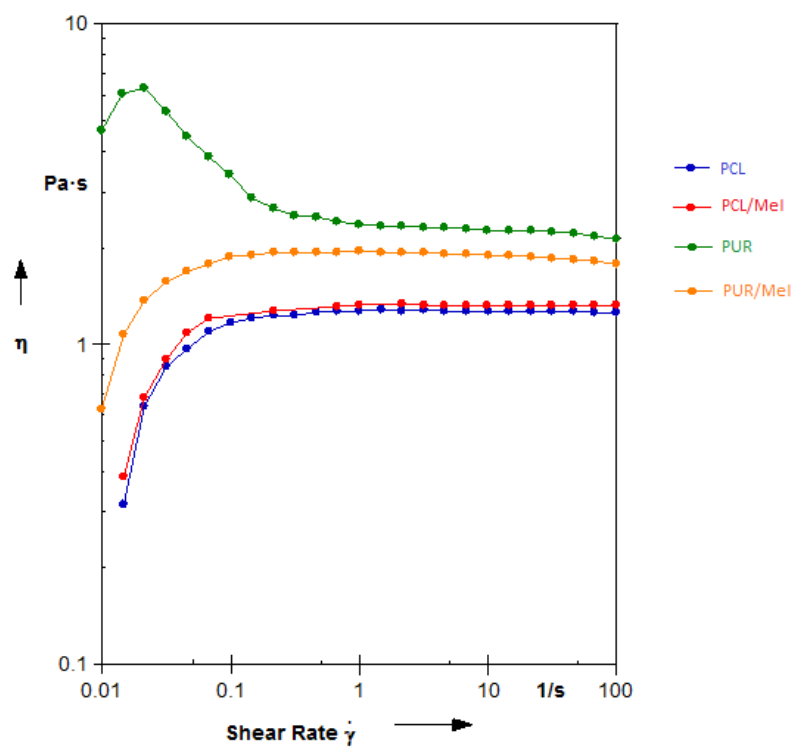


Fig. S 1 Viscosity flow curve of PCL, PCL/Mel, PUR and PUR/Mel spinning dispersions

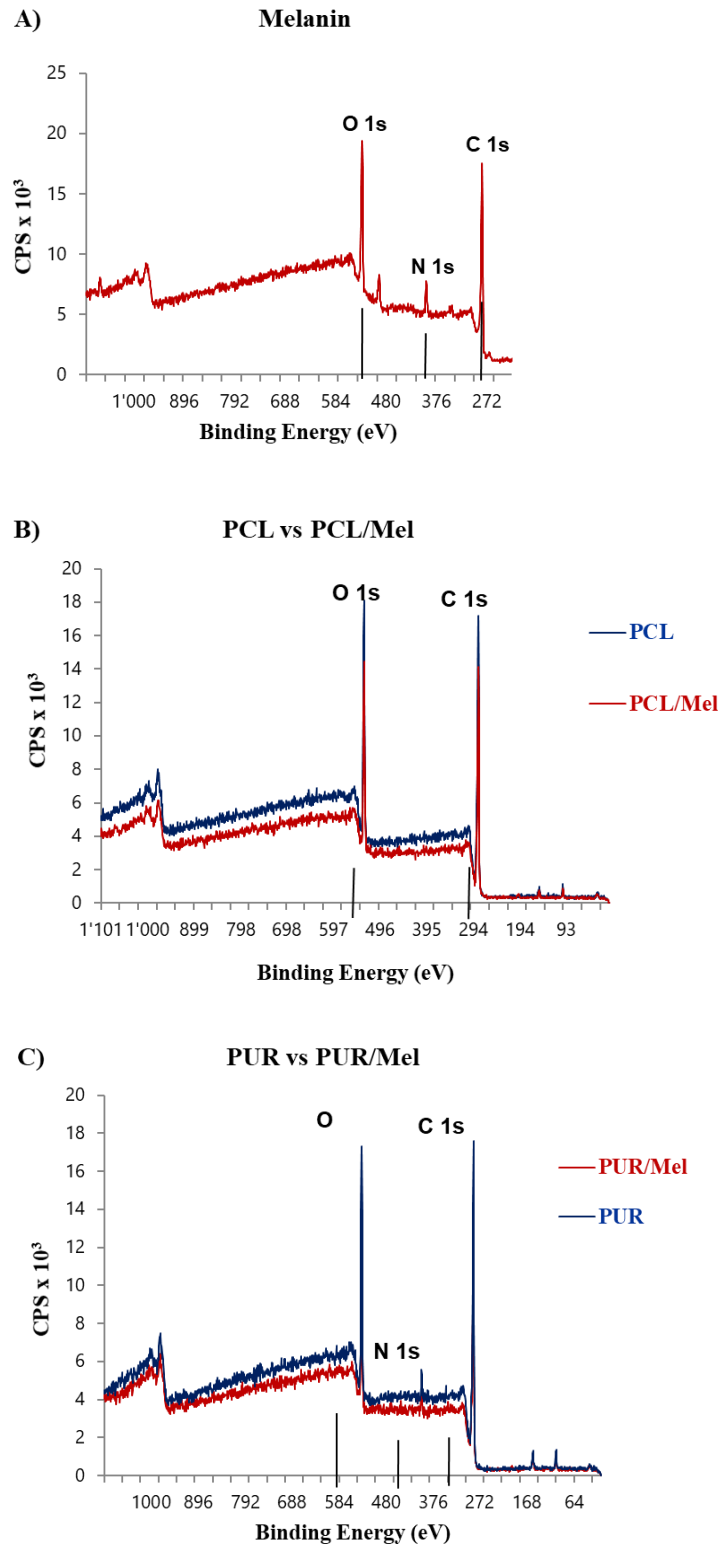


Fig. S 2 Representative XPS spectra of A) Raw melanin; B) PCL and PCL/Mel; C) PUR and PUR/Mel

Table S 1. Comparison of heavy metal adsorption of melanised membranes with other adsorbents

Heavy metal	Adsorbents	Time to reach maximum adsorption capacity (h)
-------------	------------	---

	Saw dust	3
	Activated carbon from Algerian dates stones of <i>Phoenix dactylifera.L</i>	2
	Activated carbon from <i>Eichhornia</i>	100 min
Pb ²⁺	Activated carbon from plant biomass of <i>Euphorbia rigida</i>	50 min
	<i>Mucor rouxii</i> biomass	6
	PAN/MOF electrospun membrane	3
	Melanin from marine bacteria <i>Pseudomonas stutzeri</i>	3
	Present study: PCL/Mel and PUR/Mel membranes	40 min
	Bone char	2
	Carbon slurry	70 min
	Coconut fiber	72
Cr ³⁺ /Cr ⁶⁺	Hazelnut shell activated carbon	72
	Tamarind Hull based adsorbent	15
	Melanin from marine bacteria <i>Pseudomonas stutzeri</i>	3
	Present study: PCL/Mel and PUR/Mel membranes	60 and 40 min
Cd ²⁺	PAN/MOF electrospun membrane	3
	Present study: PCL/Mel and PUR/Mel membranes	60 min

2.2. Melanized-Cationic Cellulose Nanofibers Foams for Bioinspired Removal of Cationic Dyes

Anh N. Tran-Ly,^{a,b} Kevin J. De France,^c Patrick Rupper,^d Francis W.M.R. Schwarze,^a Carolina Reyes,^c Gustav Nyström,^c Gilberto Siqueira,^c Javier Ribera^a

^aLaboratory for Cellulose & Wood Materials, Empa – Swiss Federal Laboratories for Materials Science and Technology, Lerchenfeldstrasse 5, 9014 St. Gallen, Switzerland

^bDepartment of Civil, Environmental and Geomatic Engineering, ETH Zurich, Stefano-Francini Platz 5, Postfach 193, CH-8093 Zurich, Switzerland

^cLaboratory for Cellulose & Wood Materials, Empa – Swiss Federal Laboratories for Materials Science and Technology, Überlandstrasse 129, 8600 Dübendorf, Switzerland

^dLaboratory for Advanced Fibers, Empa – Swiss Federal Laboratories for Materials Science and Technology, Lerchenfeldstrasse 5, 9014 St. Gallen, Switzerland

ABSTRACT

In recent years, water pollution has developed into a severe environmental and public health problem due to rapid urbanization and industrialization, especially in some developing countries. Finding solutions to tackle water pollution is urgently required and is of global importance. Currently, a range of water treatment methods are available, however, a water remediation process that is simple, inexpensive, ecofriendly, and effective for removal of pollutants down to ppm/ppb concentrations, has long been sought after. Herein, we describe a novel approach using fungal melanin for developing melanized-cationic cellulose nanofibers (melanized-C-CNF) foams that can successfully remove pollutants in water systems. The foam can be recycled several times while retaining its adsorption/desorption property, indicating high practicability for adsorbing the cationic dye crystal violet. This work highlights the opportunity to combine both advanced features of sustainable polymers such as cellulose and the unique properties of fungal melanin to manufacture bio-hybrid composites for water purification.

2.2.1. Introduction

Water is the most important resource on earth. All living organisms depend on water for their survival. Even though access to clean water is recognized as a basic human right, one out of every eight people lack access to safe drinking water.¹ Due to increased human activity and industrialization, a wide range of physical, chemical, and biological pollutants have entered into various water resources, with several negative consequences. Among these pollutants, organic contaminants such as dyes that are widely used in textile, plastic, paint, and paper industries are of great concern because of their high toxicity and non-degradable properties as well as their bio-accumulation and bio-magnification in the food chain.² Industrial effluents must be free of organic dyes before being released into the environment. A wide range of technologies for organic dye removal from water have been established, and are mainly based on two general strategies; degradation and adsorption.³ While degradation technologies such as photo catalysis allow the complete conversion of dye molecules into CO₂ and water, resulting in highly clean water, their high operational cost and need for sophisticated instruments hinder their use in low-income areas. Adsorption technologies, which rely on adsorbents that are designed for binding of organic dyes, are simpler in terms of applications and can be performed by non-experts.⁴ The use of sustainable materials for water treatment need to be manufactured at a large scale. They must be efficient in removing organic dyes down to ppm/ppb level within a short time, and should allow for multiple use cycles.

Melanins are natural biopolymers, with a black or dark brown color, and are ubiquitous in all biological kingdoms including humans, plants, bacteria and fungi.^{5, 6} Melanins are complex molecules, most often organized in supramolecular polymer structures, which result from the oxidative polymerization of phenolic compounds such as catechol and 1,8-dihydroxynaphthalene (DHN) (allomelanin, pyromelanin), 3,4-dihydroxyphenylalanine (DOPA) (eumelanin) and cysteinyl-DOPA (pheomelanin).⁵ In nature, many different sources of melanin are available, however, the most commonly used sources are ink of cephalopods (such as in squid, *Sepia*

officinalis), sheep wool, human hair and different types of bacteria and fungi.⁷ The melanin extracted from fungi can be obtained at a large scale with a simple preparation procedure thus facilitating its practical application. Moreover, the ability of the negatively charged melanin to form stable complexes with metals and a wide range of organic molecules (including drugs and antibiotics) makes melanin interesting for the development of bioremediation technologies.⁸ Recent studies demonstrated that fungal melanin that is incorporated into electrospun Polyurethane/Polycaprolactone membranes could remove up to 90% of heavy metals in single-component solutions indicating its potential for water treatment.⁹

Cellulose is the most abundant biopolymers on earth and can be used as a sustainable alternative for traditional polymers. Cellulose has been reported in various types of bio filters for effluent treatment. For instance, Sehaqui et al.^{10, 11} studied several cellulose and chitin modifications to introduce negative charges on the surface of the fibers to retain silver, copper, nickel, chromium and zinc ions demonstrating the removal of up to 64% silver ions and 55% crystal violet in water solutions. Crystal violet is a common synthetic molecule that belongs to the group of cationic triphenylmethane dyes and has been extensively used in paper and textile industry.¹² This dye has been extensively studied due to its teratogenic and carcinogenic effects in living organisms.¹³

Combining melanin with biopolymers (e.g. cellulose,¹⁴ chitosan,¹⁵ silk fibroin¹⁶ and lignin nanoparticles¹⁷) has attracted great attention recently. However, the potential of melanin in combination with the latter biopolymers for water purification systems has been rarely studied to date. Thus herein, we present the possibility to use melanized-C-CNF foams with improved mechanical properties and minimal shrinkage in bio-filtration systems, immobilizing water contaminants such as the model dye crystal violet.

2.2.2. Materials and methods

Cationic cellulose nanofibers (C-CNF) preparation

Elemental chlorine free (ECF) cellulose fibers were mixed with an aqueous solution of 5 wt% sodium hydroxide (NaOH) to obtain a suspension of 7.5 wt% cellulose pulp. Subsequently, 1.25 mL of glycidyltrimethylammonium chloride per gram of cellulose pulp was added under stirring conditions and mixed at 65 °C for 8 h.¹⁸ The modified cellulose was then neutralized with hydrochloric acid 37% and filtered to remove the liquid phase. The produced cellulose nanofibers (CNF) were washed with distilled water 3 times to remove impurities. This chemically modified pulp was dispersed in water at a concentration of 1 wt% and disintegrated into cationic cellulose nanofibers (C-CNF) using a grinding device (Supermass Colloider MKZA10-20J CE).

Fungal melanin biosynthesis

Fungal growth medium was prepared according to previous studies by Ribera et al.¹⁹ containing 1% peptone, 1% D-glucose, 0.1% yeast extract with 0.05% KH_2PO_4 , 0.02% $\text{MgSO}_4 \cdot 7\text{H}_2\text{O}$, 0.01% $\text{FeSO}_4 \cdot 7\text{H}_2\text{O}$, 0.0005% CuSO_4 and 3% L-tyrosine. Erlenmeyer flasks containing 300 mL of the growth medium were sterilized by autoclaving for 20 min at 121 °C and 1 bar. Five plugs of the fungus *Armillaria cepistipes* (Empa 655) were extracted from the margins of freshly growing cultures on 4% Malt Extract Agar and used to inoculate the Erlenmeyer flasks. Fungal cultures were cultivated in the flasks under constant shaking (150 rpm) at 22 °C and 70% relative humidity. After 16 weeks, the supernatant was filtered and centrifuged at 4000 rpm for 1 min to remove the biomass and cell debris. The obtained supernatant was extracted and autoclaved, which is hereafter referred to as "melanin solution". The concentration of melanin was quantified with the UV-Vis spectrophotometer (GENESYS™ 10S, Thermo Fischer Switzerland). A standard curve for natural melanin (obtained by melanin from *Sepia officinalis*, Sigma Aldrich) was used as a reference. (Figure S1).

Fabrication of melanized- C-CNF foams

Different amounts of melanin solution were added to 10 mL of C-CNF suspension 1 wt% in falcon tubes and the volume was filled up to 40 mL with milli-Q water and shaken overnight at 150 rpm. The pH of the solutions was adjusted at pH=6.5 as the use of the fabricated melanized-C-CNF foams was expected to perform at the standard pH ranges for drinking water. The mixtures were subsequently centrifuged at 4000 rpm for 20 min. The C-CNF with adsorbed melanin (hereafter melanized-C-CNF) was brought to the bottom of the tube. The supernatant was collected and measured with a UV-Vis spectrophotometer to determine the concentration of excess free melanin.

After defining the optimal ratio of CNF:Melanin (550 mg melanin per g of C-CNF), mixtures of melanized-C-CNF were produced in batches with the same ratio for experiments to ensure the consistency of the results. Thereafter, the melanized-C-CNF samples were frozen at -20 °C overnight before lyophilizing under vacuum at ambient temperature using an Alpha 3-4 LSC basic freeze-dryer (Martin Christ GmbH, Germany). The density of the melanized-C-CNF foams was determined by the weight and volume of the yielded foams. C-CNF foams with similar density were prepared in the same manner for control experiments.

Characterization of melanized-C-CNF foams

Optical density measurements were performed using a Genesys 10S UV-Vis spectrophotometer with standard poly(styrene) cuvettes (optical path 1 cm), scanning a wavelength range from 300 nm to 800 nm. Attenuated total reflection Fourier-transform infrared spectra (ATR-FTIR) were measured directly with the lyophilized samples using a Varian 640-IR Spectrometer equipped with a diamond window. Scans were taken from 650 to 4000 cm^{-1} with a resolution of 4 cm^{-1} . Scanning electron microscopy (SEM) was carried out using a Hitachi S-4800 scanning electron microscope (Hitachi) equipped with an INCA X-Sight EDS (Oxford Instruments) detector. The samples were fixed on a conductive carbon tape and sputter-coated with 5 nm of Au/Pd alloy

to facilitate imaging. The surface chemical composition of the various samples (CNF foam, melanin, melanized-C-CNF foam) was analyzed by X-ray photoelectron spectroscopy (XPS) using a Scanning XPS Microprobe (PHI VersaProbe II spectrometer, Physical Electronics) with monochromatic Al K α radiation (1486.6 eV) and a take-off angle of 45° (with respect to the sample surface). Two to three random spots per sample were analyzed with a microfocused X-ray beam of 100 μm diameter (operated at a power of 25 W at 15 kV) and dual beam charge neutralization. The melanin sample was pressed onto an indium foil (no indium signal was observed in the spectra), while the two other foam samples (CNF and melanized-C-CNF) were directly adhered to a stainless steel holder via double-sided-adhesive tape. Survey scan spectra (0-1100 eV) were acquired with 0.8 eV energy step width, 187.85 eV pass energy and 200 ms acquisition time per data point. In addition, higher-resolution narrow spectra for the elements carbon C 1s, oxygen O 1s and nitrogen N 1s were acquired (0.125 eV energy step width, 29.35 eV pass energy, 2.4 s acquisition time per data point). Obtained spectra were shifted relative to the aliphatic carbon (C-C) at 285.0 eV. Intensity determination and curve fitting was carried out with CasaXPS (software version 2.3.16) using a fixed 70% Gaussian, 30% Lorentzian product function to fit the XPS spectra. Thereby, a Shirley type background was used to calculate atomic concentrations. More details and parameters about the XPS measurements were previously published by Ribera et al.¹⁹ To perform zeta potential measurements, 1 mL of melanin suspensions in ethanol were centrifuged for 10 min at 20000 rpm. The resulting pellet was re-dispersed in an aqueous solution of 10% phosphate buffered saline (PBS, pH = 7.4). The conductivity of the samples was kept below 2 mS cm⁻¹. Each sample was measured three times and the results were averaged. Specific surface area was calculated by the Brunauer-Emmett-Teller (BET) method on a Micromeritics 3 Flex (Micromeritics, USA) device, whereby samples were degassed at 75 °C for 18 h under vacuum prior to the measurements. Note that for samples with BET surface area values below $\sim 30 \text{ m}^2 \text{ g}^{-1}$, equipment error

estimates are in the range of 10% of the measured values. Compression testing was performed on a Zwick Z010 device equipped with a 20 N load cell. Samples were compressed at a rate of 1 mm min⁻¹ to 80% strain, whereby the E-modulus was calculated from the initial linear portion of the stress-strain curves, and the compressive stress was taken as the recorded stress at maximum strain (80%). Compression testing was repeated in at least quadruplicate, with results presented as the average \pm standard deviation.

Water purification studies with melanized-C-CNF foams

In batch adsorption studies, a stock dye solution (5 g L⁻¹) was prepared by dissolving crystal violet (Merck, Germany) in deionized water. Different crystal violet solutions at defined concentrations were obtained by diluting from the stock solution. To determine the optimal contact time to reach the maximum adsorption capacity, 15 mg melanized-C-CNF foams were submerged in 40 mL of crystal violet solution at concentrations of 25 mg L⁻¹. The falcon tubes were shaken at 150 rpm and aliquots of dye solutions were taken at different time intervals from 0 to 480 min. The adsorbed concentrations were measured with the UV-Vis spectrophotometer at 590 nm. A calibration curve with different crystal violet concentrations was prepared for the adsorption calculations (Figure S2). After the optimum time was determined (1h), a new set of experiments was performed to assess the effect of initial dye concentration (5-200 mg L⁻¹) on the adsorption efficiency of the melanized-C-CNF foams using the above method.

The C-CNF foams without melanin and raw melanin were also tested as controls. Dye adsorption capacity (q_e) and removal rate (Y %) were calculated as follows:

$$Y\% = \frac{C_0 - C_e}{C_0} \times 100\% \quad (1)$$

$$q_e = \frac{(C_0 - C_e) \times V}{m} \quad (2)$$

where C_0 and C_e are the initial and equilibrium crystal violet concentrations (mg L⁻¹); V is the solution volume (L); m is the amount of used adsorbent in the adsorption process (g), q_e (mg g⁻¹) is the adsorption concentration at equilibrium.

Adsorption isotherm models

Three isotherm models, Langmuir,²⁰ Freundlich²¹ and Redlich-Peterson,²² which establish the relationship between the adsorption capacity (q_e) and equilibrium concentration (C_e) at constant temperature (25 °C) and pH = 6.5, were employed to study how the adsorbate (crystal violet) interacts with the adsorbent (melanized-C-CNF foams).

The Langmuir model assumes that the adsorbent surface is homogeneous and the adsorption is a monolayer process. The expression of the Langmuir isotherm is represented by the following equation:

$$\frac{1}{q_e} = \frac{1}{Q_m} + \frac{1}{K_L Q_m} \times \frac{1}{C_e} \quad (3)$$

where Q_m (mg g⁻¹) is the maximum adsorption capacity, C_e is the concentration at equilibrium and K_L (L g⁻¹) is the Langmuir constant, which represents the energy of adsorption. The plot of $1/q_e$ as a function of $1/C_e$ allows the determination of Q_m and K_L .

Furthermore, the separation factor R_L was obtained from the following equation:

$$R_L = \frac{1}{1 + K_L C_0} \quad (4)$$

The constant R_L indicates the favorability of the adsorption process. If $R_L=0$, the adsorption is irreversible; if $0 < R_L < 1$ the adsorption is favorable. The adsorption profile is linear when $R_L = 1$ ($K_L = 0$). When $R_L > 1$ ($K_L < 0$), the adsorption is unfavorable.

The Freundlich isotherm describes non-ideal, multilayer adsorption at a heterogeneous adsorbent surface. The adsorptive sites are presumed to exhibit different binding energies. The model is represented by the following equation:

$$\log(q_e) = \log K_F + \left(\frac{1}{n}\right) \log C_e \quad (5)$$

where K_F and $1/n$ are the Freundlich constants that indicate the adsorption capacity and the adsorption intensity, respectively. When $1/n < 1$, the adsorption is strong, e.g. chemisorption,

whereas $1/n > 1$ is indicative of cooperative adsorption. The values of K_F and n were obtained from the plot of $\log(q_e)$ versus $\log C_e$.

Finally, the Redlich-Peterson (R-P) model was used as a combination of both Langmuir and Freundlich approaches. The model can be applied in either homogeneous or heterogeneous systems, providing a more accurate representation of adsorption equilibrium over a wide range of concentration. The equation for R-P model is described as follows:

$$q_e = \frac{K_R C_e}{1 + a_R C_e^\beta} \quad (6)$$

where K_R ($L g^{-1}$) and a_R ($L mg^{-1}$) are the R-P constants and the exponent β varies between 0 and 1. A nonlinear plot of q_e versus C_e gives out the values of K_R , a_R and β .

2.7 Adsorption kinetic models

The adsorption kinetics control the adsorption rate, which determines the time needed for the foams to reach the equilibrium. Three kinetic models, namely pseudo-first-order, pseudo-second-order and Weber's intraparticle diffusion, were applied to understand the characteristics of the adsorption process such as the adsorption pathways and probable mechanism involved.

According to Lagergren,²³ the pseudo-first-order model is expressed as:

$$\frac{dq_t}{dt} = k_1(q_e - q_t) \quad (7)$$

Equation (7) can, however, be converted to the linear form:

$$\log(q_e - q_t) = \log(q_e) - \frac{k_1}{2.303} t \quad (8)$$

where q_e and q_t ($mg g^{-1}$) are the adsorption capacities at equilibrium and at time t , respectively; k_1 is the rate constant (min^{-1}) in the pseudo-first-order kinetic model. The value of k_1 can be found from the linear plot of $\log(q_e - q_t)$ versus time.

The differential equation for the pseudo-second-order kinetic model was given by Ho and McKay²⁴ as follows:

$$\frac{dq_t}{dt} = k_2(q_e - q_t)^2 \quad (9)$$

After mathematical development, the linearized form of the above equation is expressed as:

$$\frac{t}{q_t} = \frac{1}{k_2 q_e^2} + \frac{t}{q_e} \quad (10)$$

where q_e and q_t (mg g^{-1}) are the adsorption capacity at equilibrium and at time t while k_2 ($\text{g mg}^{-1} \text{ min}^{-1}$) is the pseudo-second-order rate constant. By plotting t/q_t as a function of time t , the values of q_e and k_2 were calculated.

To study the diffusion mechanism in the adsorption process, the intraparticle mass transfer diffusion model proposed by Weber and Morris²⁵ was employed:

$$q_t = k_i t^{0.5} + C \quad (11)$$

where k_i ($\text{mg g}^{-1} \text{ min}^{-1/2}$) is the intraparticle diffusion rate while C gives information about the thickness of the boundary layer.

Desorption and recyclability of the melanized-C-CNF foams

Desorption experiments were conducted to investigate the reusability of the melanized-C-CNF foams. For this purpose, 15 mg of crystal violet-loaded foams at the equilibrium were placed in falcon tubes filled with 40 mL of 0.1 M HCl and were shaken for 2 h at 150 rpm. After that, the foams were washed again in similar manner with 40 mL of Ethanol 90% (2 h, 150 rpm). The re-collected foams were then used for 5 more adsorption/desorption cycles by repeating the same procedure.

2.2.3. Results and discussion

Fabrication of melanized-C-CNF foams

C-CNF was mixed with different concentrations of fungal melanin to obtain bio-hybrid composites whereby the melanin incorporation was maximized during the freeze drying process (Figure 1). The results demonstrated that at low concentrations (below 600 mg g^{-1}), the incor-

poration of fungal melanin into the C-CNF network followed a linear relationship. At concentrations above 700 mg of fungal melanin per gram of C-CNF, melanin loading plateaued, indicating a saturation of the C-CNF network. The maximum adsorption capacity of 1 gram of C-CNF was in the range of up to 548.4 mg of fungal melanin, representing saturation of the cationic residues for C-CNF by the negatively charged melanin. Importantly, the adsorption capacity obtained here via electrostatic complexation between C-CNF and melanin was significantly higher than previous values reported in the literature. For instance, Sehaqui et al.¹¹ reported a maximum adsorption capacity of 310 mg humic acid per gram of C-CNF. When compared to other sorbents such as chitosan beads (150 mg g⁻¹),²⁶ ZnO nanoparticles (100 mg g⁻¹)²⁷ or goethite and gibbsite (100 and 70 mg g⁻¹, respectively),²⁸ the adsorption capacity was more than 5 times higher in the current study.

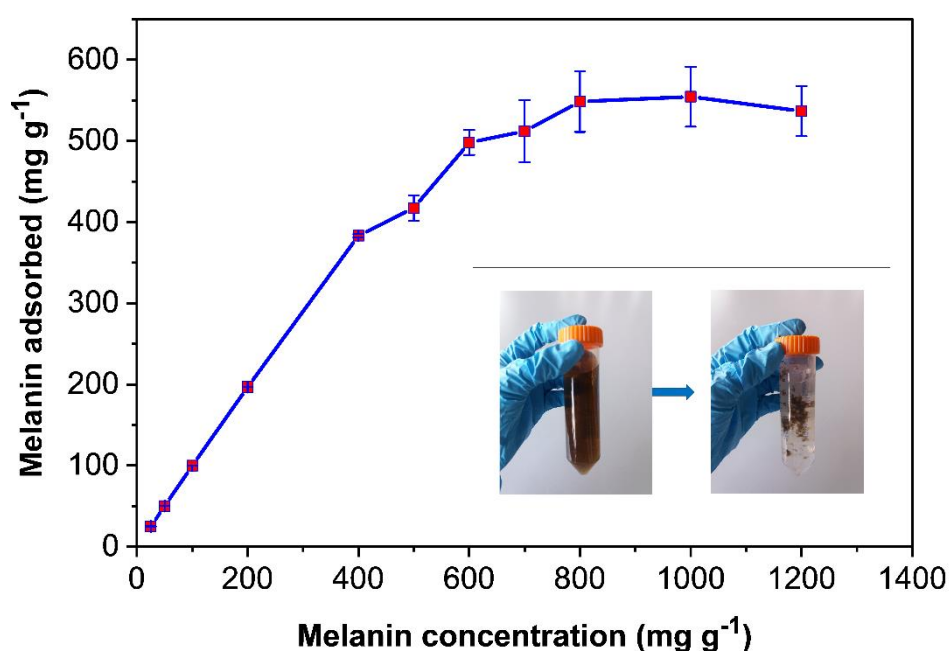


Figure 1. Adsorption capacity of fungal melanin by C-CNF versus loading (the unit mg g⁻¹ expresses the amount of adsorbed melanin per gram of C-CNF). Inset: left: a dark brown solution of melanin showing 10 mg L⁻¹ added to 10 mL of C-CNF suspension; right: the adsorption of melanin by C-CNF after shaking overnight showing a clear supernatant solution.

Characterization of melanized-C-CNF foams

i) Scanning electron microscopy

Freeze-drying the suspensions resulted in highly porous foams which displayed a density of 0.015 g cm^{-3} . SEM micrographs of the fabricated C-CNF foams (with and without fungal melanin) are shown in Figure 2. The control C-CNF foams showed a typical highly porous network structure as demonstrated also in other studies for C-CNF foams/aerogels.¹¹ The incorporation of fungal melanin leads to a more compact and organized porous structure, associated with increased crosslinking and reinforcement, leading to increased stability. This was mainly attributed to the electrostatic interactions between the negatively charged fungal melanin and the positively charged C-CNF.

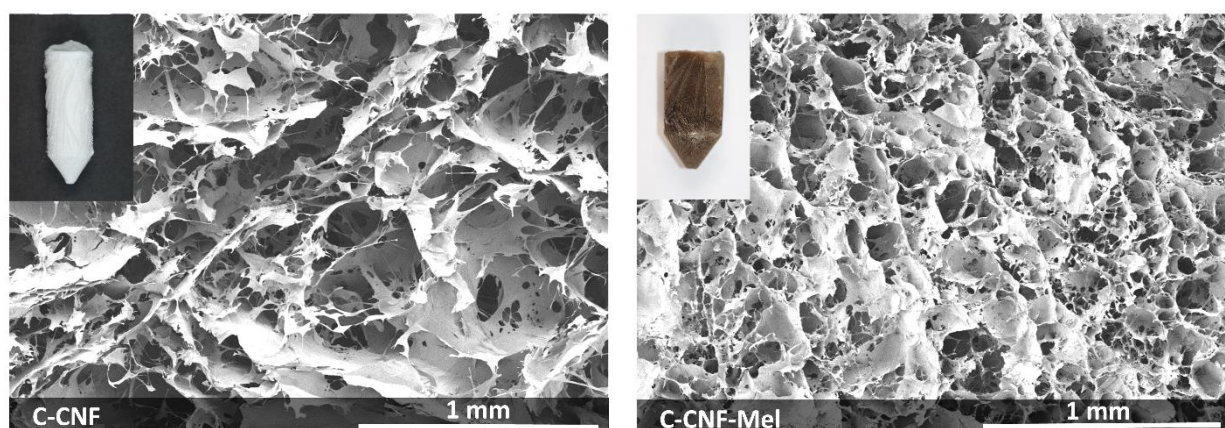


Figure 2. SEM image of the microscopic structure of C-CNF (left) and melanized-C-CNF foams (right).

ii) BET analysis and Zeta potential

The effects of the combination of fungal melanin and C-CNF foams were further investigated via BET analysis (Table 1). The C-CNF foams displayed a specific surface area of $\sim 16.4 \text{ m}^2 \text{ g}^{-1}$, which was consistent with other cellulose nanofibers foams prepared via freeze drying.²⁹ The addition of fungal melanin resulted in a decrease in the specific surface area to $\sim 8.5 \text{ m}^2 \text{ g}^{-1}$, which can be attributed to the electrostatic complexation between the positively charged cellulose nanofibers and negatively charged melanin as discussed above. This strong complexation leads to a collapse in nanopores between individual cellulose nanofibers, manifesting a decrease

in total pore volume of pores less than 10 nm in size (Figure S3). This electrostatic complexation was further confirmed by Zeta potential measurements (Table 1), whereby the melanized-C-CNF foams had a zeta potential in-between that of the two control biopolymers.

Table 1. Physical properties of melanin, C-CNF foams and melanized-C-CNF foams.

	Melanin	C-CNF	C-CNF-Mel
Zeta potential (mV)	-47.7	+56.45	-32.6
BET surface area (m ² g ⁻¹)	-	16.4	8.5
Shrinkage (%)	-	22.6 ± 2.1	3.2 ± 0.1
E-Modulus (kPa)	-	24 ± 4	370 ± 93
σ ₈₀ (kPa)	-	52 ± 8	152 ± 23

iii) Mechanical properties of the melanized-C-CNF foams

The effects of combining fungal melanin to the C-CNF foams on the mechanical properties were also investigated. Compression strength was performed up to 80% strain as shown in Figure 3 and Figure S4. Here, C-CNF foams exhibited an E-modulus of 24 ± 4 kPa, reaching an average maximum stress of 52 ± 8 kPa at 80% strain. The addition of fungal melanin resulted in a drastic increase in both values, up to 370 ± 93 kPa (E-modulus) and 152 ± 23 kPa (maximum stress), respectively. Notably, the E-modulus increased by over an order of magnitude, demonstrating the strong interactions between C-CNF and melanin via electrostatic complexation. This was also evidenced in the shape of the stress-strain curves for both samples; the pure C-CNF foams exhibited a smooth gradual increase in stress with increasing strain, indicative of material densification with little structural resistance towards the applied stress. On the other hand, melanized-C-CNF foams exhibited a more traditional 3-stage response to increasing strain; initially, a strong linear response was observed, corresponding to the foam cell-walls providing structural resistance against strain. This was followed by a plateau region where the

pore walls begin to buckle due to the applied stress, and finally by a densification region corresponding to material compaction. This was also supported by the SEM analysis mentioned above, whereby the melanized-C-CNF foams showed a relatively regular cellular pore structure while the C-CNF foams showed a much more heterogeneous and irregular morphology. Finally, these results were further supported by foam shrinkage measurements, whereby the C-CNF foams exhibited an average shrinkage of $22.6\% \pm 2.1$, indicative of a relative lack of pore-wall integrity leading to partial collapse upon drying. Conversely, the melanized-C-CNF foams exhibited an average shrinkage of only $3.2\% \pm 0.1$, demonstrating an increased structural integrity.

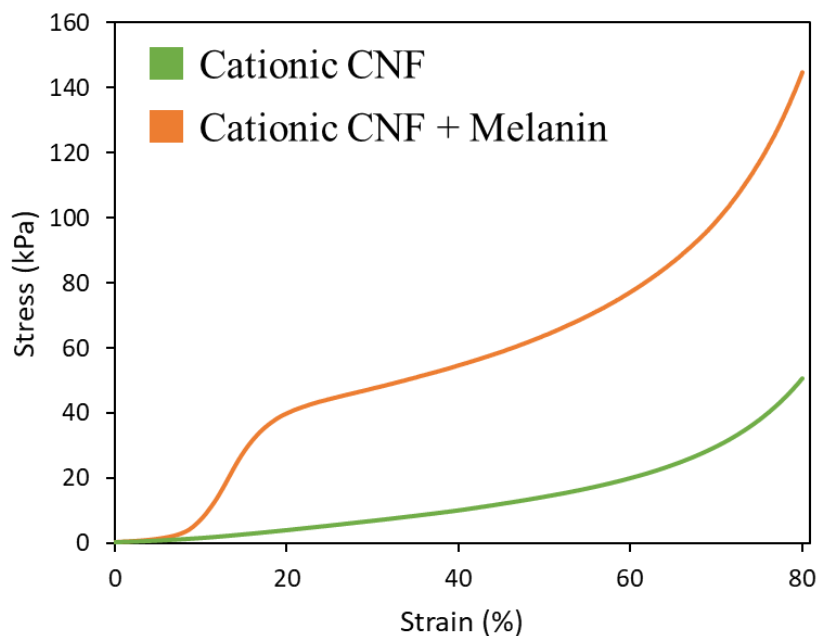


Figure 3. Representative compressive stress-strain curves of the C-CNF and melanized-C-CNF foams.

iv) X-ray photoelectron spectroscopy

To gain insight into the surface composition of the foams as well as the structure of melanin, XPS measurements were performed. Table 2 compares the elemental concentrations for C-CNF foams, melanin powder and melanized-C-CNF foams, and Figure 4a depicts the corresponding XPS survey spectra. While, as expected, in C-CNF foams only carbon (C) and oxygen (O) elements were observed, nitrogen (N) was additionally present in both melanin as well as melanized-C-CNF. This confirmed the presence of melanin in the melanized-C-CNF foams and

hence the success of the fabrication method. Small impurities of silicon (≤ 1 atomic %), attributed to production of the melanized-C-CNF sample, were present in the sample. The energetic positions of the element silicon, hardly visible at the chosen intensity scale, are marked with asterisks in Figure 4a. The melanin sample itself contained some contamination with sodium chloride (partly associated with the growth medium), which was not present anymore in the melanized-C-CNF foams due to a thorough washing during the samples fabrication. All samples were quite homogenous, as no position-dependent variation in the XPS elemental composition was observed, resulting in adequate standard deviations from a few measurements at different areas on the sample (Table 2). The elemental ratio between carbon, oxygen and nitrogen (atomic ratio C/O/N obtained by the survey scan) of melanin was 9.5/4.2/1 and in good agreement with the melanin samples investigated by Ribera et al.¹⁹ having a C/O/N = 9.1/4.0/1. Because C-CNF did not contain any nitrogen, the nitrogen content was reduced compared to that of oxygen and carbon in the melanized-C-CNF samples, resulting in a C/O/N ratio of 15.9/9.4/1. Assuming dihydroxyindole as the main component in melanin¹⁹ and using a maximum adsorption of 1 part melanin per 1.6 parts of CNF (see before, and using the molecular weights of cellulose and dihydroxyindole), a final nitrogen concentration of 3.5% would result for the melanized-C-CNF foam. This was in good agreement with the measured value (see Table 2). The mixture of C-CNF and melanin was also observed in the high-resolution XPS C 1s spectra (Figure S5). Whereas melanin mostly consisted of C-C bonds with some C-N and C-O bonds and minor part of C=O and O-C=O bonds (see Ribera et al.¹⁹), the strongest peak in the cellulose sample was, as expected from the chemical structure, the C-O bond with some smaller amount of O-C-O. The C 1s spectrum of melanized-C-CNF showed strong contributions from C-C, C-N as well as C-O.

In order to compare the chemical state of raw melanin and in the melanized-C-CNF foam, high-resolution scans for nitrogen were obtained as illustrated in Figure 4b. The dotted lines represent the fitted composite peaks according to the presence of possible different nitrogen groups in

melanin: namely primary amines (399.1 eV), pyrrolic nitrogen in an indole ring (400.2 eV) and charged amine groups (401.2 eV). Thereby, the component peak energies were restricted to ± 0.5 eV of corresponding literature values.³⁰ No significant change on the surface chemistry of melanin was observed after incorporation of the melanin into the CNF foams. For both samples, the strongest component was pyrrolic nitrogen ($\geq 80\%$ of all nitrogen). Therefore, no major indole ring opening had taken place nor significant positively charged melanin was formed. It seems likely that negative charges in the oxygen functionalities of melanin lead to electrostatically bonding to the CNF. Thus, the intact melanin structure of the melanized-C-CNF foams provides the full potential of melanin for removal of charged dyes.

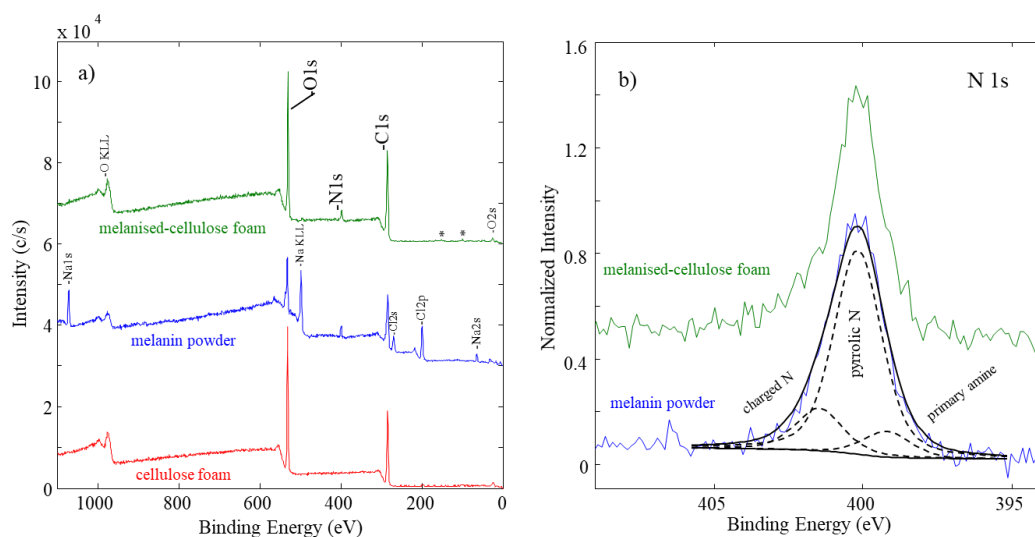


Figure 4. (a) Comparison of XPS survey spectra of C-CNF foam, raw melanin and melanized-C-CNF foams. Peak positions of silicone are marked with asterisks. (b) N 1s high-resolution scans (full lines) and functional components from the curve fitting (dotted lines) for raw melanin as well as melanized-C-CNF foam. In both figures, the spectra are offset in the y-direction for better visualization.

Table 2. Elemental composition^a for C-CNF foams, raw melanin and melanized-C-CNF foams obtained from XPS survey scans.

Sample	O	C	N
C-CNF foam	44.2 ^b \pm 0.8 ^c	55.8 \pm 1.0	-
Melanin	28.7 \pm 1.0	64.5 \pm 2.8	6.8 \pm 0.5

Melanized-C-CNF foam	35.7 ± 1.2	60.5 ± 1.5	3.8 ± 0.6
----------------------	----------------	----------------	---------------

^aSilicon (in the case of melanized-C-CNF) was only detected in minor concentrations. Melanin was slightly contaminated with sodium chloride (from the growth medium). In order to directly compare the three samples, Si, Na and Cl were not taken into account in the analysis.

^bThe values are given in atomic percentage concentrations and were normalized to 100%. ^cStandard deviation in the average of three measurements at different areas of the sample.

v) Fourier transform infrared spectroscopy

Melanized-C-CNF foams complexation was also investigated via FTIR (Figure 5). For C-CNF, prominent peaks centered around 3340 cm^{-1} and 1040 cm^{-1} were observed, corresponding to O-H and C-O stretching vibrations, respectively, as expected for cellulosic samples.³¹ Complexation with melanin resulted in an increase in peak intensity around 1630 cm^{-1} , corresponding to C=C, C=N, and C=O vibrations of melanin, indicating successful complexation.

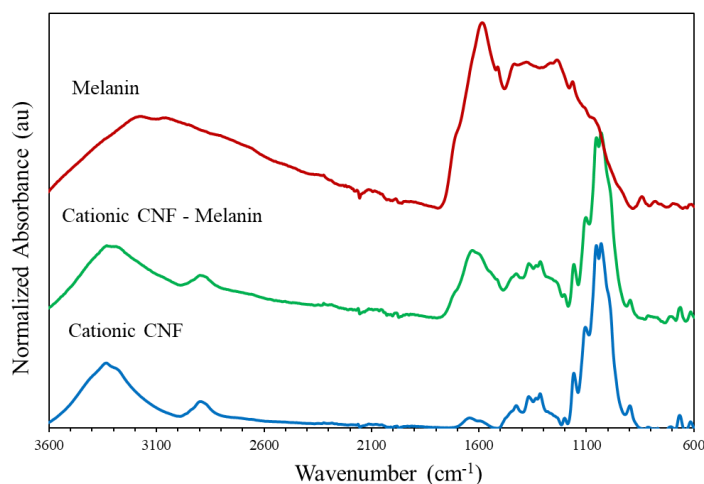


Figure 5. FTIR spectra of melanin, C-CNF and melanized-C-CNF foams.

Water purification studies with melanized-C-CNF foams

vi) Effect of contact time on crystal violet adsorption

The effect of contact time on the adsorption of crystal violet by the melanized-C-CNF foams is displayed in Figure 6. An increase in contact time had a positive effect on the adsorption within the first 45 min; however, the process slowed down at 60 min and appeared to plateau after 180

min. At this point, most of the adsorptive sites were occupied, thus, there were fewer sites available for the remaining adsorbate molecules. At the dye concentration of 25 mg L^{-1} , melanized-C-CNF foams achieved a maximal adsorption of 98.3% crystal violet within 90 min, which was among the fastest adsorbents for crystal violet. For upscaling applications, bioadsorbent materials for organic dyes need an average contact time of 300 min to reach adsorption equilibrium.³² In other studies, different materials such as Korean cabbage biochar,³³ EDTA functionalized corncob,³⁴ alginate/acid activated beads³⁵ and carboxylated sugarcane bagasse³⁶ required 180, 200, 240, 720 min to reach equilibrium, respectively. The dye concentration in the solution after adsorption was reduced to 0.425 ppm. This sub-ppm indicates a remarkable performance of the foam for dye removal. Raw fungal melanin and C-CNF foams were used as controls exhibiting negligible effect on dye removal ($< 2\%$). This was expected in the case of C-CNF foams as both the adsorbent and adsorbate shared the same positive charges. In the case of raw melanin, it can be inferred that melanin particles self-aggregated into supramolecular structures,³⁷ resulting in less surface area and therefore lower adsorption. The synergistic effect between fungal melanin and cellulose nanofibers allowed for a higher degree of surface reactivity for melanin resulting in an efficient bio-hybrid composite. This high performance during the initial 45 min can be attributed to the strong interactions between the adsorbent and adsorbate.

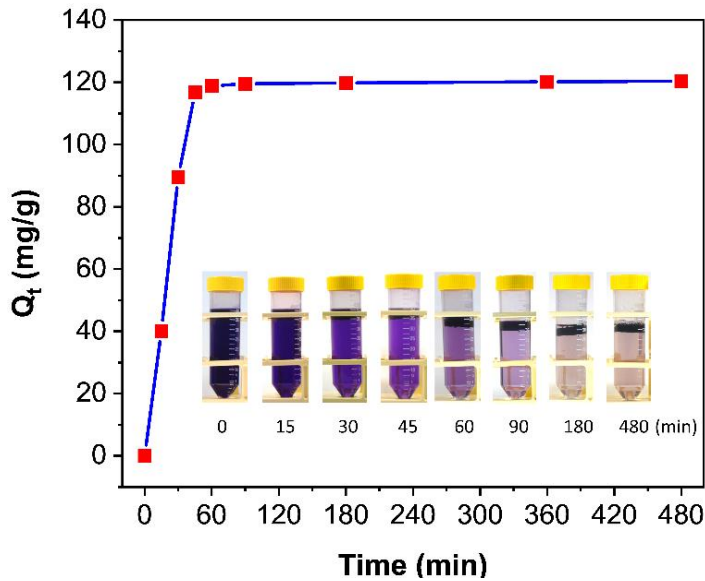


Figure 6: Effect of contact time on the removal percentage of crystal violet (conditions: Volume = 40 mL, pH = 6.5, adsorbent dose = 15 mg foams corresponding to 8.226 mg melanin, initial dye concentration = 25 mg L⁻¹).

vii) Effect of initial dye concentration on adsorption

The influence of initial concentrations of crystal violet on the removal efficiency of melanized-C-CNF foams is illustrated in Figure 7. At low concentrations (from 5 to 15 mg L⁻¹) and 60 min of contact time, the dye removal percentages were 94-96%. At higher initial concentrations of crystal violet, the percentage of dye removal was decreased. This can be explained by the decreased ratio of biosorptive surface to adsorbate molecule number and the saturation of all available binding sites as the equilibrium was gradually reached at higher concentration. Therefore, melanized-C-CNF foams demonstrated promising results to reduce the concentrations of water contaminants such as crystal violet to ppb level (< 30 mg L⁻¹).

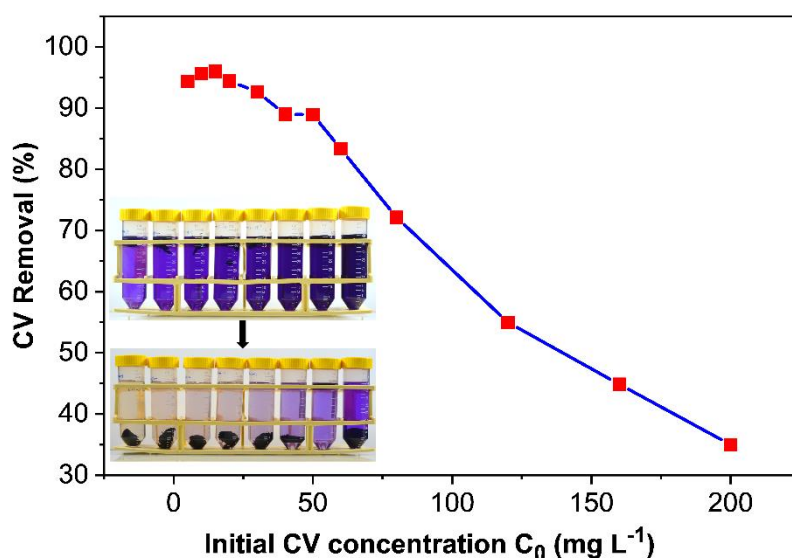


Figure 7: Effect of initial concentration on removal percentage of crystal violet (conditions: volume = 40 mL, pH = 6.5, adsorbent dose = 15 mg foams corresponding to 8.23 mg of melanin, dye concentration ranges from 5 to 200 mg L⁻¹).

viii) Adsorption isotherm studies

Different adsorption isotherm models were developed to analyze the interactions between the crystal violet adsorbate and the melanized-C-CNF foams. The isotherm results provided an estimation of the capacity of the adsorbent as well as the sorption process characteristics such as the surface properties and the adsorption mechanism. Therefore, well-fitted models facilitate the design of effective and economical treatment for various application purposes.³⁸ Among various models available in the literature, Langmuir,²⁰ Freundlich²¹ and Redlich-Peterson²² models are commonly selected to assess the adsorption values. The applicability of the models to best fit the experimental data was checked by the correlation coefficient R^2 .

The fits are shown in Figure S6, and the parameters obtained from each fit are presented in Table 3. As shown in Figure S6, the adsorption profile was best fit by the Redlich-Peterson model, suggesting that the mechanism of adsorption was complex and did not follow ideal monolayer adsorption. The β value was close to 1, indicating that the adsorption was close to

the Langmuir model. We propose that the adsorption was mainly due to the electrostatic interaction between the negatively charged melanized-C-CNF foams (Table 1, zeta potential = -32.6 mV) and the positively charged dye molecules however, a small number of dye molecules can also be adsorbed via weak van der Waals interactions.

As indicated in Table 3, the calculated Q_m achieved by melanized-C-CNF foam was 425.5 mg g^{-1} . Studies by Lin et al.³⁹ showed the possibility to use fungal mycelium prepared from grinded mycelial biomass of *Ceriporia lacerate*. The produced biosorbent composite was applied in a water purification system with a maximum uptake of 239 mg of crystal violet per gram of biomass. Kumari et al.⁴⁰ achieved a maximum removal of 30 mg Kg^{-1} crystal violet by using a mixture of *Typha latifolia* activated carbon/Chitosan composite. Another study by Wang et al.⁴¹ proposed the use of a combination of EDTA and corncob to remove a maximum concentration of 185-203 mg g^{-1} crystal violet at optimal conditions. In this context, the adsorption capacity of melanized-C-CNF foam was among the most efficient biosorbent materials found in the literature.

Table 3. Langmuir, Freundlich and Redlich-Peterson model isotherm parameters for crystal violet adsorption by melanized-C-CNF foams.

Isotherm model	Parameter	
Langmuir	Q_m (mg g^{-1})	425.532
	K_L	0.229
	R_L	0.068
	R^2	0.9469
Freundlich	K_F (mg g^{-1})(mg L^{-1}) ⁿ	75.706
	N	2.581
	R^2	0.852

Redlich-Peterson	K_R (L g ⁻¹)	127.759
	a_R (L mg ⁻¹)	0.502
	B	0.930
	R^2	0.993

ix) Adsorption kinetic studies

Three kinetic models (pseudo-first order, pseudo-second order, and Weber's intra-particle diffusion) were used to gain insight into the adsorption pathways and probable mechanism. The adsorption kinetic parameters are shown in Table 4. As shown in Figure S7, the adsorption profile was not fit to the pseudo-first order model ($R^2 = 0.380$) but fit well to the pseudo-second order model ($R^2 = 0.999$). The q_e obtained from the fit corresponded well with the experimental one. This indicated that chemisorption was dominant for the adsorption of crystal violet by the melanized-C-CNF foams.

However, the above models may not give the full picture of the adsorption process. According to Güzel et al.,⁴² the adsorption commonly comprises four steps: i) bulk diffusion: transportation of the adsorbate from the bulk to the liquid film surrounding the adsorbent, ii) external diffusion: the adsorbate molecules diffuse across the surface liquid film, iii) intraparticle diffusion: the adsorbate molecules diffuse to the surface of the adsorbent via pore diffusion or surface diffusion depending on the porosity of the adsorbent, and iv) interaction with the surface sites, either by physi- or chemisorption. The first and last steps are relatively fast and are not considered as rate controlling steps. To investigate the diffusion mechanism involved in the process, the Weber and Morris kinetic model was employed. As the data exhibited multilinear plots, the adsorption profile shown in Figure S7c was separated into two parts (Stage I: Q_t changes rapidly with time, and Stage II \rightarrow III: the adsorption was stabilized and finally reached an equilibrium). For the Weber and Morris model, $C = 0$ (the plot passes through the origin) indicated that intraparticle diffusion was the rate-limiting step. When $C > 0$, both external mass transfer and

intraparticle diffusion were the rate limiting steps. When the fit provides negative value of C , as in this case for Stage I, this can be interpreted as an external film diffusion resistance causing the time lag for the adsorption.^{43, 44} Despite this, the study suggests that the organic dyes are rapidly adsorbed on the surface (Stage I), before intraparticle diffusion is controlled where the adsorbates move slowly from larger pores to micropores causing a slow adsorption rate (Stage II \rightarrow III).

Table 4. Adsorption kinetic parameters for crystal violet onto melanized-C-CNF foams.

Kinetic model	Parameters	
Pseudo-first order	k_1 (min^{-1})	0.090
	q_e (mg g^{-1})	7.441
	R^2	0.380
Pseudo-second order	k_2 ($\text{g mg}^{-1} \text{min}^{-1}$)	0.071
	q_e (mg g^{-1})	121.065
	R^2	0.999
Intra-particle diffusion (Stage I)	k_i ($\text{g mg}^{-1} \text{min}^{-1}$)	210.807
	C (mg g^{-1})	-63.562
	R^2	0.984
Intra-particle diffusion (Stage II \rightarrow III)	k_i ($\text{g mg}^{-1} \text{min}^{-1}$)	0.263
	C (mg g^{-1})	119.172
	R^2	0.737

Reusability of melanized-C-CNF foams

Reusability of an adsorbent is a crucial indicator for the economic feasibility of water treatments. In order to compete with the existing purification technologies, the materials must be produced at industrial scale and low cost, as well as be reusable. In this experiment, the removal

efficiency of melanized-C-CNF foams was reduced about 10% over 6 adsorption/desorption cycles (from 93.0% to 83.7%) (Figure 8). Previous studies reported that gel beads of $\text{Fe}_3\text{O}_4/\text{CD}/\text{AC}/\text{SA}$ polymer nanocomposite lost about 5% of its removal efficiency after 6 cycles⁴⁵ and about 20% for EDTA/graphene oxide functionalized corncob after 9 cycles.⁴¹ However, it can be noticed that these composites required more complex fabrication processes. Therefore, even with partial loss of the removal efficiency, melanized-C-CNF foams proved to be an interesting adsorbent for cationic dyes after 6 recycling cycles. We hypothesize that the reduced efficiency may be due to the loss of fungal melanin through the recycling process. Thus, further work to improve the stability of the foam will enhance the reusability and performance of melanized-C-CNF foams for water treatment.

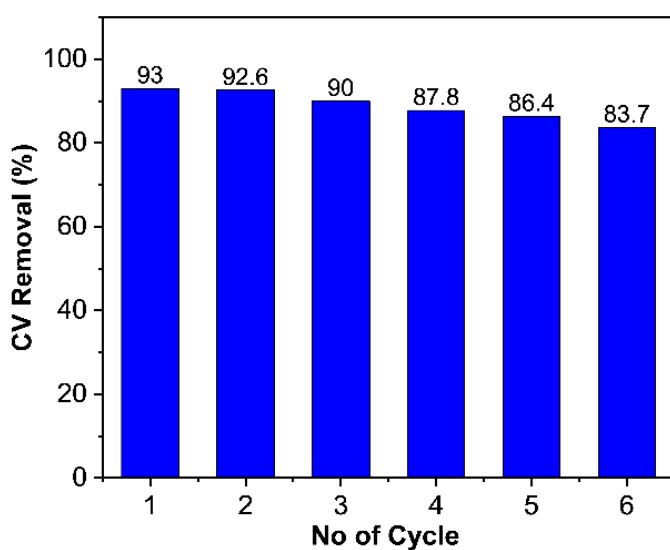


Figure 8. Reusability tests of crystal violet using regenerated melanized-C-CNF foams.

2.2.4. Conclusions

Melanized-C-CNF foams were successfully prepared via electrostatic complexation of negatively charged fungal melanin and positively charged CNF. Importantly, the use of melanized-C-CNF foams, which are environmentally friendly materials, as a promising biosorbent for water purification systems was demonstrated, whereby up to 93% of crystal violet was absorbed during the first adsorption cycle. The removal efficiency of crystal violet by the melanized-C-

CNF foams remained higher than 80% even after 6 adsorption/desorption cycles. These findings on melanized bio-hybrid composites can also be used to explore future multifunctional materials in different fields such as bioelectronics, biomedicine or environmental sensing devices.

Supporting Information: Standard curve of fungal melanin; Standard curve of crystal violet dye; Adsorption–desorption isotherms curves and pore size distributions; Compression properties; High-resolution XPS C 1s spectra; Adsorption isotherm models for crystal violet removal.

Conflict of interest

There are no conflicts to declare.

Acknowledgements

The authors thank Deeptanshu Sivaraman for help with BET measurements. K.D. gratefully acknowledges funding from the Natural Sciences and Engineering Research Council of Canada (NSERC) Postdoctoral Fellowship program.

References

1. Assembly, U. N. G., Resolution A/RES/64/292: The human right to water and sanitation. **2010**.
2. Toth, G.; Hermann, T.; Da Silva, M. R.; Montanarella, L., Heavy metals in agricultural soils of the European Union with implications for food safety. *Environ. Int.* **2016**, *88*, 299-309.
3. Ahmad, A.; Mohd-Setapar, S. H.; Chuong, C. S.; Khatoon, A.; Wani, W. A.; Kumar, R.; Rafatullah, M., Recent advances in new generation dye removal technologies: novel search for approaches to reprocess wastewater. *RSC Adv.* **2015**, *5* (39), 30801-30818.
4. Kyzas, G. Z.; Fu, J.; Matis, K. A., The Change from Past to Future for Adsorbent Materials in Treatment of Dyeing Wastewaters. *Materials.* **2013**, *6* (11), 5131-5158.
5. Solano, F., Melanin and Melanin-Related Polymers as Materials with Biomedical and Biotechnological Applications-Cuttlefish Ink and Mussel Foot Proteins as Inspired Biomolecules. *Int. J. Mol. Sci.* **2017**, *18* (7), 1561.
6. d'Ischia, M.; Wakamatsu, K.; Cicoira, F.; Di Mauro, E.; Garcia-Borron, J. C.; Commo, S.; Galvan, I.; Ghanem, G.; Kenzo, K.; Meredith, P.; Pezzella, A.; Santato, C.; Sarna, T.; Simon, J. D.; Zecca, L.; Zucca, F. A.; Napolitano, A.; Ito, S., Melanins and

melanogenesis: from pigment cells to human health and technological applications. *Pigm. Cell Melanoma Res.* **2015**, *28* (5), 520-544.

7. Piatelli, M.; Fattorusso, E.; Nicolaus, R. A.; Magno, S., Structure of Melanins and Melanogenesis .5. Ustilagomelanin. *Tetrahedron.* **1965**, *21* (11), 3229-3236.

8. Thaira, H.; Raval, K.; Manirethan, V.; Balakrishnan, R. M., Melanin nano-pigments for heavy metal remediation from water. *Sep. Sci. Technol.* **2019**, *54* (2), 265-274.

9. Anh, N. T. L.; Ribera, J.; Schwarze, F. W. M. R.; Brunelli, M.; Fortunato, G., Fungal melanin-based electrospun membranes for heavy metal detoxification of water. *Sustainable Mater. Technol.* **2020**, *23*, e00146.

10. Sehaqui, H.; de Larraya, U. P.; Liu, P.; Pfenninger, N.; Mathew, A. P.; Zimmermann, T.; Tingaut, P., Enhancing adsorption of heavy metal ions onto biobased nanofibers from waste pulp residues for application in wastewater treatment. *Cellulose.* **2014**, *21* (4), 2831-2844.

11. Sehaqui, H.; de Larraya, U. P.; Tingaut, P.; Zimmermann, T., Humic acid adsorption onto cationic cellulose nanofibers for bioinspired removal of copper(II) and a positively charged dye. *Soft Matter.* **2015**, *11* (26), 5294-5300.

12. Ayati, A.; Shahrak, M. N.; Tanhaei, B.; Sillanpaa, M., Emerging adsorptive removal of azo dye by metal-organic frameworks. *Chemosphere.* **2016**, *160*, 30-44.

13. Roy, D. C.; Biswas, S. K.; Saha, A. K.; Sikdar, B.; Rahman, M.; Roy, A. K.; Prodhon, Z. H.; Tang, S. S., Biodegradation of Crystal Violet dye by bacteria isolated from textile industry effluents. *PeerJ.* **2018**, *6*, e5015.

14. Roy, S.; Kim, H. C.; Kim, J. W.; Zhai, L. D.; Zhu, Q. Y.; Kim, J., Incorporation of melanin nanoparticles improves UV-shielding, mechanical and antioxidant properties of cellulose nanofiber based nanocomposite films. *Mater. Today Commun.* **2020**, *24*, 100984.

15. Roy, S.; Van Hai, L.; Kim, H. C.; Zhai, L.; Kim, J., Preparation and characterization of synthetic melanin-like nanoparticles reinforced chitosan nanocomposite films. *Carbohydr. Polym.* **2020**, *231*, 115729.

16. Manchineella, S.; Thirivikraman, G.; Khanum, K. K.; Ramamurthy, P. C.; Basu, B.; Govindaraju, T., Pigmented Silk Nanofibrous Composite for Skeletal Muscle Tissue Engineering. *Adv. Healthcare Mater.* **2016**, *5* (10), 1222-1232.

17. Xing, Q. Q.; Buono, P.; Ruch, D.; Dubois, P.; Wu, L. B.; Wang, W. J., Biodegradable UV-Blocking Films through Core-Shell Lignin-Melanin Nanoparticles in Poly(butylene adipate-co-terephthalate). *ACS Sustainable Chem. Eng.* **2019**, *7* (4), 4147-4157.

18. Pei, A. H.; Butchosa, N.; Berglund, L. A.; Zhou, Q., Surface quaternized cellulose nanofibrils with high water absorbency and adsorption capacity for anionic dyes. *Soft Matter*. **2013**, *9* (6), 2047-2055.
19. Ribera, J.; Panzarasa, G.; Stobbe, A.; Osypova, A.; Rupper, P.; Klose, D.; Schwarze, F. W. M. R., Scalable Biosynthesis of Melanin by the Basidiomycete *Armillaria cepistipes*. *J. Agric. Food Chem.* **2019**, *67* (1), 132-139.
20. Langmuir, I., The Adsorption of Gases on Plane Surfaces of Glass, Mica and Platinum. *J. Am. Chem. Soc.* **1918**, *40*, 1361-1403.
21. Freundlich, H., Concerning adsorption in solutions. *Z. Phys. Chem-Stoch. Ve.* **1906**, *57* (4), 385-470.
22. Redlich, O.; Peterson, D. L., A Useful Adsorption Isotherm. *J. Phys. Chem.* **1959**, *63* (6), 1024-1024.
23. Lagergren, S., About the Theory of so Called Adsorption of Soluble Substances. *K. Sven. Vetenskapsakad. Handl.* **1898**, *24*, 39.
24. Ho, Y. S.; McKay, G., Pseudo-second order model for sorption processes. *Process Biochem.* **1999**, *34* (5), 451-465.
25. Weber, J. W. J., Morris, J.C., Kinetics of adsorption on carbon from solution. *J. Sanit. Eng. Div.* **1963**, *89*, 28.
26. Chang, M. Y.; Juang, R. S., Adsorption of tannic acid, humic acid, and dyes from water using the composite of chitosan and activated clay. *J. Colloid. Interface Sci.* **2004**, *278* (1), 18-25.
27. Yang, K.; Lin, D. H.; Xing, B. S., Interactions of Humic Acid with Nanosized Inorganic Oxides. *Langmuir*. **2009**, *25* (6), 3571-3576.
28. Parfitt, R. L.; Fraser, A. R.; Russell, J. D.; Farmer, V. C., Adsorption on Hydrous Oxides .2. Oxalate, Benzoate and Phosphate on Gibbsite. *Eur. J. Soil Sci.* **1977**, *28* (1), 40-47.
29. De France, K. J.; Hoare, T.; Cranston, E. D., Review of Hydrogels and Aerogels Containing Nanocellulose. *Chem. Mater.* **2017**, *29* (11), 4609-4631.
30. Beamson, G. B., D., *High Resolution XPS of Organic Polymers*. John Wiley & Sons: Chichester, U.K., 1992.
31. Soni, B.; Hassan, E. B.; Mahmoud, B., Chemical isolation and characterization of different cellulose nanofibers from cotton stalks. *Carbohydr Polym.* **2015**, *134*, 581-589.
32. Behera, S. S.; Das, S.; Parhi, P. K.; Tripathy, S. K.; Mohapatra, R. K.; Debata, M., Kinetics, thermodynamics and isotherm studies on adsorption of methyl orange from aqueous

solution using ion exchange resin Amberlite IRA-400. *Desalin. Water Treat.* **2017**, *60*, 249-260.

33. Sewu, D. D.; Boakye, P.; Woo, S. H., Highly efficient adsorption of cationic dye by biochar produced with Korean cabbage waste. *Bioresour. Technol.* **2017**, *224*, 206-213.

34. Chowdhury, A.; Kumari, S.; Khan, A. A.; Hussain, S., Selective removal of anionic dyes with exceptionally high adsorption capacity and removal of dichromate (Cr₂O₇²⁻) anion using Ni-Co-S/CTAB nanocomposites and its adsorption mechanism. *J. Hazard. Mater.* **2020**, *385*, 121602.

35. Oladipo, A. A.; Gazi, M., Enhanced removal of crystal violet by low cost alginate/acid activated bentonite composite beads: Optimization and modelling using non-linear regression technique. *J. Water Process Eng.* **2014**, *2*, 43-52.

36. Ferreira, B. C. S.; Teodoro, F. S.; Mageste, A. B.; Gil, L. F.; de Freitas, R. P.; Gurgel, L. V. A., Application of a new carboxylate-functionalized sugarcane bagasse for adsorptive removal of crystal violet from aqueous solution: Kinetic, equilibrium and thermodynamic studies. *Ind. Crops Prod.* **2015**, *65*, 521-534.

37. Pralea, I. E.; Moldovan, R. C.; Petrache, A. M.; Ilies, M.; Heghes, S. C.; Ielciu, I.; Nicoara, R.; Moldovan, M.; Ene, M.; Radu, M.; Uifalean, A.; Iuga, C. A., From Extraction to Advanced Analytical Methods: The Challenges of Melanin Analysis. *Int. J. Mol. Sci.* **2019**, *20* (16), 3943.

38. Yagub, M. T.; Sen, T. K.; Afroze, S.; Ang, H. M., Dye and its removal from aqueous solution by adsorption: A review. *Adv. Colloid Interface Sci.* **2014**, *209*, 172-184.

39. Lin, Y. H.; He, X. B.; Han, G. M.; Tian, Q. J.; Hu, W. Y., Removal of Crystal Violet from aqueous solution using powdered mycelial biomass of *Ceriporia lacerata* P2. *J. Environ. Sci.* **2011**, *23* (12), 2055-2062.

40. Kumari, H. J.; Krishnamoorthy, P.; Arumugam, T. K.; Radhakrishnan, S.; Vasudevan, D., An efficient removal of crystal violet dye from waste water by adsorption onto TLAC/Chitosan composite: A novel low cost adsorbent. *Int. J. Biol. Macromol.* **2017**, *96*, 324-333.

41. Wang, H.; Lai, X.; Zhao, W.; Chen, Y. N.; Yang, X. L.; Meng, X. H.; Li, Y. H., Efficient removal of crystal violet dye using EDTA/graphene oxide functionalized corncob: a novel low cost adsorbent. *RSC Adv.* **2019**, *9* (38), 21996-22003.

42. Guzel, F.; Saygili, H.; Saygili, G. A.; Koyuncu, F., Decolorisation of aqueous crystal violet solution by a new nanoporous carbon: Equilibrium and kinetic approach. *J. Ind. Eng. Chem.* **2014**, *20* (5), 3375-3386.

43. Zhu, Q. Y.; Moggridge, G. D.; D'Agostino, C., Adsorption of pyridine from aqueous solutions by polymeric adsorbents MN 200 and MN 500. Part 2: Kinetics and diffusion analysis. *Chem. Eng. J.* **2016**, *306*, 1223-1233.
44. Zhu, Q. Y.; Moggridge, G. D.; Ainte, M.; Mantle, M. D.; Gladden, L. F.; D'Agostino, C., Adsorption of pyridine from aqueous solutions by polymeric adsorbents MN 200 and MN 500. Part 1: Adsorption performance and PFG-NMR studies. *Chem. Eng. J.* **2016**, *306*, 67-76.
45. Yadav, S.; Asthana, A.; Singh, A. K.; Chakraborty, R.; Vidya, S. S.; Susan, M. A.; Carabineiro, S. A. C., Adsorption of cationic dyes, drugs and metal from aqueous solutions using a polymer composite of magnetic/beta-cyclodextrin/activated charcoal/Na alginate: Isotherm, kinetics and regeneration studies. *J. Hazard. Mater.* **2021**, *409*, 124840.

Supporting Information

Melanized-Cationic Cellulose Nanofibers Foams for Bioinspired Removal of Cationic Dyes

Anh N. Tran-Ly,^{a,b} Kevin J. De France,^c Patrick Rupper,^d Francis W.M.R. Schwarze,^a Carolina Reyes,^c Gustav Nyström,^c Gilberto Siqueira,^c Javier Ribera^a

^aLaboratory for Cellulose & Wood Materials, Empa – Swiss Federal Laboratories for Materials Science and Technology, Lerchenfeldstrasse 5, 9014 St. Gallen, Switzerland

^bDepartment of Civil, Environmental and Geomatic Engineering, ETH Zurich, Stefano-Francisini Platz 5, Postfach 193, CH-8093 Zurich, Switzerland

^cLaboratory for Cellulose & Wood Materials, Empa – Swiss Federal Laboratories for Materials Science and Technology, Überlandstrasse 129, 8600 Dübendorf, Switzerland

^dLaboratory for Advanced Fibers, Empa – Swiss Federal Laboratories for Materials Science and Technology, Lerchenfeldstrasse 5, 9014 St. Gallen, Switzerland

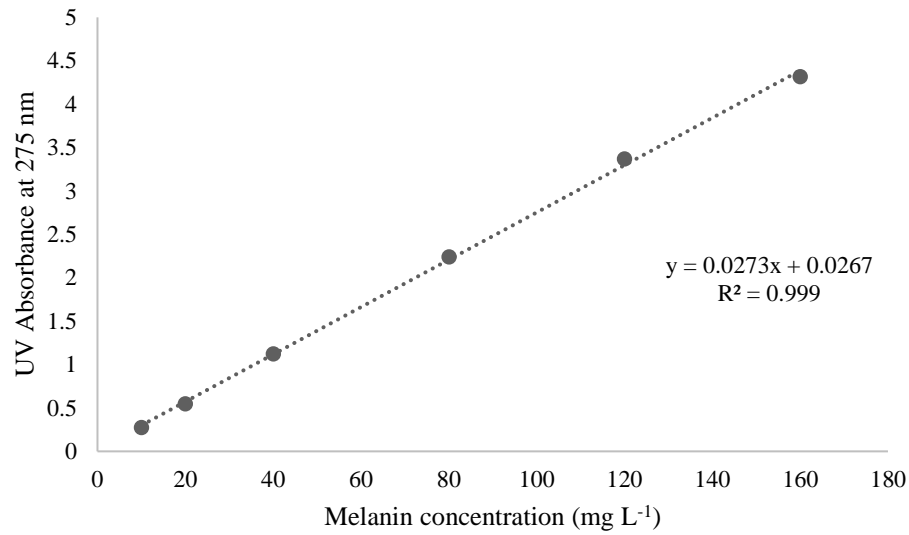


Figure S1. Standard curve of fungal melanin extracted from *Armillaria cepistipes* (Empa 655).

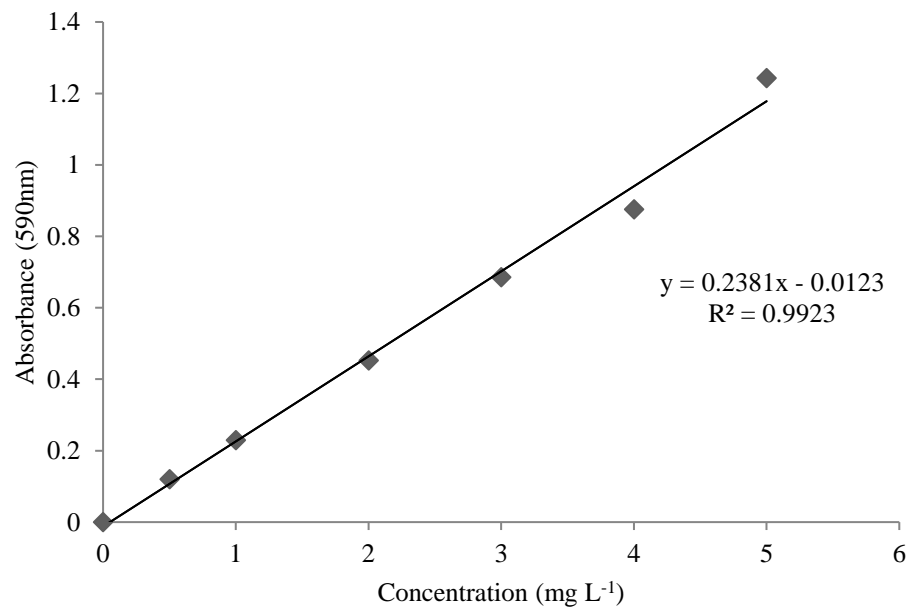


Figure S2. Standard curve of crystal violet dye.

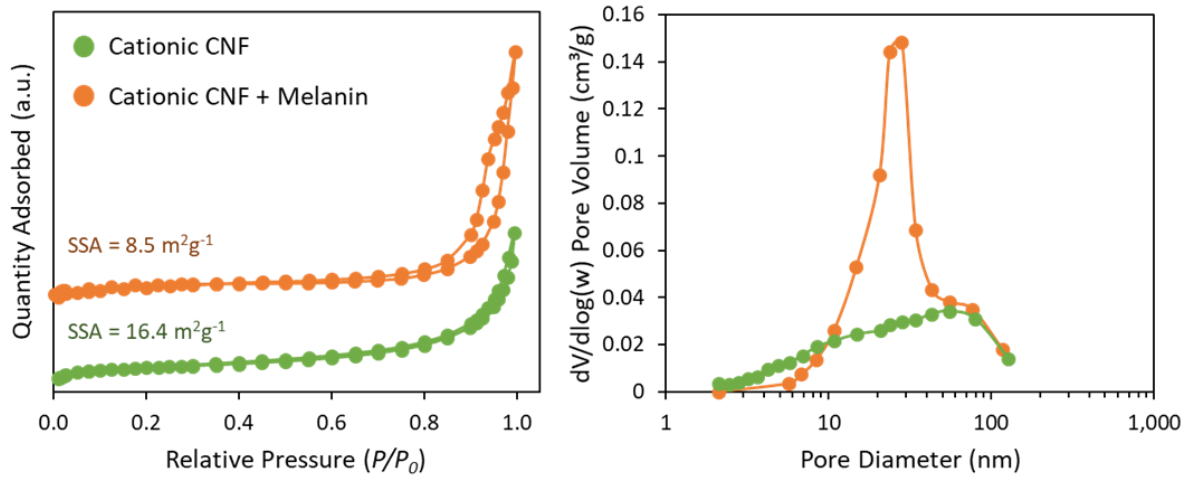


Figure S3. (left) Typical N_2 adsorption–desorption isotherms and (right) BJH pore size distributions of Cationic CNF and melanised-cellulose foams.

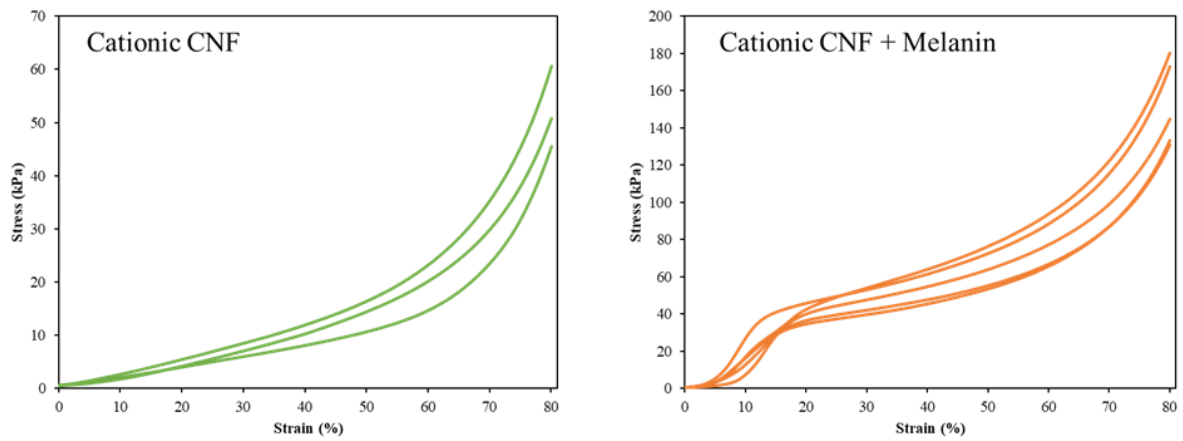


Figure S4. Compression measurements of the cationic cellulose (left) and melanised-cellulose foams (right).

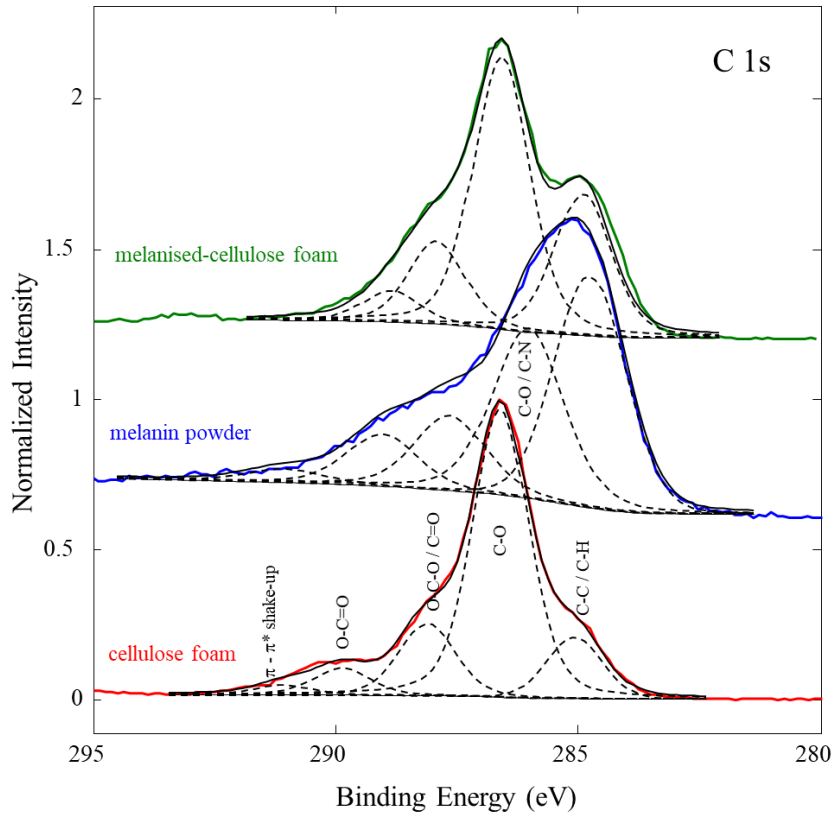


Figure S5. High-resolution XPS C 1s spectra.

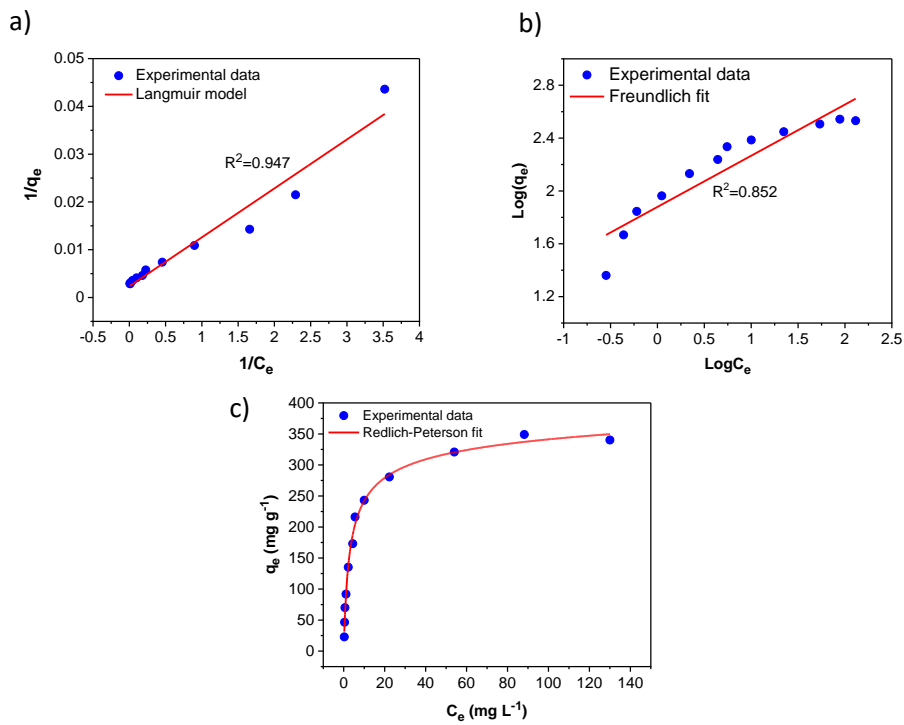


Figure S6. Different adsorption isotherm models for crystal violet removal by melanised-cellulose foams.

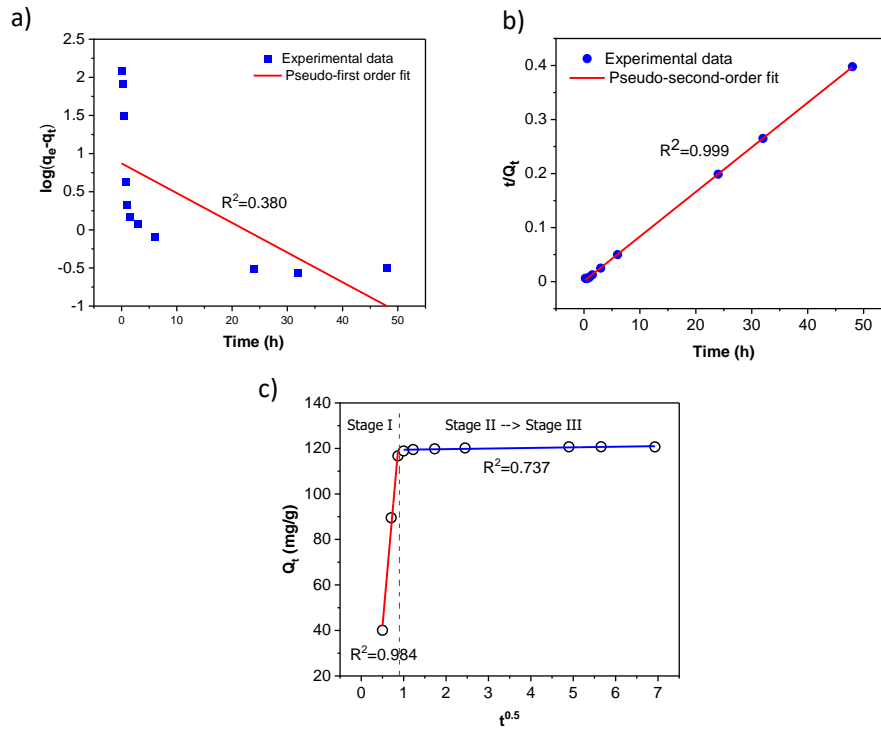


Figure S7. a) Pseudo-first order, b) Pseudo-second order and c) Weber-Morris intra-particle diffusion plots of crystal violet on melanised-cellulose foams.

2.3. Antimicrobial Effect of Fungal Melanin in Combination with Plant Oils for the Treatment of Wood

Anh N. Tran-Ly^{1,2}, Markus Heeb¹, Tine Kalac¹, Francis W.M.R. Schwarze¹

¹Laboratory for Applied Wood Materials, Empa, Lerchenfeldstrasse 5, St. Gallen 9014, Switzerland

²Department of Civil, Environmental and Geomatic Engineering, ETH Zurich, Stefano-Francini-Platz 5, Postfach 193, CH-8093 Zurich, Switzerland

Abstract

Microbial deterioration of wood has gradually destroyed precious and historic musical instruments. Serpentino (English: serpent/little snake), a wind instrument used over 400 years ago and considered the godfather of modern instruments such as the saxophone and the tuba, was totally ruined as the last original specimens were consumed due to the invasion of bacteria and fungi. Reconstructing the serpent in particular and other ancient instruments in general requires the preservation of wood from bio-deterioration. Conventional chemical preservatives based on copper and borate compounds have been used in wood processing industry; however, they are not ideal for protecting musical instruments and may pose a negative impact on the health and safety of musicians with direct contact. Non-biocidal preservatives, such as plant oils, have attracted a lot of attention. Herein, we report the antimicrobial efficacy of plant oils, alone and in combination with fungal melanin, in protecting walnut wood used to make the serpent against oral bacteria and wood-decay fungi. Linseed and tea tree oils were found to have a strong antibacterial effect, inhibiting the survival of *S. mutans*, the bacteria commonly found in human saliva, to below 1%. When melanin was also used, the double-impregnation of plant oils and melanin resulted in an accelerated and superior antibacterial response compared to that of the oil(s). A satisfactory antifungal effect was also achieved, with the survival rate of *Chaetomium globosum* on the radial longitudinal surface below 10% after 2 weeks. In addition,

the treated wood samples absorbed less water than the untreated ones and preserved their dimensions at different humidity conditions, highlighting the practicability of this approach for wood preservation.

2.3.1. Introduction

Wood used in historical buildings, ancient artworks or antique furniture is of great importance to human cultural heritage, as it provides valuable information about the past. However, wood is susceptible to various bio-deteriorating agents, which makes restoration and preservation of historical objects and features a significant and complicated process. In this work, reconstruction of Serpentino (in English: serpent/little snake), an ancient musical instrument used from the end of the 16th century to the middle of the 19th century,¹ is such an example. In the past this wind instrument was played in churches to support singing, as it covers the vocal registers of the human voice and can "carry" a choir.²

In the 19th century the serpent was replaced by less fragile, easier to manufacture and more virtuoso to play brass instruments such as ophicleide and tuba.³ However, with today's trend towards historically based performances, the renaissance of the serpent, along with other historical instruments, is of great interest.

In 2008, the Swiss serpent maker, Stephan Berger, developed a new processing method for production of the serpent, in order to counteract the technical inadequacies of the traditional instruments and to produce sound-perfect and robust instruments. However, the snake shape of the instrument (Figure 1) made of walnut (*Juglans regia* L.) wood does not only create an incomparable sound, but also ideal conditions for wood deterioration. Due to the water condensation from the musician's breath, a humid microclimate within the tube develops, which promotes the growth of wood decay fungi and bacteria. This was also the reason for the decomposition of the centuries-old instrument, with the last original specimens gradually being

destroyed as shown in Figure 1. To the best of our knowledge, no studies have to date investigated the microorganisms that colonize the serpent and cause wood decay.

To inhibit wood decay, chemical preservatives, either water-borne or oil-borne, are used. However, the preservation of wood instruments such as the serpent with wood preservatives is challenging since active substances, e.g. metal salts such as copper sulfate or zinc borate, although normally considered to have low mammalian toxicity, may pose negative impact on health and safety of musicians with direct contact.^{4,5} The interior tube of serpents is traditionally treated with linseed/ flaxseed (*Linum usitatissimum* L.) oil. Linseed oil is an inexpensive, biodegradable, and nontoxic vegetable oil with antimicrobial properties, which has recently attained a lot of interest for manufacturing of coatings.⁶⁻⁸ Humar and Lesar (2013) demonstrated that linseed oil is an effective substitute for the biocidal treatment of wood in less hazardous applications.⁹ Not only did linseed oil prove effective against wood decay fungi, but also reduced short-, medium-, and long-term water uptake. Panov and Terziev (2015) showed that epoxidized linseed oil is also efficient as a hydrophobic agent in combination with biocides, forming a suitable protective formulation for wood in both above- and in-soil exposure.¹⁰ Nevertheless, the use of linseed oil alone for the treatment of serpents is not adequate to prevent wood from biodeterioration by wood-decay fungi and bacteria.

In this work, we investigate the efficacy of environmentally friendly plant oils in combination with melanin, a bio-derived polymer, for the protection of wood of serpents. Melanin can be produced from *Armillaria* species, which are long lived and are among the largest living organisms in the world.¹¹ They are widespread wood decomposing fungi that spread in the soil by melanised rhizomorphs. Due to high amounts of incorporated melanin, the rhizomorphs can bind heavy metals¹² and are protected from environmental stresses, such as UV-radiation, elevated temperatures, antimicrobial agents and competition by antagonistic fungi and bacteria.¹³ We recently developed a simple and inexpensive method to synthesize and utilize

melanin produced by *A. cepistipes*¹⁴ for a range of industrial applications in several research fields.^{15,16}

Herein, we show that the combination of plant oils and melanin is an effective method to protect the wood of serpents against deterioration. Bacteria and fungi from naturally infected serpents were first isolated and used to artificially infect walnut wood. We conducted a number of bioassays on the efficacy of melanin-based coatings against the casual wood decay agents. This work highlights the potential use of the combination of melanin and plant oils as a simple and environmentally benign method for wood preservation.

2.3.2. Materials and methods

Isolation and identification of the casual decay microorganisms from infected wood

The microorganisms causing deterioration were isolated from a serpent no.18 made in January – February 2013 by Stephan Berger from walnut wood. In 2019 initial signs of internal decay were detected (Figure 1a). A wood sample containing decayed internal areas, approximately 5 cm × 2 cm (diameter × thickness), was excised from the serpent tube as indicated in Figure 1a. First, the extracted wood sample was lightly sprayed with ethanol to disinfect the exposed surface. Then, under sterile conditions, the sample was carefully broken across the decayed area, to expose a surface free of any potential contaminants. Using a sterile scalpel, wood samples approx. 5 × 5 mm in dimension were excised from the freshly exposed wood surface. The samples were then placed with sterile forceps in Petri dishes with 2% MEA (Malt Extract Agar, OXOID) for the isolation of deuteromycetes, or in addition with 20 ml of 2% MEA with 2 ml of thiabendazole dissolved in lactic acid (Merck, Darmstadt, Germany).¹⁷ This procedure was repeated ten times per growth media. The Petri dishes were sealed with Parafilm and maintained in the dark at 25°C and 65% relative humidity (RH) and growth was monitored daily. The successful isolations were then maintained on a cellulose-mineral-agar medium containing NaNO₃ (3.0 g), K₂HPO₄ (1.0 g), MSO₄ × 7 H₂O (0.25 g), KCl, (0.25 g),

bacteriological agar (10.0 g) and distilled H₂O (1000.0 g). Sterile, transparent, cellophane pieces about 30 µm thick with dimensions of 1 × 1 cm were placed onto the growth media. After colonization by the fungus, the cellophane square was lifted off the growth medium and placed on a glass slide with Lactophenol Cotton Blue, which is commonly used for the microscopic examination and identification of fungi. All cultures were identified microscopically using the keys of Stalpers (1978) for basidiomycetes¹⁸ and that of Barnett & Hunter (1998) for deuteromycetes.¹⁹

For the antibacterial assays, three bacterial strains were used: *Staphylococcus arlettae* Rosenbach (gram positive), *Pseudomonas fluorescens* Migula (gram negative) and a common oral bacterium, *Streptococcus mutans* Clarke ATCC 25175 (gram positive). Pure cultures of *S. arlettae* and *P. fluorescens* were provided by Swissatest AG, St. Gallen, Switzerland. *S. mutans* was isolated from the surface of walnut wood samples that were exposed to human saliva. All selected bacterial strains were cultivated in Petri dishes on Tryptic Soy Agar (TSA, OXOID) and subsequently sub-cultured on Tryptic Soy Broth (TSB, OXOID) at 30°C or 35°C.

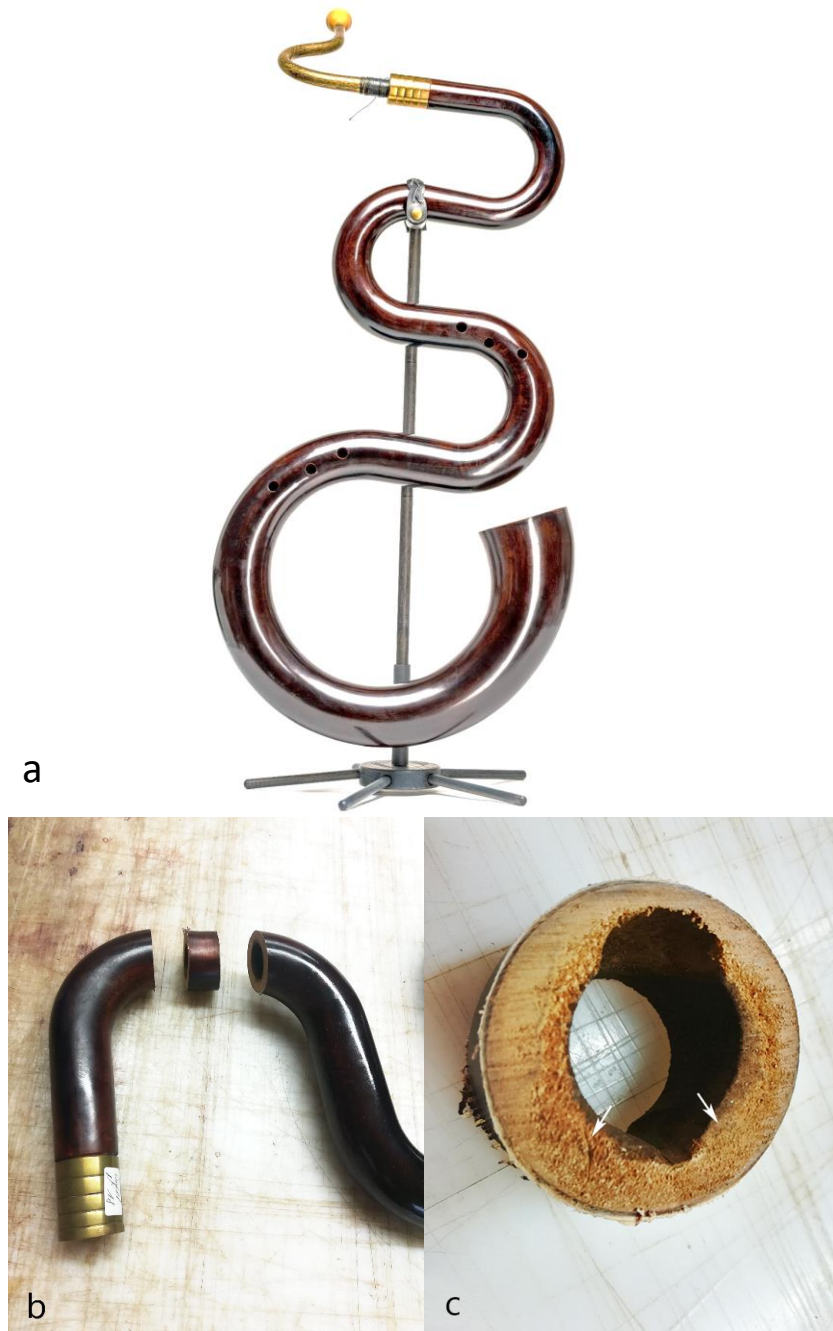


Figure 1. a: The snake-like shape of the serpent helps to position the finger holes in reach. b: European walnut wood samples showing distinctive interior decay (1c), were sawn (circle) from the wooden conical tube (b). c: Isolations were made from wood chips extracted from the decayed wood (arrows) and placed onto Petri dishes with different growth media.

Light microscopy observation of naturally infected walnut wood from a serpent

For light microscopy of naturally infected walnut wood from a serpent (Figure 1), samples of approx. $20 \times 5 \times 5$ mm were sawn. The samples, with transverse and radial faces exposed for examination, were infiltrated with acetone and embedded in a methacrylate medium. The embedded samples were sectioned at approx. 2 and 4 μm using a rotary microtome (Reichert-Jung/Leica 2040, Jung/ Leica Instruments GmbH, Nussloch bei Heidelberg, Germany) fitted with a diamond knife. The sections were finally stained for 12 h in safranin and then counter-stained for 3 min in methylene blue and for 30 min in auramin. Micrographs were taken with a Leica DM4000 B LED microscope using the LAS software version 4.13.0.

Antimicrobial substances

Three types of natural plant oils were used for wood impregnation: linseed (*Linum usitatissimum* L.) oil, tea tree (*Melaleuca alternifolia* (Maiden & Betche) Cheel) oil and eucalyptus (*Eucalyptus citriodora* (Hook.) K.D.Hill & L.A.S.Johnson) oil. The oils were obtained from Drogerie Spillmann AG, Dübendorf, Switzerland. All oils were used with their original concentration (purity $\geq 99\%$) for the antimicrobial tests.

Fungal melanin was biosynthesized via cultivation of *Armillaria cepistipes* (Empa 665) according to Ribera et al. (2019).¹⁴ Melanin was prepared with a concentration of 0.25 g/L, by diluting the original collected melanin solution from culture with milli-Q water and confirmed by UV-Vis spectroscopy. Different test concentrations and combinations of melanin, plant oils, copper sulfate and chitosan were selected for these experiments. All combinations that were used in preliminary studies are summarized in Table S1, whereas Table 1 only includes the four most promising combinations of plant oils and melanin. Finally, Sanitized® Preservation (Switzerland) was used as a benchmark.

Table 2. Abbreviation for different treatments

Abbreviation	Content	
	Impregnation I	Impregnation II
LO	Linseed oil	/
Mel-LO	Melanin (0.25 g/L)	Linseed oil
MO	Mix oils (linseed oil : tea tree oil 9:1 v/v)	/
Mel-MO	Melanin (0.25 g/L)	Mix oils (linseed oil : tea tree oil 9:1 v/v)
Sanitized®	Benchmark preservative	/
Control	/	/

Wood treatment

The wood samples used for the tests were excised from the heartwood of European walnut trees. For the antimicrobial tests, the samples were cut into small blocks with dimensions of 25 mm × 15 mm × 10 mm. For every test, wood samples were prepared with two different fiber orientations i.e. radial longitudinal (RL) and tangential longitudinal (TL) directions. Wood specimens were oven-dried and the dry weight was measured. Then the wood specimens were conditioned for two weeks at 25 °C and 65%RH and placed into glass beakers filled with antimicrobial substances. The glass beakers were sealed in a vacuum chamber. Impregnation was performed for 20-30 min under vacuum (100 hPa), followed by 60 min under ambient pressure for substance uptake. For the linseed and tea tree oil treatment, the oil mixture was prepared with a ratio of 9:1 (linseed:tea tree). For the combination of the other oils and melanin, the impregnation was performed in a two-step process, as the substances are immiscible liquids. First, samples were impregnated with melanin, dried overnight at 45 °C and finally impregnated with the plant oil(s). After treatment, the samples were stored for at least 2 weeks in a climate

chamber at 20 °C / 65%RH. Then the treated wood samples were sterilized with ethylene oxide for 5 hours.

The preservative uptake was determined by weighing wood samples immediately after impregnation. Excess oil on the wood surface was removed using clean filter papers. Preservative uptake by walnut wood samples was calculated as follows:

$$\text{Preservative uptake} = \frac{W_e - W_i}{V} \quad (1)$$

where, W_i and W_e are the weight of wood sample before and after impregnation in kg, V is the volume of wood sample in m^3 .

Antimicrobial efficacy test

The antimicrobial efficacy tests for the potential wood preservatives was conducted according to the Antimicrobial Efficacy Test, GMP and Investigations with slight modification to suit the requirements of wood (Figure 2).²⁰ In the antifungal assay, *Chaetomium globosum* spores collected from two petri dishes of 4-week cultivation were suspended into a sterile antarox solution. Treated and untreated wood samples were placed in the spore suspension for 1-2 min and then air-dried at 25 °C and 50%RH. After 1 day, 3 days, 7 days and 14 days, the tested samples were placed again for 10-15 min in a sterile antarox solution. Then the solutions were diluted several times and placed into Petri dishes with 2% MEA at 25 °C to count the number of surviving colonies.

In a similar manner, approximate 10^6 colony forming unit (CFU)/mL suspensions of *S. arlettae*, *P. fluorescens* and *S. mutans* were prepared with quarter-strength Ringers solution (Oxoid Thermo Fischer Scientific, Germany). Treated and control wood samples were placed in the microbial suspension for 1-2 min, then immediately transferred to a pre-conditioned desiccator at 23 °C, 95%RH. After 1h and 3h, all samples were rinsed again for 10-15 min in a sterile Ringer solution. Two extra time points of 7h and 24h were applied for *S. mutans* exposed samples. From the solutions, two serial, 1/10 dilutions were made, and 0.1 mL was plated in

TSA agar. Petri dishes with *S. mutans* were incubated at 30°C, whereas *S. arlettae* and *P. fluorescens* were incubated at 35°C.

The antimicrobial efficacy of melanin and natural oils was determined by measuring the survival rate of bacteria as follows:

$$\text{Survival rate (\%)} = \frac{N \times 100}{N_0} \quad (2)$$

where N_0 is the total viable count on the surface of control wood samples at the time of incubation (CFUs/cm²) and N is the total viable count of survival after determined time periods.

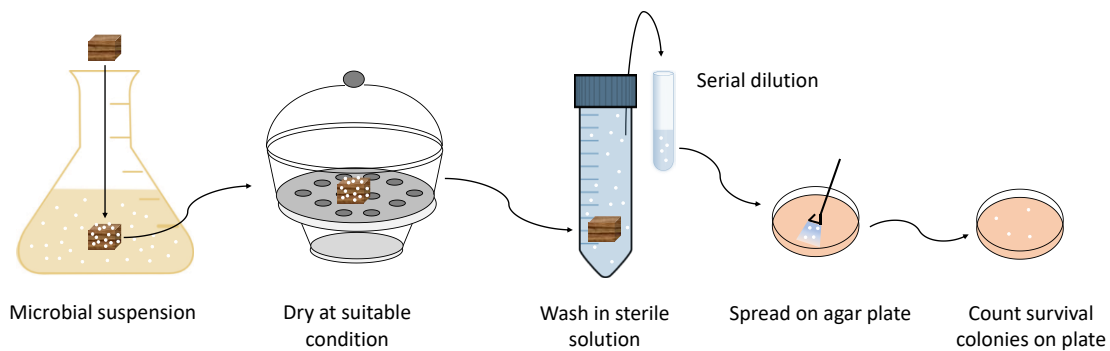


Figure 2. Scheme of antimicrobial efficacy test.

Water absorption and dimensional stability test

For the dynamic determination of wood moisture and dimensions at different climate conditions, wood specimens with dimensions 40 mm × 40 mm × 10 mm were prepared according to DIN 52182, 52183 and 52184.²¹ After impregnation, wood samples were conditioned for 4 weeks in different climate chambers starting with 35%RH, subsequently followed by 65% and 85%RH. Manual measurements of mass and length changes of samples were performed with a caliper directly within the climate chambers. Water absorption (WA) and dimensional stability (DS) were calculated according to equations (3) and (4):

$$WA = \frac{M_e - M_i}{M_i} \times 100 \quad (3)$$

$$DS = \frac{T_e - T_i}{T_i} \times 100 \quad (4)$$

where M_i and M_e are the mass of wood samples before and after test, T_e is the dimension of the samples at a conditioned climate (35%RH or 85%RH) and T_i is the dimension of samples at 65%RH.

Statistical analysis

All measurements were performed in triplicates and results were presented as mean value \pm SD. Statistical differences were analyzed by an independent sample t-test. The difference was considered significant when the $P < .05$.

2.3.3. Results and discussions

Isolation and identification of the casual decay fungus from infected wood

Isolations from wood samples extracted from the damaged serpent did not show any fungal growth in MEA containing 0.2% thiabendazole. The latter growth media is commonly used as a selective media for isolating basidiomycetes. On MEA the appearance of colonies of the aerial mycelium was pale or olivaceous, often with yellow, grey green, green or red exudates. A daily growth rate of (6–) 7–8 mm was observed. Olive, grey-green or brown ovate ascomata (Figure 3a) up to 500 μm long, with numerous coiled, unbranched hairs developed within 7–9 days (Figure 3). Flat lemon-shaped to globose ascospores, brownish when matured, with dimensions of 9–12 \times 8–10 \times 6–8 μm were produced within the asci of the ascomata (Figure 3b). All these microscopic features are typical for *Chaetomium globosum* Kunze. *C. globosum* is one of the most prevalent fungi in the world and it can be found either on living plants or in the debris of decaying plants and wood.²²

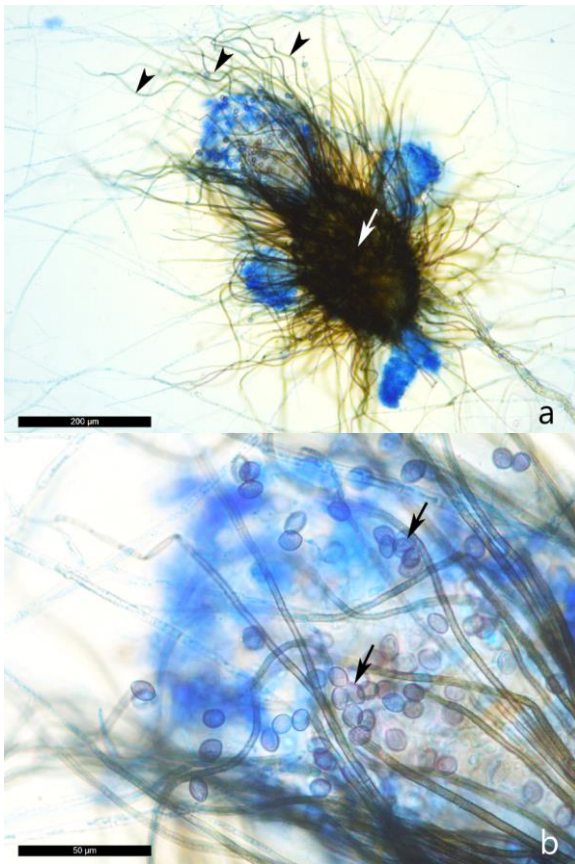


Figure 3. a: Perithecium (white arrow) of *Chaetomium globosum* with a large number of apical hairs which are spirally coiled (black pointer). b: Lemon-shaped, olive-brown colored ascospores (black arrows) of *Chaetomium globosum*, entrapped in the apical hairs.

Light microscopy observation of naturally infected walnut wood from a serpent

The presence of soft rot in the walnut wood caused by *C. globosum* was revealed by high-resolution light microscopy. The cell walls show hyphal tunnelling along the cellulose microfibrils of the S2 layer, resulting in the appearance of minute cavities in transverse sections (Figure 4a). This mode of attack is typical of a Type 1 soft rot.²³ Even at advanced stages, the persistence of a ‘lignin-rich’ skeleton (Figure 4b, 4c), representing the most lignified components of the wood, remained mostly intact, preserving stiffness so that the wood becomes brittle.²⁴ The persistence of lignin-rich regions of the wood matrix in trees decayed by *C. globosum* is not only due to their high lignin content per se, but also to their high percentage of guaiacyl lignin. Some ascomycetes have relatively poor lignolytic ability, and this is mainly confined to the decomposition of syringyl lignin (Nilsson et al. 1989).²⁵ These results are in

good agreement with Popescu et al. (2011) who described a typical soft rot pattern by *C. globosum* in lime wood using SEM.²⁶

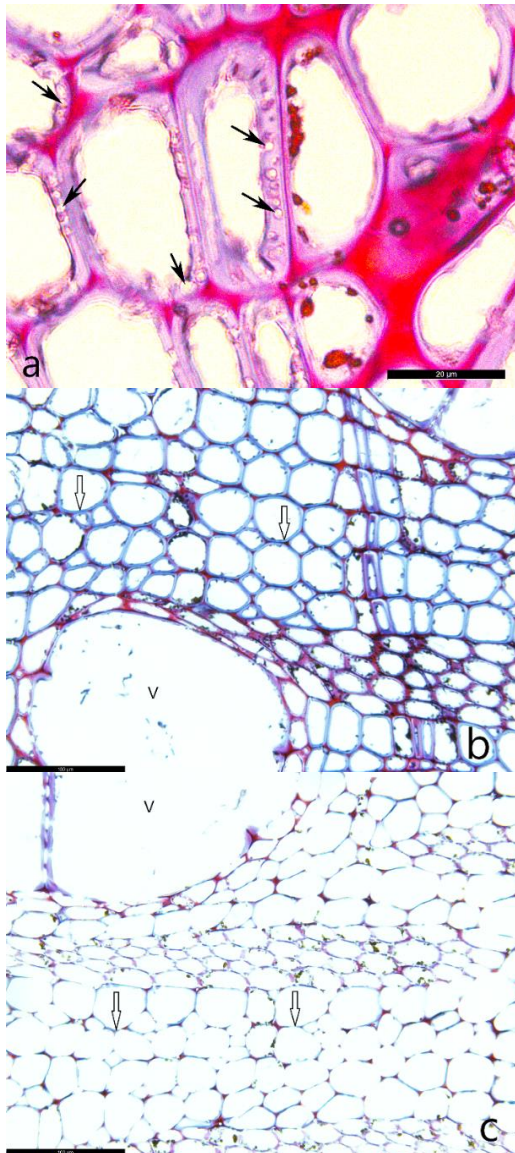


Figure 4. a: Transverse sections of walnut wood naturally infected by *Chaetomium globosum* showing cavities (arrows) within the secondary walls of fibre-tracheids. Bar, 20 μm . b: During early stages of decay, abundant hyphae are apparent within the cell lumina, whereas the secondary walls (arrows) remain intact. Bar, 100 μm . c: Progressive cell wall thinning of the fibre-tracheids (arrows) occurs from the lumen outwards. Bar, 100 μm .

Uptake of melanin and natural oils in treated wood

The preservative uptake results after impregnation are presented in Table 2. The RL wood samples, with more exposed parenchyma cells in multiseriate xylem rays retained a greater amount of melanin and natural oils than that of the TL wood samples. Studies show that

preservatives diffuse more easily in wood through the simple pits of the xylem ray.²⁷ Uptake of melanin was significantly higher in the RL samples than in the TL samples. Colonization of the parenchyma cells by fungi and bacteria may also be facilitated by the presence of readily degradable carbohydrates.

For both RL- and TL wood samples, the oil uptake was similar for both linseed oil and mixed oil. The linseed oil uptake in treated walnut wood is comparable to beech wood, but lower than that of pine- or spruce wood.⁹ This is due to the higher density and lower porosity of hardwood like beech and walnut compared to that of softwoods. It is worth noting that after impregnation with melanin, there is a slight change in the amount of oil absorbed, however, these changes are not statistically significant. This indicates that the first impregnation of melanin does not hinder the wood from uptake of other plant oils during subsequent impregnation processes.

Table 3. Uptake of melanin and natural oils in walnut wood.

Treatment	RL (strongly exposed parenchyma cells)		TL (weakly exposed parenchyma cells)	
	Melanin uptake (kg/m ³)	Oil uptake (kg/m ³)	Melanin uptake (kg/m ³)	Oil uptake (kg/m ³)
LO	/	414 ± 28	/	350 ± 22
Mel-LO	15 ± 1	389 ± 26	12 ± 1	368 ± 25
MO	/	413 ± 25	/	377 ± 35
Mel-MO	15 ± 1	399 ± 25	13 ± 1	355 ± 12

Efficacy of preservatives against bacteria

In preliminary tests (see Table S2), the survival of *S. arlettae*, *P. fluorescens* and *S. mutans* on the untreated walnut wood samples at 23 °C and 55%RH was investigated during 1-, 2-, and 3-hour periods. Significant reduction in CFUs was recorded after 1h, and almost all bacterial species died within 3h, with the exception of *S. mutans*. This suggests that walnut wood has

intrinsic antibacterial properties e.g. a naturally occurring high tannin content that suppresses the growth of *S. arlettae* and *P. fluorescens*. Studies by Hon and Shiraishi (2000) on the discoloration of hardwoods suggests that black walnut heartwood contains 2% tannin.²⁸ Previous studies have shown that some wood species possess specific porous structure and hygroscopic properties, which can remove the water required for bacterial colonization, inhibiting bacterial survival propagation on wooden surface.²⁹ Moreover, some naturally existing polyphenols in wood have been proven to have the antibacterial effect.³⁰

A second test was repeated, but at higher moisture conditions (> 90%RH, 23 °C) in a closed chamber. Similar to the incubation at low RH, CFUs of *P. fluorescens* (gram negative) decreased significantly after 1h (Figure 5), from 850 to 120 CFUs/cm² and almost no CFU was evident after 3h. Starting at 1050 – 1300 CFUs/cm², the number of CFUs of *S. arlettae* also decreased rapidly by 85-90% for both untreated and treated samples after 3h. This indicates that *P. fluorescens* and *S. arlettae* cannot readily colonize walnut wood. Since the growth of both bacterial species is inhibited on walnut wood, the addition of different plant oils and melanin did not reveal an enhanced antibacterial effect. *S. mutans*, the bacteria commonly found in human saliva, however, survives for a longer time. In fact, in both untreated RL and TL wood samples, CFUs of *S. mutans* increased significantly after one day, with the RL samples accumulating a greater number of CFUs (985 CFUs/cm²) compared to the TL samples (778 CFUs/cm²) right at the beginning and this pattern continued at all later time points.

Impregnation of walnut wood with plant oils clearly had an antibacterial effect. CFUs of *S. mutans* decreased by more than 50% after only 1h compared to that of the untreated controls. However, the combination of linseed oil with tea tree oil did not enhance the efficacy of linseed oil against bacteria, whereas melanin showed an improved antibacterial effect, especially at early stages of treatment. For instance, the addition of melanin in combination with oil(s) increased the antibacterial effect by 20 – 25% after 3h. This suggests that the two-step impregnation of melanin and linseed oil treatment has an enhanced efficacy against *S. mutans*.

Although linseed oil has a lethal effect on most bacteria after 24h, the addition of melanin significantly increases the antibacterial effect.

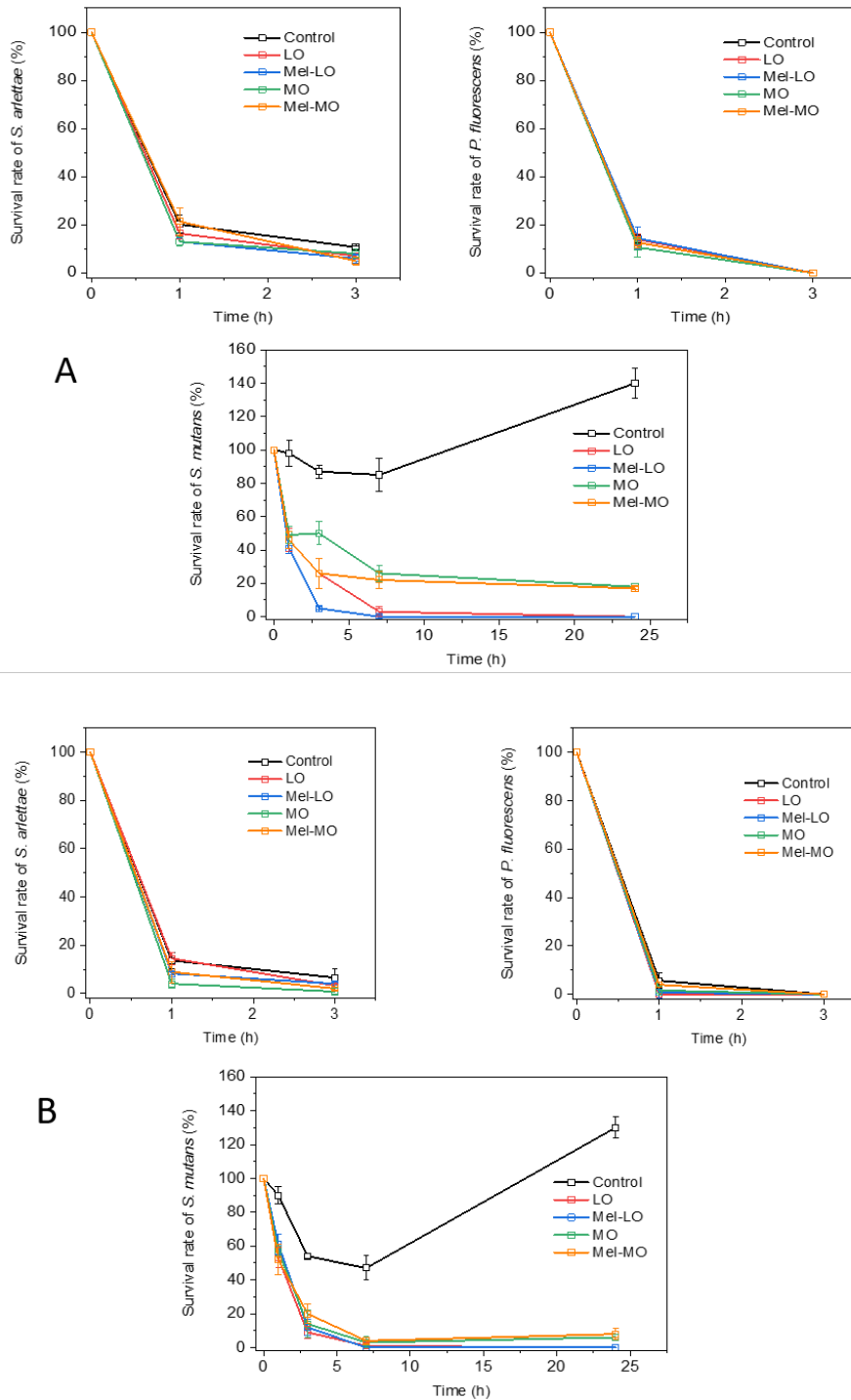


Figure 5. Survival rate of tested bacteria over time on A) radial-longitudinal and B) tangential-longitudinal wood samples.

Efficacy of natural oils and melanin against Chaetomium globosum

From the initial inoculum of around 950 - 1100 CFUs/cm², *C. globosum* survived on wood for a long period and its survival rate remained above 50% on the untreated control wood samples after 14 days. When the wood samples were treated with plant oils, a positive antifungal effect was recorded in all cases. The benchmark preservative (Sanitized®) had a stronger efficacy after a short period (1 day), however, inhibition of *C. globosum* rapidly reduced over the time. This is probably related with the water-based formulation of Sanitized®, as part of it may be leached out of the suspension during the dipping step of the assay.

Unlike the benchmark, the plant oils alone and in combination with melanin (LO, MO, Mel-LO and Mel-MO) are highly hydrophobic, and counteract leaching when in contact with water. As indicated in Figure 6, although the initial antimicrobial efficacy of these substances were lower than the benchmark, they showed better results in the long term. It is worth noting that the wood samples were impregnated with melanin, which is water-soluble, prior to the treatment with plant oils to minimize leaching. It is conceivable that the plant oils formed a water-repelling layer on the outside of the samples protecting the melanin within the wood.

A strong antifungal effect against *C. globosum* was observed on RL wood samples. The best performance was recorded from wood treated with Mel-MO, which was closely followed by Mel-LO. Both of these combinations provided a 25% better efficacy than the benchmark product, and approximately 5-10% better efficacy than the linseed and mixed oils combination after 14 days. At that time, less than 10% of the fungal spores of the initial inoculum were able to survive. This indicates that the addition of melanin significantly enhances the antifungal effect of plant oils on walnut wood.

The antifungal effect of all the plant oil-type combinations was also stronger than the benchmark product for TL samples i.e. the survival rate of *C. globosum* conidia was reduced by 20-25%. It should be noted that similar to the study with bacteria, more colonies were found

on the RL than the TL samples of the untreated wood. However, the opposite situation was observed on the treated wood samples, as more colonies were present on the TL than on the RL wood samples. This is due to the higher number of exposed parenchyma cells on the RL- than the TL wood samples, which allows more microbial cells to colonize the untreated wood. In addition, the higher porosity of the RL wood samples can increase the uptake of melanin by the simple pits in the xylem ray parenchyma, boosting the antifungal effect against *C. globosum*. This is in good agreement with the recorded amounts of melanin uptake for treated wood samples (Table 2).

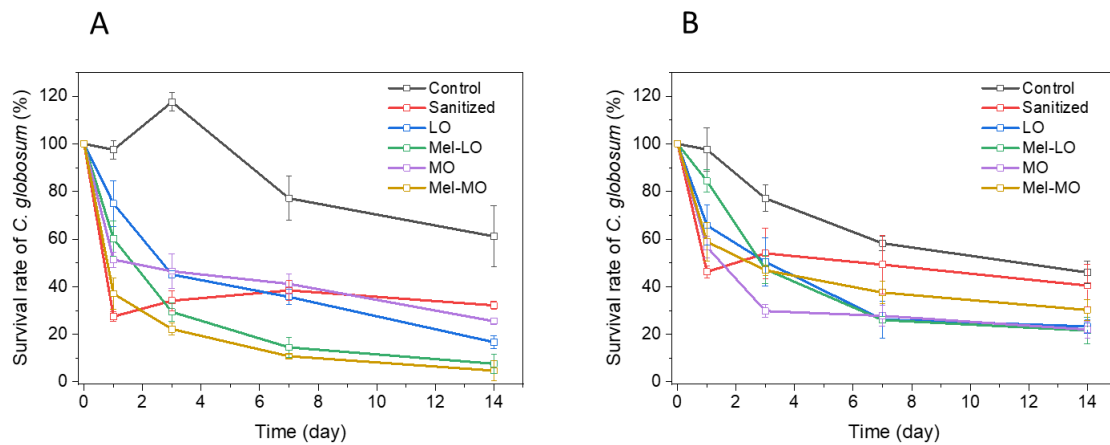


Figure 6. Survival rate (%) of *C. globosum* over time on A) radial-longitudinal and B) tangential-longitudinal wood samples.

Sorption dynamic

Dimensional changes, which result in a shrinking or swelling of wood volume, are an important factor that may affect the visual and structural properties of a musical instrument. For untreated wood, dimensional changes occur when the moisture content in the wood decreases or increases in response to changes in the relative humidity (RH) of the atmosphere, i.e. at a high RH, wood absorbs moisture and swells while at a low RH, wood loses moisture and shrinks. For treated wood, dimensional changes can also be induced by the adsorption of natural oils or melanin. It is ideal if shrinking and swelling rates of the treated wood are lower or at least not significantly higher than that of the untreated wood.

The dimensions of the wood samples are provided in SI. For all walnut wood samples, the length and mass changes at a low RH (35%) and a high RH (85%) were calculated in comparison to wood samples stored at 65%RH (Table 3).

Table 4. Shrinkage and swelling rate of walnut wood after different treatments with plant oils and melanin

		Control	LO	Mel-LO	MO	Mel-MO
Longitudinal direction	Shrinkage (%)	0.05	0.06	0.04	0.1	0.02
	Swelling rate (%)	0.16	0.15	0.11	0.09	0.13
Tangential direction	Shrinkage rate (%)	0.16	0.22	0.14	0.24	0.13
	Swelling rate (%)	1.45	1.35	1.26	1.36	1.27
Radial direction	Shrinkage rate (%)	0.34	0.41	0.52	0.43	0.39
	Swelling rate (%)	2.05	2.04	2.07	3.05	2.78
Theoretical volume change (%)	Shrinkage rate (%)	0.55	0.70	0.62	0.76	0.20
	Swelling rate (%)	3.70	3.58	3.47	4.54	4.22
Mass change (%)	Desorption	0.59	0.48	0.35	0.22	0.37
	Absorption	6.62	4.14	4.42	4.16	4.60

As indicated in Table 3, wood samples treated with plant oils show similar shrinkage and swelling rates of the dimensions and volume to that of the controls. Along the longitudinal direction, shrinkage and swelling rates are minor (below 0.2%) as the cellulose, the main component of the cell, is stiff and strong and negligible dimensional changes are measured in the direction parallel to cellulose microfibrils.³¹ The shrinking rates are also insignificant in the tangential and radial directions, whereas the swelling rates were slightly higher, but less than 3% for all wood samples. It is worth noting that the impregnation of the wood samples with oil

reduces the uptake of moisture as the mass change percentage due to water absorption is much lower than for the control wood samples.

In summary, we have found that the combination of melanin and plant oils is an efficient method to protect walnut wood from bio-deterioration, without affecting the wood's dimensions. This allows low maintenance of the musical instruments made by walnut wood. This method might be applicable for other precious wood species, and this work is in progress. Looking back to the development of wood preservatives in general,³² the high toxicity of the first-generation preservatives such as creosote and chromated copper arsenate have raised significant concerns over health issues; therefore, their usage is no longer permitted in Europe. The second-generation of wood preservatives are mainly water-borne copper-rich compounds such as alkaline copper quat, copper azole, copper xylogen, and copper betaine, which have good effectiveness. Water-borne borates also belong to the second generation and together with the copper compounds, they are suited for residential applications. However, environmental concerns on the leaching of copper and borate to the environment, especially the aquatic system, have led to the preference of non-metallic organic preservatives, which are of the third generation. Environmentally friendly and nature-derived substances such as essential oils have been investigated and used in many wood preserving practices.³³ However, an effective preservation requires the match between the oil types, the wood species and the targeted deteriorating microorganisms. There are limited reports on preservatives used for walnut wood, especially walnut wood used in musical instruments. Nevertheless, efficacy of linseed oil and tea tree oil against wood-decay fungi has been proven on other European wood species such as spruce and beech wood.^{9,33,34} It is worth noting that the conventional methods used to evaluate the antimicrobial efficacy in those studies are either agar disk diffusion, broth dilution or wood surface contact.³⁵ With the first two, the results are quantitative and can be achieved within 24 – 72 hours, but they lack practical results on real wood samples. The last one gives results directly on wood samples, but requires relatively long time (weeks to months) due to the slow

growth of fungi. The convenience of our testing method is the advantages combined from both methodologies, where the results are quantitative and can be obtained in shorter time than the traditional methods. Moreover, this is among the first research that investigates the combining effect of plant oils and melanin in wood preservation. The synergic antimicrobial efficacy of the combination reported in this work significantly contributes to the third generation of preservatives, as they are safe for use without health and environmental concerns.

2.3.4. Conclusions

In this study, walnut wood treated with a combination of melanin and plant oils such as linseed oil showed a higher antimicrobial effect than the benchmark substance Sanitized®. The addition of melanin significantly enhanced the antibacterial and antifungal effect of plant oils. Walnut wood samples treated with melanin and plant oils also maintained their sizes and volume under different humidity conditions, which is a crucial factor for the treatment of wood musical instruments such as the serpent. This work opens a new strategy for using plant oils in combination with melanin, which can be used as an additive to boost the inherent antimicrobial properties of environmentally friendly wood preservatives.

Supporting Information

The file contains information about fungal melanin production and preliminary screening of potential wood preservatives, and is available free of charge.

AUTHOR INFORMATION

Corresponding Author

* francis.schwarze@empa.ch

Notes

The authors declare no competing financial interest.

ACKNOWLEDGMENT

The authors are grateful to acknowledge the financial support by the Innosuisse (Project No. 36301.1 IP-ENG). We thank Daniel Heer for the preparation of walnut wood samples for conducting the bioassays.

References

- (1) Holman, C. Rhythm and Metre in French Classical Plainchant. *Early Music* **2017**, *45* (4), 657–664. <https://doi.org/10.1093/em/cax087>.
- (2) Six, A. The black gold of mushrooms <https://www.empa.ch/web/s604/melanin-aus-pilzen>.
- (3) Palmer, P. R. In Defense of the Serpent. *Hist. brass Soc. J.* **1990**, *2*, 132–186.
- (4) Vallero, D.; Isukapalli, S.; Zartarian, V.; McCurdy, T.; McKone, T.; Georgopoulos, P.; Dary, C. Chapter 44 - Modeling and Predicting Pesticide Exposures. In *Hayes' Handbook of Pesticide Toxicology (Third Edition)*; Krieger, R., Ed.; Academic Press: New York, 2010; pp 995–1020. <https://doi.org/10.1016/B978-0-12-374367-1.00044-6>.
- (5) Jorge, F. C.; Nunes, L.; Botelho, C. Boron in Wood Preservation: Problems, Challenges and Proposed Solutions. An Overview on Recent Research. *J. Fac. Sci. Technol.* **2004**, *1*, 3–15.
- (6) Echard, J.-P.; Bertrand, L.; von Bohlen, A.; Le Hô, A.-S.; Paris, C.; Bellot-Gurlet, L.; Soulier, B.; Lattuati-Derieux, A.; Thao, S.; Robinet, L.; et al. The Nature of the Extraordinary Finish of Stradivari's Instruments. *Angew. Chemie Int. Ed.* **2010**, *49* (1), 197–201. <https://doi.org/10.1002/anie.200905131>.
- (7) Vidholdová, Z.; Slabejová, G.; Šmidriaková, M. Quality of Oil- and Wax-Based Surface Finishes on Thermally Modified Oak Wood. *Coatings* **2021**, *11* (2). <https://doi.org/10.3390/coatings11020143>.
- (8) Lu, K.-T.; Chang, J.-P. Synthesis and Antimicrobial Activity of Metal-Containing Linseed Oil-Based Waterborne Urethane Oil Wood Coatings. *Polymers (Basel)*. **2020**, *12* (3). <https://doi.org/10.3390/polym12030663>.
- (9) Humar, M.; Lesar, B. Efficacy of Linseed- and Tung-Oil-Treated Wood against Wood-Decay Fungi and Water Uptake. *Int. Biodeterior. Biodegradation* **2013**, *85*, 223–227. <https://doi.org/10.1016/j.ibiod.2013.07.011>.
- (10) Panov, D.; Terziev, N. Durability of Epoxi-Oil Modified and Alkoxysilane Treated Wood in Field Testing. *BioResources* **2015**, *10*, 2479–2491.

- (11) Smith, M. L.; Bruhn, J. N.; Anderson, J. B. The Fungus *Armillaria Bulbosa* Is among the Largest and Oldest Living Organisms. *Nature* **1992**, *356* (6368), 428–431. <https://doi.org/10.1038/356428a0>.
- (12) Rigling, D.; Günthardt-Goerg, M. S.; Blauenstein, H.; Frey, B. Accumulation of Heavy Metals into *Armillaria* Rhizomorphs from Contaminated Soils. *For. Snow Landsc. Res.* **2006**, *80* (2), 213–220.
- (13) Tran-Ly, A. N.; Reyes, C.; Schwarze, F. W. M. R.; Ribera, J. Microbial Production of Melanin and Its Various Applications. *World J. Microbiol. Biotechnol.* **2020**, *36* (11). <https://doi.org/10.1007/s11274-020-02941-z>.
- (14) Ribera, J.; Panzarasa, G.; Stobbe, A.; Osypova, A.; Rupper, P.; Klose, D.; Schwarze, F. W. M. R. Scalable Biosynthesis of Melanin by the Basidiomycete *Armillaria Cepistipes*. *J. Agric. Food Chem.* **2019**, *67* (1), 132–139. <https://doi.org/10.1021/acs.jafc.8b05071>.
- (15) Tran-Ly, A. N.; Ribera, J.; Schwarze, F. W. M. R.; Brunelli, M.; Fortunato, G. Fungal Melanin-Based Electrospun Membranes for Heavy Metal Detoxification of Water. *Sustain. Mater. Technol.* **2020**, *23*, e00146. <https://doi.org/https://doi.org/10.1016/j.susmat.2019.e00146>.
- (16) Tran-Ly, A. N.; De France, K. J.; Rupper, P.; Schwarze, F. W. M. R.; Reyes, C.; Nyström, G.; Siqueira, G.; Ribera, J. Melanized-Cationic Cellulose Nanofiber Foams for Bioinspired Removal of Cationic Dyes. *Biomacromolecules* **2021**, *22* (11), 4681–4690. <https://doi.org/10.1021/acs.biomac.1c00942>.
- (17) Sieber, T. N. *Pyrenochaeta Ligni-Putridi* Sp. Nov., a New Coelomycete Associated with Butt Rot of *Picea Abies* in Switzerland. *Mycol. Res.* **1995**, *99* (3), 274–276. [https://doi.org/https://doi.org/10.1016/S0953-7562\(09\)80897-6](https://doi.org/https://doi.org/10.1016/S0953-7562(09)80897-6).
- (18) Stalpers, J. A. Identification of Wood-Inhabiting Aphylophorales in Pure Culture Studies in Mycology 16. *CBS Baarn Netherlands.* **1978**.
- (19) Barnett, H. L.; Hunter, B. B. *Illustrated Genera of Imperfect Fungi*, 4th ed.; APS Press: St. Paul, MN, USA, 1998.
- (20) Sutton, S. The Antimicrobial Efficacy Test, GMP and Investigations.
- (21) Nopens, M.; Riegler, M.; Hansmann, C.; Krause, A. Simultaneous Change of Wood Mass and Dimension Caused by Moisture Dynamics. *Sci. Rep.* **2019**, *9* (1), 10309. <https://doi.org/10.1038/s41598-019-46381-8>.
- (22) Bahmani, M.; Schmidt, O. Plant Essential Oils for Environment-Friendly Protection of Wood Objects against Fungi. *Maderas. Cienc. y Tecnol.* **2018**, *20*, 325–332.

- (23) Corbett, N. H. Micro-Morphological Studies on the Degradation of Lignified Cell Walls by Ascomycetes and Fungi Imperfecti. *J. Inst. Wood Sci.* **1965**, *14*, 18–29.
- (24) Schwarze, F. W. M. R. Wood Decay under the Microscope. *Fungal Biol. Rev.* **2007**, *21* (4), 133–170. <https://doi.org/https://doi.org/10.1016/j.fbr.2007.09.001>.
- (25) Nilsson, T.; Daniel, G.; Kent, K.; Obst, J. R. Chemistry and Microscopy of Wood Decay by Some Higher Ascomycetes. **1989**, *43* (1), 11–18. <https://doi.org/doi:10.1515/hfsg.1989.43.1.11>.
- (26) Popescu, C.-M.; Tibirna, C.; Manoliu, A. L.; Petronela, G.; Vasile, C. Microscopic Study of Lime Wood Decayed by *Chaetomium Globosum*. *Cellul. Chem. Technol.* **2011**, *45*, 565–569.
- (27) Schwarze, F. W. M. R.; Landmesser, H.; Zraggen, B.; Heeb, M. Permeability Changes in Heartwood of *Picea Abies* and *Abies Alba* Induced by Incubation with *Physisporinus Vitreus*. **2006**, *60* (4), 450–454. <https://doi.org/doi:10.1515/HF.2006.071>.
- (28) Hon, D. N.-S.; Shiraishi Nobuo. *Wood and Cellulosic Chemistry, Revised, and Expanded*; CRC Press: Boca Raton, 2000.
- (29) Munir, M. T.; Pailhories, H.; Eveillard, M.; Aviat, F.; Lepelletier, D.; Belloncle Christophe; Federighi, M. Antimicrobial Characteristics of Untreated Wood: Towards a Hygienic Environment. *Health (Irvine. Calif.)* **2019**, *11*, 152–170.
- (30) Plumed-Ferrer, C.; Väkeväinen, K.; Komulainen, H.; Rautiainen, M.; Smeds, A.; Raitanen, J.-E.; Eklund, P.; Willför, S.; Alakomi, H.-L.; Saarela, M.; et al. The Antimicrobial Effects of Wood-Associated Polyphenols on Food Pathogens and Spoilage Organisms. *Int. J. Food Microbiol.* **2013**, *164* (1), 99–107. <https://doi.org/https://doi.org/10.1016/j.ijfoodmicro.2013.04.001>.
- (31) Yamashita, K.; Hirakawa, Y.; Nakatani, H.; Ikeda, M. Tangential and Radial Shrinkage Variation within Trees in Sugi (*Cryptomeria Japonica*) Cultivars. *J. Wood Sci.* **2009**, *55* (3), 161–168. <https://doi.org/10.1007/s10086-008-1012-2>.
- (32) Schultz, T. P.; Nicholas, D. D.; Preston, A. F. A Brief Review of the Past, Present and Future of Wood Preservation. *Pest Manag. Sci.* **2007**, *63* (8), 784–788. <https://doi.org/https://doi.org/10.1002/ps.1386>.
- (33) Broda, M. Natural Compounds for Wood Protection against Fungi—A Review. *Molecules* **2020**, *25* (15). <https://doi.org/10.3390/molecules25153538>.

(34) Mantil, E.; Daly, G.; Avis, T. J. Effect of Tea Tree (*Melaleuca Alternifolia*) Oil as a Natural Antimicrobial Agent in Lipophilic Formulations. *Can. J. Microbiol.* **2015**, *61* (1), 82–88. <https://doi.org/10.1139/cjm-2014-0667>.

(35) Munir, M. T.; Pailhories, H.; Eveillard, M.; Irle, M.; Aviat, F.; Dubreil, L.; Federighi, M.; Belloncle, C. Testing the Antimicrobial Characteristics of Wood Materials: A Review of Methods. *Antibiotics* **2020**, *9* (5). <https://doi.org/10.3390/antibiotics9050225>.

Supporting Information

Antimicrobial Effect of Fungal Melanin in Combination with Plant Oils for the Treatment of Wood

Anh N. Tran-Ly^{1,2}, Markus Heeb¹, Tine Kalac¹, Francis W.M.R. Schwarze¹

¹Laboratory for Applied Wood Materials, Empa, Lerchenfeldstrasse 5, St. Gallen 9014, Switzerland

²Department of Civil, Environmental and Geomatic Engineering, ETH Zurich, Stefano-Francini-Platz 5, Postfach 193, CH-8093 Zurich, Switzerland

1. Fungal melanin production

Growth medium was prepared according to Ribera et al. (2019)¹ and contained 1% (w/v) peptone, 1% (w/v) D-Glucose, 0.1% (w/v) yeast extract with 0.05% (w/v) KH₂PO₄, 0.02% (w/v) MgSO₄·7H₂O, 0.01% FeSO₄·7H₂O, 0.0005% (w/v) CuSO₄ and 2.5% (w/v) tyrosine. The growth medium was sterilised by autoclaving for 20 min at 121°C. It was then inoculated with five plugs taken with a cork borer from fresh cultures of *A. cepistipes* (Empa 655). The fungus was cultivated in 500 mL Erlenmeyer flasks with 300 mL of the growth medium under continuous shaking at 150 rpm and 22°C for 4 months. Thereafter, the supernatant was centrifuged at 4800 rpm for 15 min to remove the biomass and other debris. The collected supernatant was filtered through a 0.45 µm nitrocellulose membrane (Merck) to remove all the leftover cell

debris. The filtered liquid was then sterilized by autoclaving for 20 min at 121 °C and 1 bar and was stored at room temperature as melanin solution.

To determine the melanin content, standard curve for natural melanin (obtained by melanin from *Sepia officinalis*, Sigma-Aldrich) was used as a reference:

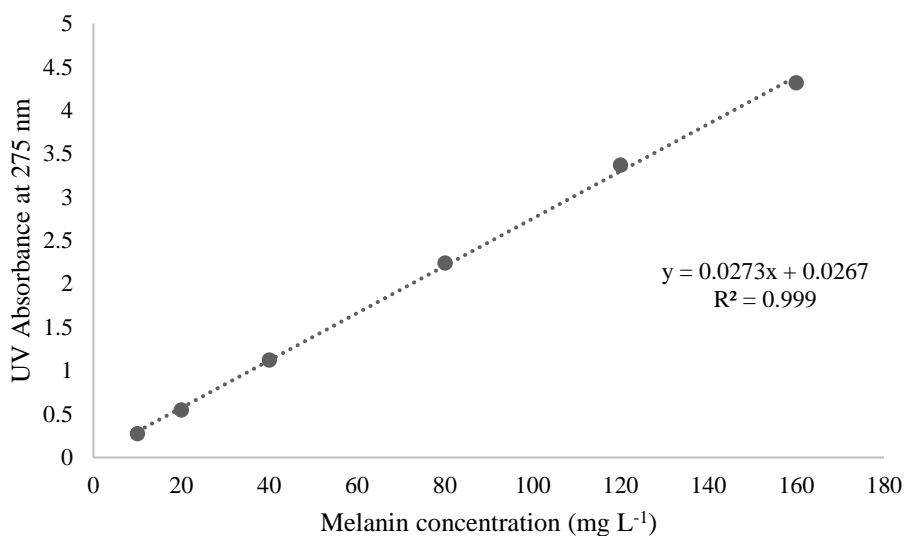


Figure S1. Standard curve of fungal melanin extracted from *Armillaria cepistipes* (Empa 655).²

2. Preliminary screening of potential wood preservatives

Table S1. Efficacy of different antimicrobial substances against *C. globosum* on wood samples

Substances	Total survival colonies on the wood surface (CFUs) after			Efficacy after 7 days (%)
	24h	3 days	7 days	
Untreated wood	16781	17225	10360	0
Melanin 2.5%	mold	-	-	-
CuSO ₄ 250 ppm	28497	10080	11928	-15.1
CuSO ₄ 500 ppm	24150	8113	9443	8.9
CuSO ₄ 1000 ppm	16931	15913	9873	4.7

2. Main investigations

CuSO ₄ 1000 ppm	13218	16088	9371	9.5
+ Melanin 0.25%				
Linseed oil	7940	952	1484	85.7*
Melanin 0.25%	13691	5376	2092	79.8*
+ Linseed oil				
Melanin 2.5%	26851	11841	8610	16.9
+ Linseed oil				
Tea tree oil	16802	8431	7391	28.7
Melanin 0.25%	14915	10059	8689	16.1
+ Tea tree oil				
Melanin 2.5%	22910	8442	10991	-6.1
+ Tea tree oil				
Eucalyptus oil	15520	10507	13757	-32.8
Melanin 0.25%	25941	10926	10032	3.2
+ Eucalyptus oil				
Melanin 2.5%	18028	7676	19058	-83.9
+ Eucalyptus oil				
Linseed + Tea tree oil	10772	6150	6431	37.9*
Melanin 0.25%	11897	8361	3938	62.0*
+ Mix (LS+TT) oil				

(*) Chosen substances/combination to perform official antimicrobial test (with 6 replicates for each)

Table S2. Survival of bacteria on untreated wood samples at ambient condition (23-25°C, ~50%RH)

Bacterial strain	Survival colonies (CFUs) after			
	1h	2h	3h	24h
<i>S. arlettae</i>	1722	98	0	0
<i>P. fluorescens</i>	1960	0	0	0
<i>S. mutans</i>	600	160	360	1000

References

- (1) Ribera, J.; Panzarasa, G.; Stobbe, A.; Osypova, A.; Rupper, P.; Klose, D.; Schwarze, F. W. M. R. Scalable Biosynthesis of Melanin by the Basidiomycete *Armillaria Cepistipes*. *J. Agric. Food Chem.* 2019, 67 (1), 132–139. <https://doi.org/10.1021/acs.jafc.8b05071>.
- (2) Tran-Ly, A. N.; De France, K. J.; Rupper, P.; Schwarze, F. W. M. R.; Reyes, C.; Nyström, G.; Siqueira, G.; Ribera, J. Melanized-Cationic Cellulose Nanofiber Foams for Bioinspired Removal of Cationic Dyes. *Biomacromolecules* 2021, 22 (11), 4681–4690. <https://doi.org/10.1021/acs.biomac.1c00942>.

3. General discussion and conclusions

Biocompatibility along with the distinctive photoprotective, metal chelating, toxin binding, and antimicrobial properties are among the key values that promote the use of melanin in practical applications. However, neither the animal sources nor the synthetic ones are sustainable for the large-scale supply of melanin, thus holding up further progress of applied melanin research. In this research, a newly developed scalable source of melanin – fungal melanin – was used to explore the application potential and to improve the understanding of this biopolymer from the material perspective. Following the preceding work of synthesis and characterization of fungal melanin extracted from *Armillaria cepistipes* [10], the focus of my doctoral thesis was set on using this melanin source to develop functional materials for various applications. By applying different material processing techniques, melanin's properties and functions as well as its interaction with other matrix materials were investigated. Based on the obtained results, I will discuss several aspects that need to be considered for the development and design of melanin-based materials, from the synthesis, extraction to the processing procedure.

3.1. Relationship between Synthesis, Extraction and Structure of Melanin

Melanin belongs to a group of ubiquitous pigments that can be found in almost all living kingdoms. Traditionally, melanin is isolated from animal sources such as *Sepia* cuttlefish, hair follicle melanosomes or bovine eyes. However, the source dependence makes the production of natural melanin costly (e.g. Sigma Aldrich, melanin from *sepia officinalis* costs CHF 1760 per gram), impeding its use for large-scale applications. Motivated by the astonishing array of melanin's functions, the past two decades have witnessed many efforts from polymer chemists to reduce the cost by developing synthetic melanin from different precursors e.g. tyrosine. As discussed in sub-chapter 1.3, both production methods have their own drawbacks. In our work, we utilized microorganisms such as fungi to synthesize melanin, which helps overcome these

weaknesses of the conventional production methods. This approach allows natural melanin production at a lower cost (~CHF 25 per gram). However, besides the cost efficiency, it is important to understand the effect of each production as well as extraction method on the melanin structure, because it will affect the functions and properties of the final melanin-based products. The traditional melanin isolation process from animal sources usually involves harsh chemical treatments, including extensive hydrolysis by boiling in mineral acids or bases followed by successive washing steps with organic solvents [11, 12]. These treatments can cause significant chemical alterations to the melanin's polymer chains [13]. On the other hand, the artificial synthetic route is mostly based on the oxidation of dopamine in alkaline-pH environments with the presence of metal catalysts to create polydopamine (PDA), which has served as a typical analogue of synthetic melanin [14]. Although PDA has shown some similar properties to that of natural melanin, its structure is not entirely the same. First, an important feature of natural melanin structure is the presence of 5,6-dihydroxyindole-2-carboxylic acid (DHICA) subunits. Certain natural melanins have more than 50% of DHICA-derived subunits [15]. By contrast, the synthetic PDA-based melanin contains mostly 5,6-dihydroxyindole (DHI) and no DHICA subunits [16]. This lack of $-\text{COOH}$ groups from DHICA subunits leads to several changes in the structural features and functions of melanin. In DHICA-containing natural melanins, the pendant $-\text{COOH}$ groups give rise to atropisomers, which is attributed to the larger rotation energy barrier along the C-C inter-DHICA bond [14]. On the other hand, PDA has a more planar oligomeric structure due to the resonance between the DHI subunits [17]. In addition, the zwitterionic DHICA subunits are important for natural melanin's UV radiation protection properties [18, 19]. The $-\text{COOH}$ groups also contribute to the effectiveness of melanin in scavenging of toxic compounds [20].

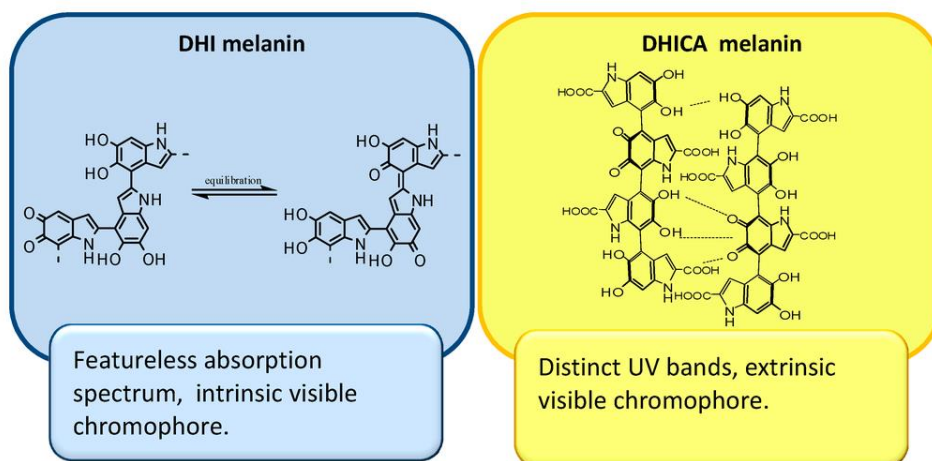


Figure 3.1. Intrinsic and extrinsic contributions to the chromophoric properties of DHI and DHICA-based melanin. Reproduced with permission from reference [15]. Copyright MDPI, 2016.

The approach of using fungi to produce melanin comprises benefits of both the animal-source extraction and artificial synthesis methods. By providing proper precursors (e.g. tyrosine) and culture conditions, melanogenesis occurs naturally in liquid media by the enzymes (e.g. laccase) released from fungi [21]. Good yields can be obtained with suitable fungal species, for instance, *Armillaria cepistipes* (Empa 655) can produce approximately 28 g of melanin per liter of the medium. In terms of quantity, this approach is sustainable and promising for industrial upscaling. The obtained fungal melanin preserves the inherited properties of melanin in nature. The structure of fungal melanin isolated from *Armillaria cepistipes* (Empa 655) was elucidated and compared with reported literature [10]. Via X-ray photoelectron spectroscopy (XPS) and electron paramagnetic resonance (EPR) studies, the authors suggested that fungal melanin contains both DHICA and DHI subunits and their derivatives (oxidized and radical forms), which is a typical eumelanin structure in nature and largely resembles sepia melanin [10]. The proposed structure of fungal melanin is shown in Figure 3.2. It is worth noting that this structure does not consider supramolecular interactions, e.g. π - π stacking and hydrogen bonding, which are important to determine the physical and chemical properties of melanin [10].

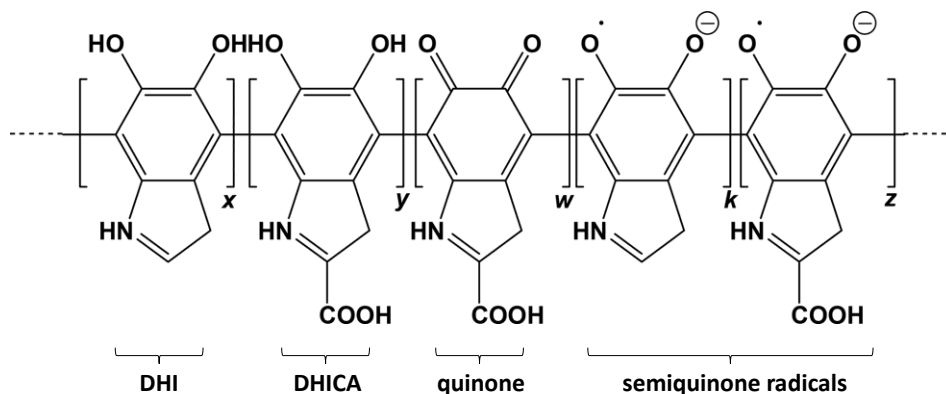


Figure 3.2. Proposed structure of fungal melanin isolated from *A. cepistipes* (EMPA 655). Reproduced with permission from reference [10]. Copyright American Chemical Society, 2019.

Once separated from biomass and cell debris, the melanin solution is ready for use as “native melanin” in the liquid form or can be further treated with acid or protease to obtain “pure melanin” in the solid form. At this point, the extraction method can affect the properties of the final melanin-based products. Previous studies have reported that *in vivo* melanin usually exists as melanoprotein complexes [22]. The association with proteins may be the reason for the solubility of the “native melanin”. On the contrary, after being deproteinized by acid treatment, the melanin subunits are spontaneously assembled into aggregates of larger amorphous structures [14]. Many of the observed properties of melanin reported in the literature (for instance, the remarkable robustness and insolubility) are the results of this supramolecular organization [12]. It is important to consider which melanin state (native vs pure melanin) to utilize in the composite because each level of structural organization may reveal or hinder certain functional groups, thus affecting the final properties of the materials.

3.2. Different Material Processing Strategies to Utilize Melanin

Powders are usually not preferred in industrial applications due to processing issues including dustiness, clogging, static charge accumulation, and challenges in handling, transportation, and

disposal. Transforming powders into shaped materials, for example embedding them into a polymer matrix to make thin films or porous foams, is often performed for certain uses, e.g. water treatment. One of the challenges in incorporating powders into polymers is that the polymeric macromolecules may affect the physicochemical properties of the powder. For instance, the polymer can block or deactivate the active sites of the incorporated powder. Maintaining the powder's intrinsic properties is thus important in powder processing. Furthermore, the synergy between the components of a composite, e.g. the enhanced interaction or cooperation between the powder and the polymer matrix, is often sought to develop a material with properties that is superior to each component.

3.2.1. Electrospinning

In sub-chapter 2.1, extracted “pure” fungal melanin in the form of powder was mixed in the polymer solutions (PCL and PUR) to make melanized membranes via electrospinning. It is worth noting that common methods for preparing polymer-melanin films included extrusion [23], casting [24], and layer-by-layer deposition [25], while no previous studies employed electrospinning. Therefore, many factors such as polymer, solvent, volatility of the solvent, processing parameters (i.e. applied voltage, distance between the spinneret and the collector, diameter of the spinneret, flow rate of the polymer solution) and the ambient conditions (i.e. temperature, relative humidity) were studied. It is known that the structure and morphology of electrospun fibers are influenced by the polymer concentration and conductivity [1]. The polymer concentration dictates the viscosity and surface tension of the spinning solution. It was found that too low concentrations of polymers, PCL and PUR, in the presence of melanin (< 0.2 g/ml for PCL and < 0.15 g/ml for PUR), impeded a formation of fibers, since the interaction between the polymer chains was too weak. Even when a film was obtained at a low polymer concentration, it contained clusters of collapsed plates, spherical beads, spindle beads, and/or bead-on-string morphologies (Figure 3.3). At an optimum polymer concentration (0.2 – 0.25 g/ml), the jet could be spun continuously and generated uniform fibers owing to the increased

chain entanglement and viscosity. If the concentration was too high (> 0.25 g/ml), the polymer solution became too viscous to eject from the spinneret.

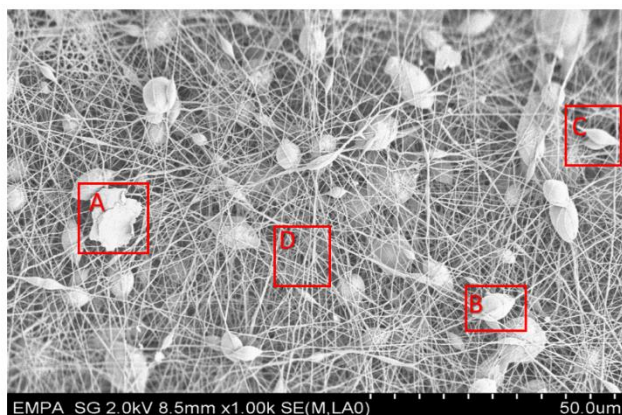


Figure 3.3. SEM image of different fiber morphologies on an electrospun melanin-based membrane. A: collapsed plates, B: spherical beads, C: spindle beads, D: cylindrical fibers.

In terms of electrical conductivity, electrospinning of an insulating PCL or PUR solution is challenging, because charges are not conducted from the solution interior to its surface. Adding melanin, which is an ionic compound, increases the conductivity of the polymer solution. Notably, a too high conductivity makes it difficult to generate a Taylor cone or initiates bending instability due to the depleted electrostatic repulsion [1]. Within a suitable range, the increase of electrical conductivity favors the formation of thinner fibers because of the extensive bending of the jet. Therefore, the amount of melanin loading needs to be measured and optimized.

“Pure” melanin powder was used to prepare films with PCL or PUR. Due to the highly aggregated structure after the extraction process, the “pure” melanin is hydrophobic and insoluble in most common organic solvents. Therefore, to maximize the dispersion of melanin in the polymer solutions, the melanin pigment had to be ground into fine powder. Furthermore, the mixtures were sonicated before starting the electrospinning process. Despite all the pre-treatments, the added melanin continuously sedimented at the bottom of the polymer reservoir. As a result, the longer the electrospinning process was performed, the less melanin was spun out. In the

manufactured melanized membranes, approximately 15 – 30% of melanin was lost when compared to the original concentration of the spinning suspension. Moreover, in a spinning material system containing both polymer and particles, the spinnability and morphology of the fibers are highly influenced by the particle aggregation and the size ratio of the particles to the fibers [26]. Under a strong electrostatic force, melanin aggregates are fragmented into nanoscale particles (Figure 3.4). At an optimized condition, the fiber size is larger than the melanin particle size, resulting in good encapsulation of particles in the fibers. If the fibers are smaller than the particle, or the particles are highly susceptible to aggregation, the morphology of the fibers will change from single particle inclusion to clusters of particles trapped in a net of short polymer fiber fragments. Both the fiber size and the level of particle aggregation can be controlled by numerous factors such as viscosity, conductivity, molecular weight, amount of particle loading etc. Due to the ability to encapsulate melanin particles and the flexible tunability of the morphology, electrospinning is a promising processing technology to develop functional melanin encapsulated nonwoven mats for various applications.

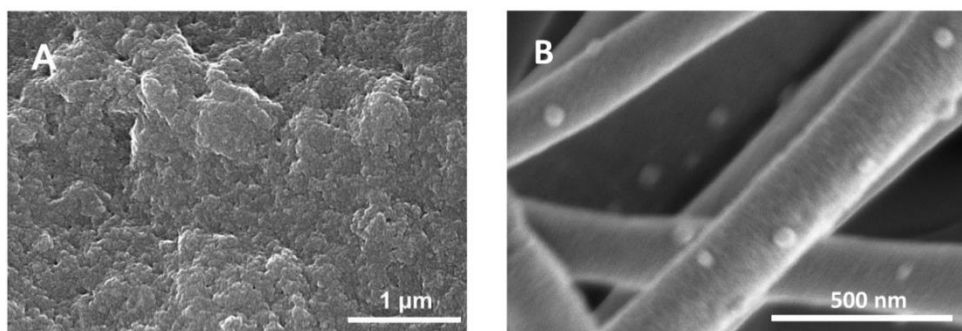


Figure 3.4. SEM images of melanin aggregates (A) and melanin nanoparticles (B) deposited on polymer fibers.

3.2.2. Freeze-drying

Lyophilization, or freeze-drying, is a common method to preserve the structure of porous materials by removing the solvent, typically water, through sublimation. This technique is among

the most facile, energy- and cost- efficient practices to fabricate shaped materials, e.g. aerogels/foams with lightweight and high porosity, from polymer solutions. It is convenient for preparing laboratory-scale materials with commercially available instruments; therefore, this method was employed in my work to prepare melanin-CNF foams. However, it is worth noting that freeze-drying is an impeding factor for upscaling.

Freeze-drying is particularly essential for use with biological compounds that are sensitive to high temperatures. For example, when protein is heated, it can be denatured as the protein molecules unfold and lose their tertiary/secondary structure [27]. With freeze-drying, the dehydrated materials, including the labile biological specimen, can preserve most of their structural features in the dry state [28–30]. This may explain the solubility of lyophilized melanin powder as most of the melanoproteins are still preserved. In contrast, solidifying melanin by acid hydrolysis results in insoluble melanin aggregates because the attached proteins are destroyed (Figure 3.5). Therefore, freeze-drying can be considered as a processing method to solidify melanin while keeping its native form and properties intact.



Figure 3.5. Insoluble (left) and soluble (right) melanin.

3.3. Metal Binding to Melanin

Natural melanins serve as a reservoir for Ca^{2+} and Zn^{2+} , with high concentrations of these ions being observed in pigmented tissues. Natural melanins also sequester reactive metals such as Fe^{3+} and Cu^{2+} , protecting biological systems from damages caused by hydroxyl radicals generated from Fenton reactions. The ability of melanin to bind a variety of metals is attributed to

the presence of functional groups within its structure, including carboxyl, amine, hydroxyl (phenolic), quinone and semiquinone groups (Figure 3.2), which can serve as the metal binding site (it is possible that more than one type of site coordinates to the same metal). Besides quinone, the binding of metals to the other functional group requires the deprotonation (Figure 3.6) and therefore is pH-dependent. The binding site is dependent on the nature of the metal ion [31]. For example, it has been known that Ca^{2+} , Mg^{2+} , and Zn^{2+} share the same binding sites in Sepia melanin, which are the carboxylate groups [32, 33]. Fe^{3+} and Cu^{2+} do not coordinate to the carboxylate groups; instead, Cu^{2+} binds to hydroxyl (OH) groups and Fe^{3+} binds to OH or amine groups. Therefore, the accumulation of Fe^{3+} and Cu^{2+} in the melanosome do not inhibit the binding of Ca^{2+} , Mg^{2+} , and Zn^{2+} to melanin [34].

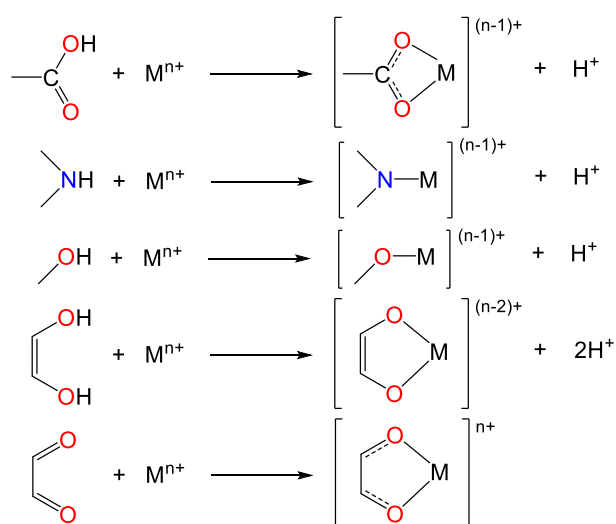


Figure 3.6. Metal binding to functional groups of melanin. It is possible that more than one type of site coordinates to the same metal.

The strength of the coordination bond between a metal ion and the functional group(s) of melanin determines the binding affinity. For an ion that has high binding affinity, it is less likely to be replaced by other ions with lower affinity. For example, in my studies, when melanin or its composites was treated with a solution containing different cations, the adsorption of Pb^{2+} was negligibly affected, while no significant amount of metals such as Ca^{2+} and Zn^{2+} was adsorbed, suggesting that Pb^{2+} has the highest binding affinity. Therefore, melanin and its composites

could be used as effective adsorbents for Pb^{2+} , which is commonly present in waste and industrial water.

3.4. Aggregation versus Dispersion Affecting Adsorption

An adsorption process has commonly four steps: (i) bulk diffusion: transportation of the adsorbate from the bulk to the liquid film surrounding the adsorbent, (ii) external diffusion: the adsorbate molecules diffuse across the surface liquid film, (iii) intraparticle diffusion: the adsorbate molecules diffuse to the surface of the adsorbent via pore diffusion or surface diffusion depending on the porosity of the adsorbent, and (iv) interaction with the surface sites, either by physio- or chemisorption [35]. The diffusion of adsorbate ions/molecules into the inner pores of the adsorbent is crucial for achieving a high adsorption capacity.

It is worth noting that diffusion is driven by the difference of concentrations and a solute will move from a region of high concentration to a region of low concentration. Diffusion is often described by Fick's laws. The Fick's first law postulates that the amount of a substance flowing through a unit area during a unit time interval (i.e. diffusion flux) is proportional to the concentration gradient and the diffusivity of that substance:

$$J = -D \frac{d\varphi}{dx} \quad (1)$$

where J is the diffusion flux, D is the diffusivity (or diffusion coefficient), φ is the concentration and x is the position. D is dependent on the temperature, the viscosity of the fluid and the size of the particles according to the Stokes–Einstein relation. Larger molecules or particles have lower diffusivity compared to that of smaller ions.

When using melanin as the adsorbent, due to the small size and high diffusivity of metal ions, they can deeply penetrate inside the aggregated structure of melanin and bind to the functional groups. However, for large cations with low diffusivity such as several organic dyes, such penetration is limited; therefore, the adsorption mainly occurs on the surface of the micrometer-scale melanin aggregates [36, 37].

When aggregated melanin particles were fragmented into nanoparticles and deposited onto polymeric fibers, their negatively charged surface was further exposed. In addition, the transport of ionic species is enhanced due to the higher surface-to-volume ratio and the reduced transport length in nanoparticles. Therefore, the positively charged molecules can interact more with the surface via electrostatic interaction. As a consequence, the adsorption of cationic dyes is significantly boosted (Figure 3.7). In fact, at the dye concentration of 25 mg L^{-1} , melanized-CNF foams were shown to adsorb 98.3% of crystal violet within 90 min, and the dye concentration in the solution after adsorption was reduced to 0.425 ppm (subchapter 2.2). Raw fungal melanin, however, exhibited a negligible effect on dye removal ($<2\%$) as expected.

This study indicates that the nanosizing of melanin by the intercalation of polymers is a promising method to tackle the issue of aggregation, allowing melanin to perform at full potential for capturing toxic chemicals.

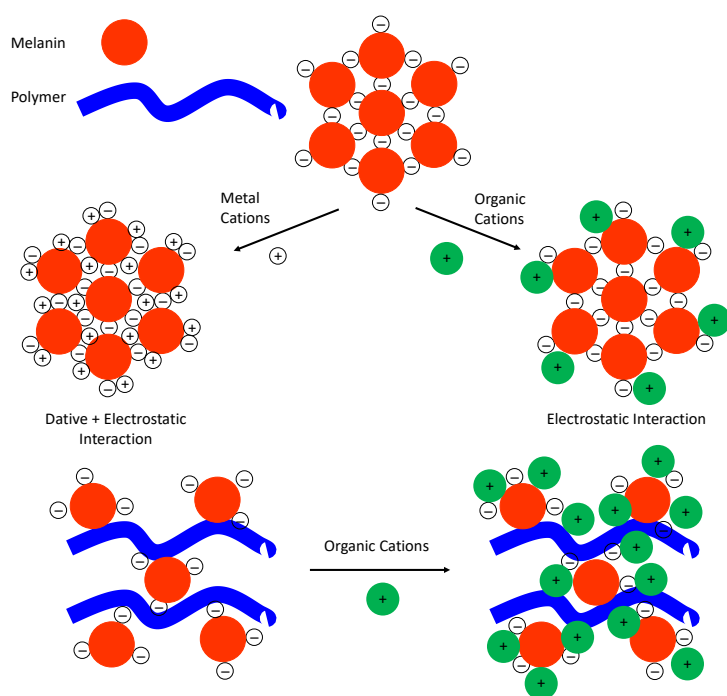


Figure 3.7. Melanin can absorb small metal cations well via electrostatic interactions but the aggregation inhibits the penetration of larger cations, limiting the uptake. The exfoliation of melanin nanoparticles by polymer chains increases the exposed surface and hence boosting the absorption of large cations.

3.5. Mechanical Improvement of Melanin-based Composites

The incorporation of melanin in polymeric substrates, besides helping to disperse the aggregates to exposed melanin's functional groups as mentioned above, allows the formation of freestanding membranes and foams. These shaped materials are preferable compared to the powder form of melanin in industrial applications.

As shown in Figure 3.4, for melanin/polymer composites, melanin nanoparticles with a size of approximately 55 ± 8 nm, act as nano-fillers that are evenly distributed along the fibers' surfaces. It was evident that to achieve desired mechanical properties, the selection of polymers is important. As shown in subchapter 2.1, electrospun PUR membranes are stiffer materials with higher elastic modulus as compared to PCL membranes. Melanin encapsulated within the polymeric fibers influences the mechanical response of membranes, causing a decrease in the elastic modulus for PUR while increasing the average modulus for PCL (Figure 3.8a). This was attributed to the different interaction between the polymer chains and melanin. Similarly, as shown in subchapter 2.2, cationic cellulose was chosen to make the foams due to its electrostatic interaction with the negatively charged melanin. Consequently, the melanized C-CNF foams exhibit a drastic increase in both E-modulus and maximum stress compared to that of C-CNF foams without melanin (Figure 3.8b), with the E-modulus being higher by over an order of magnitude. The improved mechanical performance and stability of the melanin/polymer composites in water enable their recyclability for industrial applications. If the membrane or foam is not stable in aqueous solutions, e.g. C-CNF foams without melanin disintegrate in water and can only be used once, hence increasing the overall cost of the adsorbent.

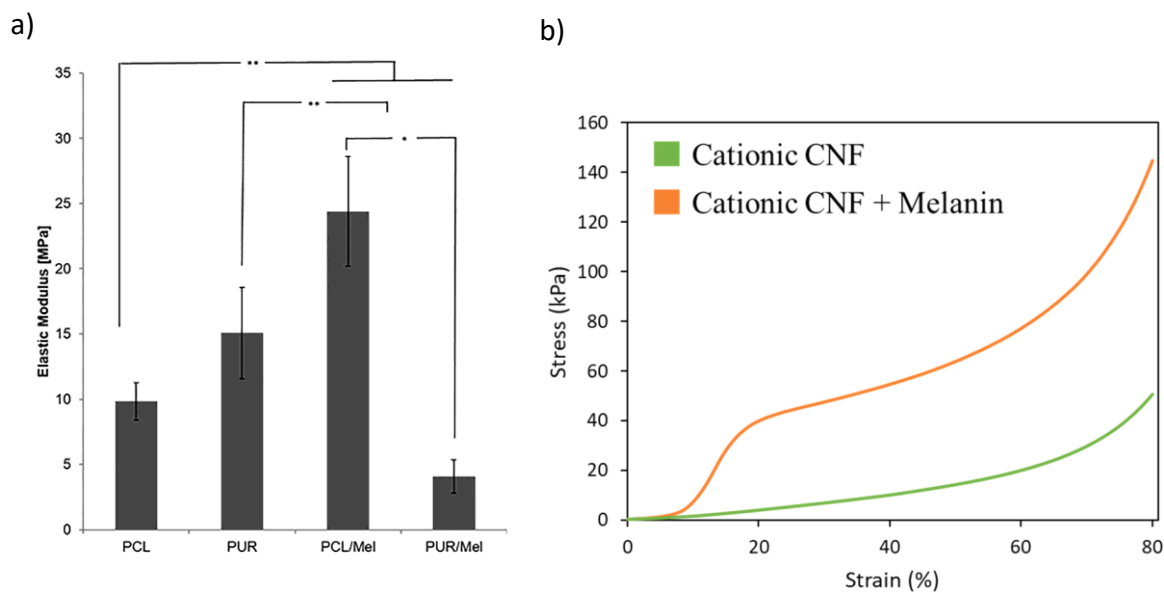


Figure 3.8. a) Young Modulus of different membranes; b) Compressive stress–strain curves of the C-CNF and melanized-C-CNF foams.

3.6. Synergy between Fungal Melanin and Plant Oils

Melanin has been known as an antimicrobial agent, with effect on many different species [38]. Plant oils are also known for their antimicrobial activity [39]; however, the treatment of wood using either fungal melanin or plant oil(s) in our study was not sufficient to protect the walnut wood samples from fungi, as shown in subchapter 2.3. On the one hand, experiments showed that wood samples freshly treated only with melanin solution were more susceptible to airborne microbes than the untreated ones (Table S1 – Subchapter 2.3). This may be due to the remaining moisture and the associated melanoproteins in the treated wood samples, which can be good nutrient sources for some bacteria or fungi. On the other hand, the hydrophobicity of the wood surface treated with plant oils and the antimicrobial properties of plant oils certainly reduce the microbial colonization when compared to untreated wood (Subchapter 2.3). However, some bacteria and wood-decay fungi can still survive in the presence of the plant oils, as they have adapted to colonizing wood, even at a very low moisture content, i.e. < 30% water content.

The double impregnation of wood with melanin and plant oils complement each other, boosting the antifungal activity compared to that of each component. On the one hand, the hydrophobicity of plant oils helps to reduce the moisture adsorption by wood when exposed to a high humidity environment. On the other hand, melanin can inhibit the growth of wood-decay microorganisms. This is significant for protecting wood of wind instruments, e.g. the serpent, as a humid microclimate within the instrument's tube often develops due to the water condensation from the musician's breath, which promotes the growth of wood decay fungi and bacteria. Although melanin does not show an antimicrobial effect against common molds found in the air, the pigment can significantly inhibit the growth of the tested wood decay fungi and bacteria. The mechanism of this selective antimicrobial effect is unclear. In a study by Correa et al. (2017), it was evident that fungal melanin showed a low antimicrobial activity against the fungal species where it had been isolated. They also showed that fungal melanin and human melanin exhibited a different antifungal activity [38]. It is, therefore, hypothesized that melanin from different sources can exhibit different antimicrobial activity, according to their original protective role in nature. This may originate from the variation of melanin structures extracted from different sources, which is worth further investigation.

In conclusion, we have shown that fungal melanin itself is an interesting biopolymer, with similar characteristics of eumelanin, which is the most common type of melanin found e.g. in sepia ink and the human body. The combination of fungal melanin with other compounds presented in this work helps to overcome limiting factors for applications, such as its aggregated structure and hydrophilicity, and can significantly improve the performance of fungal melanin.

4. Outlook

In today's world, sustainability and the circular economy have become the focus of numerous production lines. In that sense, bio-based materials science and technology have become a growing field. New active compounds are discovered and old compounds are investigated for new functions. Fungal melanin is in between. Melanin is one of the most ancient pigments in the world; yet, the understanding of this biopolymer is still far from being complete, with many unanswered questions remaining, especially regarding the exact molecular structure(s). Knowledge of the melanin structure(s) and its relationship with the precursor (e.g. tyrosine) is important to control the chemical and physical properties of melanins, i.e. with different precursors, the fungi may produce melanins with different structures. Although several techniques have been used to analyze melanin's structure, in most cases, these methods require the disruption of the material and hence only the information about the monomeric units is provided. Further work is required to get an insight into the secondary structure of melanin, e.g. how the polymer chains cross-link to form aggregates, as this organization controls the physical properties of melanin.

As shown in our work, the interaction between melanin and the polymer matrices is key for the performance of composites. If the interaction can be tuned, this will open the avenue to obtain a wide range of multifunctional materials for different applications from green technology, healthcare to bioremediation [40, 41]. In addition, a thoughtful design of melanin-based composites will optimize melanin's functions, thus helps reduce the high cost of melanin-based materials (by using less melanin for more efficiency) for practical applications.

In this work, the biodegradability of the melanin-based materials was not studied. Several fungi, such as *Aspergillus fumigatus* or *Phanerochaete chrysosporium* have been reported to be able

to degrade melanin [42]. Nevertheless, future work that will investigate the composites' biodegradability is significant to bring these materials closer to practical and sustainable applications.

The work of this thesis can be further extended to study other applications of melanin such as photo-protection, semiconductor and anti-oxidant properties. Moreover, potential applications of fungal melanin can be identified for bioelectronics and in the field of biomedicine; for example, the construction of biologically derived batteries or the preparation of biodegradable semiconducting films for nerve tissue engineering.

References of chapter 1, 3 and 4

1. Xue J, Wu T, Dai Y, Xia Y (2019) Electrospinning and electrospun nanofibers: Methods, materials, and applications. *Chem. Rev.* 119
 2. Wang J, Xu H, Huo Y, et al (2020) Progress of electrospray and electrospinning in energy applications. *Nanotechnology* 31:. <https://doi.org/10.1088/1361-6528/ab52bb>
 3. Keskinetepe L, Eroglu A (2015) Freeze-drying of mammalian sperm. *Methods Mol Biol* 1257:. https://doi.org/10.1007/978-1-4939-2193-5_25
 4. Langmuir I (1918) The adsorption of gases on plane surfaces of glass, mica and platinum. *J Am Chem Soc* 40:. <https://doi.org/10.1021/ja02242a004>
 5. Freundlich H (1907) Über die Adsorption in Lösungen. *Zeitschrift für Phys Chemie* 57U: <https://doi.org/10.1515/zpch-1907-5723>
 6. Redlich O, Peterson DL (1959) A useful adsorption isotherm. *J. Phys. Chem.* 63
 7. Lagergren SK (1898) About the theory of so-called adsorption of soluble substances. *Sven Vetenskapsakad Handlingar* 24:
 8. Ho YS, McKay G (1999) Pseudo-second order model for sorption processes. *Process Biochem* 34:. [https://doi.org/10.1016/S0032-9592\(98\)00112-5](https://doi.org/10.1016/S0032-9592(98)00112-5)
 9. Weber WJ, Morris JC (1963) Kinetics of Adsorption on Carbon from Solution. *J Sanit Eng Div* 89:. <https://doi.org/10.1061/jsedai.0000430>
 10. Ribera J, Panzarasa G, Stobbe A, et al (2019) Scalable Biosynthesis of Melanin by the Basidiomycete *Armillaria cepistipes*. *J Agric Food Chem* 67:132–139. <https://doi.org/10.1021/acs.jafc.8b05071>
 11. Liu Y, Simon JD (2003) Isolation and Biophysical Studies of Natural Eumelanins: Applications of Imaging Technologies and Ultrafast Spectroscopy. *Pigment Cell Res* 16:606–618. <https://doi.org/10.1046/j.1600-0749.2003.00098.x>
-

12. Pralea I-E, Moldovan R-C, Petrache A-M, et al (2019) From Extraction to Advanced Analytical Methods: The Challenges of Melanin Analysis. *Int J Mol Sci* 20:3943. <https://doi.org/10.3390/ijms20163943>
13. Liu Y, Kempf VR, Nofsinger JB, et al (2003) Comparison of the Structural and Physical Properties of Human Hair Eumelanin Following Enzymatic or Acid/Base Extraction. *Orig Res Artic* 16:355–365. <https://doi.org/10.1034/j.1600-0749.2003.00059.x>
14. Cao W, Zhou X, McCallum NC, et al (2021) Unraveling the structure and function of melanin through synthesis. *J Am Chem Soc* 143:. <https://doi.org/10.1021/jacs.0c12322>
15. Micillo R, Panzella L, Koike K, et al (2016) “Fifty shades” of black and red or how carboxyl groups fine tune eumelanin and pheomelanin properties. *Int. J. Mol. Sci.* 17
16. Ito S (2003) A Chemist’s View of Melanogenesis. *Pigment Cell Res.* <https://doi.org/10.1034/j.1600-0749.2003.00037.x>
17. D’Ischia M, Napolitano A, Ball V, et al (2014) Polydopamine and eumelanin: From structure-property relationships to a unified tailoring strategy. *Acc Chem Res* 47:3541–3550. <https://doi.org/10.1021/ar500273y>
18. Ligonzo T, Ambrico M, Augelli V, et al (2009) Electrical and optical properties of natural and synthetic melanin biopolymer. *J Non Cryst Solids* 355:1221–1226. <https://doi.org/10.1016/j.jnoncrysol.2009.05.014>
19. Bridelli MG, Crippa PR (2010) Infrared and water sorption studies of the hydration structure and mechanism in natural and synthetic melanin. *J Phys Chem B* 114:9381–9390. <https://doi.org/10.1021/jp101833k>
20. Kim YJ, Wu W, Chun SE, et al (2013) Biologically derived melanin electrodes in aqueous sodium-ion energy storage devices. *Proc Natl Acad Sci U S A* 110:20912–20917. <https://doi.org/10.1073/pnas.1314345110>

21. Jalmi P, Bodke P, Wahidullah S, Raghukumar S (2012) The fungus *Gliocephalotrichum simplex* as a source of abundant, extracellular melanin for biotechnological applications. *World J Microbiol Biotechnol* 28:505–512. <https://doi.org/10.1007/s11274-011-0841-0>
22. Meredith P, Powell BJ, Riesz J, et al (2006) Towards structure-property-function relationships for eumelanin. *Soft Matter* 2
23. Łopusiewicz Ł, Jedra F, Mizieńska M (2018) New poly(lactic acid) active packaging composite films incorporated with fungal melanin. *Polymers (Basel)*. <https://doi.org/10.3390/polym10040386>
24. Łopusiewicz Ł, Kwiatkowski P, Drożdowska E, et al (2021) Preparation and characterization of carboxymethyl cellulose-based bioactive composite films modified with fungal melanin and carvacrol. *Polymers (Basel)* 13:. <https://doi.org/10.3390/polym13040499>
25. Eom T, Shim BS (2015) Natural melanin composites by layer-by-layer assembly. In: *Electroactive Polymer Actuators and Devices (EAPAD) 2015*. SPIE, p 94302V
26. Ewaldz E, Patel R, Banerjee M, Brettmann BK (2018) Material selection in electrospinning microparticles. *Polymer (Guildf)* 153:. <https://doi.org/10.1016/j.polymer.2018.08.015>
27. Cerdán-Leal MA, López-Alarcón CA, Ortiz-Basurto RI, et al (2020) Influence of heat denaturation and freezing–lyophilization on physicochemical and functional properties of quinoa protein isolate. *Cereal Chem* 97:. <https://doi.org/10.1002/cche.10253>
28. Griebenow K, Klibanov AM (1995) Lyophilization-induced reversible changes in the secondary structure of proteins. *Proc Natl Acad Sci U S A* 92:. <https://doi.org/10.1073/pnas.92.24.10969>
29. Johnson RE, Kirchoff CF, Gaud HT (2002) Mannitol-sucrose mixtures - Versatile formulations for protein lyophilization. *J Pharm Sci* 91:. <https://doi.org/10.1002/jps.10094>
30. Matejtschuk P (2007) Lyophilization of proteins. *Methods Mol. Biol.* 368

31. Hong L, Simon JD (2007) Current understanding of the binding sites, capacity, affinity, and biological significance of metals in melanin. *J Phys Chem B* 111:. <https://doi.org/10.1021/jp071439h>
32. Bowness JM, Morton RA (1952) Distribution of copper and zinc in the eyes of fresh-water fishes and frogs. Occurrence of metals in melanin fractions from eye tissues. *Biochem J* 51:. <https://doi.org/10.1042/bj0510530>
33. Panessa BJ, Zadunaisky JA (1981) Pigment granules: A calcium reservoir in the vertebrate eye. *Exp Eye Res* 32:. [https://doi.org/10.1016/S0014-4835\(81\)80008-5](https://doi.org/10.1016/S0014-4835(81)80008-5)
34. Hong L, Liu Y, Simon JD (2004) Binding of Metal Ions to Melanin and Their Effects on the Aerobic Reactivity¶. *Photochem Photobiol* 80:. [https://doi.org/10.1562/0031-8655\(2004\)080<0477:bomitm>2.0.co;2](https://doi.org/10.1562/0031-8655(2004)080<0477:bomitm>2.0.co;2)
35. Güzel F, Saygılı H, Saygılı GA, Koyuncu F (2014) Decolorisation of aqueous crystal violet solution by a new nanoporous carbon: Equilibrium and kinetic approach. *J Ind Eng Chem* 20:. <https://doi.org/10.1016/j.jiec.2013.12.023>
36. Tran-Ly ANANAN, Ribera J, Schwarze FWMRFWMMR, et al (2020) Fungal melanin-based electrospun membranes for heavy metal detoxification of water. *Sustain Mater Technol* 23:e00146. <https://doi.org/10.1016/j.susmat.2019.e00146>
37. Tran-Ly AN, De France KJ, Rupper P, et al (2021) Melanized-Cationic Cellulose Nanofiber Foams for Bioinspired Removal of Cationic Dyes. *Biomacromolecules* 22:4681–4690. <https://doi.org/10.1021/acs.biomac.1c00942>
38. Correa N, Covarrubias C, Rodas PI, et al (2017) Differential antifungal activity of human and cryptococcal melanins with structural discrepancies. *Front Microbiol* 8:. <https://doi.org/10.3389/fmicb.2017.01292>

39. Petropoulos SA, Fernandes Â, Calhelha RC, et al (2021) Antimicrobial properties, cytotoxic effects, and fatty acids composition of vegetable oils from purslane, linseed, luffa, and pumpkin seeds. *Appl Sci* 11:. <https://doi.org/10.3390/app11125738>
40. Tran-Ly ANAN, Reyes C, Schwarze FWMRFWMR, Ribera J (2020) Microbial production of melanin and its various applications. *World J Microbiol Biotechnol* 36:170. <https://doi.org/10.1007/s11274-020-02941-z>
41. Mattoon ER, Cordero RJB, Casadevall A (2021) Fungal melanins and applications in healthcare, bioremediation and industry. *J. Fungi* 7
42. Butler MJ, Day AW (1998) Destruction of fungal melanins by ligninases of *Phanerochaete chrysosporium* and other white rot fungi. *Int J Plant Sci* 159:989–995. <https://doi.org/10.1086/314093>

Acknowledgements

Finally, this chapter will close soon. I know that PhD is just one of the challenges I will need to overcome during my life, but I will remember it as one of the most important milestones that help shape me into the person I am today. For that, I would like to express my gratitude to all those who gave me the possibility to complete this dissertation in specific as well as the academic support in general that I received during my PhD time at Empa and ETH Zürich.

Foremost, I would like to send my deepest gratitude to Prof. Francis W.M.R. Schwarze for introducing me to such an interesting topic for the PhD project and giving me all the conditions needed to conduct and complete it at Empa – Swiss Federal Laboratories for Materials Science and Technology. I appreciate his invaluable guidance and advice all these years. Even more than that, I am grateful for his patience, concerns, support and understanding when I hit rock bottom on my PhD journey.

I also wish to send my honest thanks to Prof. Ingo Burgert for agreeing to be my main supervisor at ETH Zürich. He always gave me the best support throughout the process from writing the research plan to submitting the final dissertation. Without him, I would not have the privilege of becoming a student of ETH, where I greatly benefited from a high quality research environment.

I was lucky to get an interdisciplinary project, which allowed me to work with experts in different fields and expand my knowledge a lot. I will never forget my late supervisor in membrane and textile engineering: Dr. Giuseppino Fortunato, may he rest in peace. His patient guidance since my first steps into the Materials Science field and his critiques on my work forms the high standard for every scientific work I have conducted later. I would also give my special thanks to Dr. Javier Ribera Regal, for his help in Mycology, his advice and assistance in keeping my progress on schedule. My thanks are extended to Mr. Adrian Wichser, Mr. Patrick Rupper, Mr.

Alexander Gogos and Mr. Markus Heeb for their technical help in performing chemical and physical analyses.

This wonderful journey would not have been fulfilled without all my colleagues at Empa, and particularly in the Department of Wood and Cellulose materials (Abt. 302): Bruno Zraggen, Markus Heeb, Javier Ribera, Alessia Pasqualini, Alessia Giuffrida, Mónica Mur, Saranya, Joao Marcos, Felix Rentschler, Yolanda Martinez, Tingting, Tine, Carolina, Kevin... Thank you for the fun, the talks, the great support in the lab and for all the memories we have had shared together.

I would like to also thank chú Chánh, cô Ngọc, chị Nhàn, cô Thịnh and my Vietnamese gang: Ngô Lan Phuong, Phan Minh Trí, chị Hạnh Dương, anh Trung Dương, em Thái, chị Đào, em Khánh, em Thi, em Huyền, chị Quy Vo-Reinhard for the delicious Vietnamese food and talks in my mother tongue whenever I feel nostalgic of my far away home.

Finally, from the deepest of my heart, I want to thank my parents for their unconditional love, support and belief in me. Thank my brother and my sister-in-law for taking care of my parents when I am not home. Thank also my little nephew for being my endless joy. And my big shout out to Dr. Tu Nguyen, my fiancé, who shares the passion for science and inspires me to do science not just for publication but for the real impact we can make on society. As a knowledgeable chemist, he helped me a lot in analyzing and understanding the results, as well as proofreading the manuscripts. I am looking forward to our coming together projects.

Did I forget to thank anyone? Ah yes. Thank myself, for not giving up. Without this persistence, this accomplishment would not have been possible. Cám ơn!




Curriculum Vitae

1

ANH N. TRAN LY

PHD CANDIDATE IN MATERIALS SCIENCE

CONTACT

 (+41) 78 791 68 23
 tranlyn@student.ethz.ch
 www.linkedin.com
/in/anhtranly

SKILLS

RESEARCH

Materials characterization methods
Molecular biology techniques
Microbiology techniques

COMPUTER

Microsoft Office
LaTeX, EndNote
ImageJ, Origin
SPSS
R

LANGUAGES

Vietnamese
English
French
German

EDUCATION

Ph.D. candidate in Materials Science

ETH Zürich, Switzerland | May 2018 - June 2022 (expected)

Project splitted between ETHZ and Empa

- Fungal & enzymatic bioengineering Dept. at EMPA, Prof. Dr. Francis F.W.R. Schwarze
- Wood Materials Science Dept. at ETHZ, Prof. Dr. Ingo Burgert

M.Sc. in Safety in the Food chain

Universität für Bodenkultur, Austria | Sep 2015 - Apr 2018

Wageningen University & Research, Netherlands | Erasmus exchange semester

Thesis grade: 1/5 (Very good - Austrian scale)

B.Sc. in Biotechnology-Pharmacology

University of Science and Technology of Hanoi (Vietnam-France University), Vietnam | Oct 2011 - July 2014

GPA: 17.2/20 (Very good - French scale) | Rank 2nd of class 2014

WORK EXPERIENCE

Trainee (2017) - Research assistant (2018 onward)

Empa - Swiss Federal Laboratories for Materials Science and Technology, Switzerland | Mar 2017 - present

- PhD project: Fungal melanin-based composites for various biotechnological applications
- Innosuisse project: The Serpentino: Development of an antimicrobial coating for a historical wind instrument

Biological technician

MycoSolutions AG, Switzerland | May 2018 - May 2019

- Support the R&D team in design, development and maintenance biocontrol agent products.
- Ensure quality standard by performing different biological tests

Research assistant

Oxford University Clinical Research Unit - Hospital for Tropical Diseases, Vietnam | Oct 2014 - Jun 2015

Malaria Group

- Participate in various research activities in clinical studies
- Support setting up for clinical trials at field sites

ANH N. TRAN-LY

2

PRESS RELEASES

The world of mushrooms: melanin from the honey mushroom
 The science series Leschs Kosmos (TV program), Sep 21, 2021

La recherche dans les HEM et son impact sociétal
 Revue Musicale Suisse, Sep 2021

La mélanine, un pigment aux étonnantes propriétés
 Radio Télévision Suisse, CQFD (radio interview), Feb 24, 2021

The black gold of mushrooms
 Empa Quarterly Nr.70, Jan 2021

HONORS & AWARDS

- Winner of Startup Campus Award for business ideas from technology in the Innosuisse Startup Campus - Swiss Innovation Agency, 2021
- Erasmus Mundus Scholarship (48,000 EUR/2 years) for full International Master Programme in Europe, 2015
- Excellent Fellowship (500 EUR/month) for top 3 students of the department to do internship at Montperlier SupAgro, France, 2014
- JENESYS 2.0 - Japan-East Asia Network of Exchange for Students and Youth Scholarship as Vietnam delegate

PUBLICATIONS

- Tran-Ly, A.N., Heeb, M., Berger, S., & Schwarze, F.W.M.R. Antimicrobial Effect of Fungal Melanin in Combination with Plant Oils for the Treatment of Wood. *Frontiers in Plant Science* (2022). (submitted)
- Tran-Ly, A.N., De France, K.J., Rupper, P., Nystöm, G. et al. Melanised-cationic cellulose nanofibers foams for bioinspired removal of cationic dye. *Biomacromolecules* (2021). <https://doi.org/10.1021/acs.biomac.1c00942>
- Tran-Ly, A.N., Reyes, C., Schwarze, F.W.M.R. et al. Microbial production of melanin and its various applications. *World J Microbiol Biotechnol* 36, 170 (2020). <https://doi.org/10.1007/s11274-020-02941-z>
- Tran-Ly, A.N., Ribera, J., Schwarze, F., Brunelli, M., & Fortunato, G. (2020). Fungal melanin-based electrospun membranes for heavy metal detoxification of water. *Sustainable Materials And Technologies*, 23, e00146. doi: 10.1016/j.susmat.2019.e00146

CONFERENCE PRESENTATIONS

- "Development of melanised nanocellulose composite for water purification systems". International Conference on Nanotechnology for Renewable Materials, June 2020. (talk)
- "Fungal melanin: a novel approach for metal detoxification". 15th European Conference on Fungal Genetics, Rome, Italy, Feb 2020. (poster)
- "Fungal melanin for waste water treatment". Annual Euroleague for Life Sciences - Scientific Student Conference, Copenhagen, Denmark, Nov 2017. (talk)
- "Phenotypic analysis of *Arabidopsis thaliana* pdf1 mutants in response to abiotic stresses". Annual Euroleague for Life Sciences - Scientific Student Conference, Hohenheim, Germany, Nov 2016. (poster)

Declaration

I, Tran Ly Nguyet Anh, declare that this thesis is my own work and has not been submitted in any form for another degree or diploma at any university or other institute.

Information derived from the published and unpublished work of others has been acknowledged in the text and a list of references is given in the bibliography.